Nuclear Structure for the Crust of Neutron Stars and Exotic Nuclei

Dissertation

zur Erlangung des Grades eines
Doktors der Naturwissenschaften
der Fakultät für Mathematik und Physik
der Eberhard–Karls–Universität zu Tübingen

vorgelegt von

Peter Gögelein
aus Rot am See – Brettheim

2007

Tag der mündlichen Prüfung:	4. Oktober 2007
Dekan:	Prof. Dr. Nils Schopohl
1. Berichterstatter:	Prof. Dr. Herbert Müther
2. Berichterstatter:	Prof. Dr. Dr. h.c. mult. Amand Fäßler

Contents

Chapter 1

Introduction

One of the major challenges in theoretical nuclear physics is the reproduction of the main properties of nuclear systems from realistic nucleon–nucleon interactions, which reproduce the experimental nucleon-nucleon (NN) scattering data up to the pion threshold of about 350 MeV. The model for such a realistic interaction may be chosen from quantum chromodynamics (QCD) [Va$^+$95], or assuming the meson exchange or one-boson exchange model [Ml89]. Another possibility is a purely phenomenological model for a local interaction a with a complete set of two–body spin–isospin operators [LP81]. The parameters of such a model are determined in a fit to the experimental nucleon–nucleon phase shifts.

After choosing the model for the realistic interaction, the many–body problem for the interacting nucleons has to be solved. The first approach to the many–body problem is the Hartree–Fock method. Unfortunately this method leads to unbound nuclear systems if a realistic NN interaction is employed in the calculation. These problems arise due to the repulsive core of the realistic interactions at short inter–nucleon distances [MP00].

Hence correlations beyond the mean–field have to be considered in such many–body calculations. Various methods have been developed to improve the many–body calculations like the Brueckner hole–line expansion, which leads to the Brueckner G–matrix, the "coupled cluster" technique, the "exponential S" method, the self–consistent Green function approach, variational methods employing correlated basis states, and quantum monte–carlo techniques [DM$^+$92, MP00, WFF88, Cep95].

These improvements enable the realistic interactions to describe nuclear systems to the same extend (see discussion below). However, different realistic interactions lead to different results and on closer inspection even the matrix elements are different

for the same partial wave due to different treatment of the short–range part of the interaction. This led to the development of an effective low–momentum interaction V_{lowk}, which results in the same matrix elements for all kinds of realistic input interaction by introducing a cutoff corresponding to the pion threshold [BK$^+$03]. This effective interaction provides a broader range of applications since the model space in the many–body calculation may be truncated to lower momenta. But also this low–momentum interaction is not without problems, which are mainly that the saturation property of homogeneous nuclear matter is lost. This problem may be cured by introduction of a density dependent effective interaction $V_{lowk}(\rho)$ in connection with a three–body force [KM$^+$03, BDM06].

A plot of the binding energy over the saturation density of nuclear matter obtained from many–body calculations employing different bare realistic potentials leads to the so–called "Coester"–line, which does not hit the experimental value [Co$^+$70]. In finite nuclei this means that the binding energies and radii can't be reproduced simultaneously. Again the inclusion of three–body forces can cure this problem, but this is somehow an artificial adjustment [Sv$^+$86].

Besides the realistic interactions, phenomenological approaches to the nucleon–nucleon interaction have been developed like the Skyrme and the Gogny forces [Sk59, RS80]. These forces result in an energy density functional for the nuclear system, which has to be minimized by a variational calculation [VB72]. The parameters of such forces are fitted to the experimental binding energies and radii of closed shell nuclei. A connection can be drawn to approaches based on realistic forces by a density matrix expansion of the Brueckner G–matrix. Such nuclear forces describe radii and binding energy of nuclei well but they are not able to reproduce phase shifts of nucleon–nucleon scattering and hence they are not counted among realistic interactions.

So far all many–body approaches has been non–relativistic ones, although the nucleons reach in the nucleus about one third of the speed of light. A second feature which is essential in nuclear structure calculations, the spin–orbit interaction, is also a relativistic effect which has been built into the non–relativistic approaches artificially.

The Dirac–Brueckner–Hartree–Fock approach (DBHF) to nuclear matter employing realistic NN interactions of the Bonn type is a relativistic extension of the Brueckner theory [An$^+$83, BM90]. The realistic interactions employed in such an approach are based on one–boson exchange (OBE). The exchanged bosons correspond to various

covariant operators in the nucleon–boson vertices. Each of these vertices denote a special meson exchange, which are the attractive scalar mesons σ and δ, the repulsive vector mesons ω and ρ and the π in the pseudo–vector channel. The exchanged mesons generate large contributions to the nucleon self–energy up to several hundred MeV. Especially the attractive scalar self–energy contribution Σ_S and the repulsive time–like vector contribution Σ_0 play an important role. They cancel each other to a large extend and the lowest states in the Fermi–sea get a usual energy of about -50 MeV. As density rises the lower component of the Dirac spinor gets larger, what results in a smaller effective mass in the nuclear medium compared to the free Dirac spinor. Anyway, this density dependent effective mass improves the saturation properties and the Dirac–Brueckner–Hartree–Fock approach provides results which are close to the experimental value or even reach it with some special realistic interactions.

Besides the relativistic Brueckner approach, which is too complex to be applied to finite nuclei, the relativistic mean–field approaches have been developed. The first attempt was done by Walecka and Serot, who applied the relativistic Hartree approach to finite nuclei [SW86]. One year later already the relativistic Hartree–Fock approach has been published [BM$^+$87]. Parameters for the models were obtained by fits to the experimental data of finite nuclei or by fits to nuclear matter properties [Rhd89]. Applying relativistic models, the ground state properties of finite nuclei are improved. The spin–orbit force, which is mainly guided by the sum of scalar and time–like vector self–energy, is state dependent in such a model in contrary to non–relativistic approaches. This feature improves the spin–orbit splitting in finite nuclei significantly. For some years such relativistic mean–field approaches were regarded as unable to reproduce concurrently experimental data for finite nuclei and nuclear matter properties with a satisfactory precision. Therefore some groups introduced non–linear terms for the σ–meson field to overcome this problem, others introduced terms similar to the Skyrme functional. It is possible to fit suitable parameter sets for such approaches, but they are even more phenomenological than the original one. Things changed with the introduction of a new method: density dependent coupling functions were introduced [FM94]. Within this method phenomenological fits to binding energy and radii of finite nuclei has been performed, which are able to reproduce the fitted properties of many nuclei with sufficient accuracy. However, from the many–body point of view a better method is to fit the coupling functions such that the self–energy contributions of the various mesons of a relativistic Brueckner

calculation are reproduced for nuclear matter. Projection methods onto covariant operators improved such a local density approximation of the Brueckner G-matrix [Sch00, SM01]. Finally, by taking rearrangement contributions into account single–particle energies and wave functions show better agreement with the experiment [FLW95].

A theory of nuclear systems, which is derived from the interaction of two nucleons in the vacuum and fits to data of finite nuclei at normal density should yield reliable predictions for nuclear systems at extreme densities, temperature and proton–neutron asymmetries, as they occur in astrophysical objects like neutron stars or supernovae. Nuclear reactions and electro–weak interactions with the light particles, the leptons, drive various astrophysical processes [CTT]. The binding energy of a nucleus shows a maximal value for the iron (^{56}Fe) nucleus. Hence light nuclei in stars set energy free by fusion to heavier nuclei. Different burning stages form layers with the heavier nuclei in the center. The exothermal nuclear reaction provides a pressure against the gravitational force and thus stabilizes the star. A relation between properties of the medium inside a star is called an equation of state (EoS). Together with the nuclear reactions the equation of state is an essential ingredient for all kinds of star simulations.

At the end of the nuclear burning in a star with a mass larger than eight times the mass of our sun the fusion of silicon generates a growing iron core in which no fusion is present any more. If the central density of such an iron core exceeds the Chandrasekhar limit, the inverse β–decay becomes energetically favorable, where protons and electrons react to neutrons and neutrinos. In this situation the core collapses until the Fermi pressure of the neutrons is reached. The infalling matter bounces onto the collapsed core and forms a shock wave running outward until it is stalled by accreting matter. Neutrino heating revives the shock until finally the envelope of the star is blasted away. The remnant of such a core collapse supernova is a neutron star or a black hole in case of more massive stars.

The remaining neutron star cools by neutrino emission. If the so–called direct Urca process sets in, it enhances the cooling rate of a neutron star significantly. Neutron stars may rotate very fast due to the angular momentum conservation during the collapse. In the center of the neutron star there may exist strange baryons besides the neutrons if a certain density is exceeded, pion and kaon condensates may occur and even a transition to quark matter is taken into consideration. The outer core is dominated by superfluid neutrons with a small abundance of protons and

electrons. In the crust of a neutron star a transition from nulcei in the outer layers to homogeneous matter on the inside takes place, which is investigated in this work. This crust may influence the neutrino opacity and thus the cooling rate of the star. The envelope consists mainly of iron nuclei and is very smooth because of the large gravitational force. Changes of the properties of superfluid nuclear matter may cause sudden changes in the rotational frequency of the neutron star which are called "glitches". In connection with huge magnetic fields so–called "pulsars" emit X–ray bursts.

The crust of a neutron star is a very intriguing object for theoretical nuclear structure physics, as it contains the transition from stable nuclei in the outer crust to a system of homogeneous nuclear matter, consisting of protons, neutrons and leptons in β–equilibrium, in the inner part of this crust. The question of how matter consisting of isolated nuclei melts into uniform matter with increasing density has evoked a large number of studies [PR95, HS$^+$84, Oya03, OI07]. Already at moderate densities the Fermi energy of the electrons is so high that the β–stability enhances the neutron fraction of the baryons so much that a part of these neutrons drip out of the nuclei. This leads to a structure, in which quasinuclei, clusters of protons and neutrons, are embedded in a sea of neutrons. In order to minimize the Coulomb repulsion between the protons, the quasinuclei form a lattice.

These structures are typically described in form of the Wigner–Seitz (WS) cell approximation. One assumes a geometrical shape for the quasinuclei and determines the nuclear contribution to the energy of such a WS cell from a phenomenological energy density functional. Such Thomas–Fermi calculations yield a variety of structures: Spherical quasinuclei, which are favored at small densities, merge with increasing density to strings, which then may cluster to parallel plates. At even larger densities inverse structures may be formed until the homogeneous nuclear matter phase is reached. These geometrical structures have been the origin for the popular name of this phase: Pasta phase.

Such Thomas–Fermi calculations, however, are very sensitive to the surface tension under consideration. Furthermore they do not account for characteristic features of the structure of finite nuclei, like the shell–effects. Shell effects favor the formation of closed shell systems and may have a significant effect on the formation of inhomogeneous nuclear structures in the crust of neutron stars. These shell effects are incorporated in self–consistent Hartree-Fock or relativistic mean–field calculations, which can treat finite nuclei, infinite matter and inhomogeneous structures in be-

tween within a consistent frame based on an effective nucleon–nucleon interaction. Such calculations employing the density–dependent Skyrme forces have been done more than 25 years ago by Bonche and Vautherin[BV81] and by a few other groups. These studies show indeed that shell effects have a significant influence on details like the proton abundance of the baryonic matter in the inhomogeneous phase [MMM04]. They also provide the basis for a microscopic investigation of properties beyond the equation of state. This includes the study of pairing phenomena, excitation modes and response functions as well as the effects of finite temperature.

Self–consistent Hartree–Fock calculations for such inhomogeneous nuclear structures have typically been performed assuming a WS cell of spherical shape. This assumption of quasinuclei with spherical symmetry reduces the numerical work–load considerably. However, it does not allow the exploration of quasinuclear clusters in form of strings or plates as predicted from Thomas–Fermi calculations. Furthermore the limit of homogeneous matter can not be described in a satisfactory manner in a spherical WS cell. Employing the representation of plane wave single–particle states in terms of spherical Bessel functions leads to a density profile, which, depending on the boundary condition chosen, exhibits either a minimum or a maximum at the boundary of the cell. Bonche and Vautherin [BV81] therefore suggested to use a mixed basis, for which, depending on the angular momentum, different boundary conditions were considered. However, even this optimized choice leads to density profiles with fluctuations [MMM04].

Therefore the investigations presented in this work consider cubic WS cells, which allows for the description of non–spherical quasinuclear structures and contains the limit of homogeneous matter in a natural way. Self–consistent Hartree–Fock calculations are performed for β–stable matter in a density range for which the quasinuclear structures discussed above are expected to appear. For the nuclear Hamiltonian we consider Skyrme forces but also perform calculations within the relativistic mean–field approximation. Special attention will be paid to the comparison between results obtained in the effective microscopic approaches and corresponding Thomas–Fermi calculations.

After this introduction the Skyrme Hartree–Fock approach will be reviewed in chapter 2. Afterwards the relativistic Hartree–Fock approach is introduced and extended to triaxial application and asymmetric nuclear matter in chapter 3. The superfluidity of nuclear systems is included in the code by pair correlations, which are treated in combination with finite temperature in chapter 4. The numerical solution of the

Hartree–Fock and mean–field equations in the cubic WS cell requires sophisticated numerical methods and fast algorithms which are described in chapter 5. An essential ingredient is the application of the imaginary time step method which is extended to relativistic calculations. In chapter 6 the results of different projects are presented and discussed, which are a parametrization for a density dependent relativistic mean–field model (DDRMF) from a Dirac–Brueckner–Hartree–Fock approach (DBHF) for astrophysical use, the structure of the "Pasta" phase and the equation of state in the crust of a neutron star, and relativistic Hartree-Fock calculations for some exotic nuclei.

The summary and outlook closes this Ph.D. thesis in the final chapter 7. Parts of this thesis has been published in [GM07a]. Two further publications are in preparation, one about the DDRMF model derived from DBHF [GvD$^+$07] and another one will present the application of the low–momentum interaction V_{lowk} to finite nuclei [GM07b].

Chapter 2

The Skyrme Hartree–Fock Approach

In this chapter the general Hartree–Fock formalism is introduced to solve the nuclear many–body problem. Then we turn to the Skyrme interaction which leads to a density functional approach. These approaches can be related to a local density approximation of the Brueckner–Hartree–Fock theory [Ne70, NV75]. After the introduction of the interaction the energy functional and the Hartree–Fock equations are discussed.

2.1 The General Hartree–Fock Formalism

In this work the Hartree–Fock method is extensively used to solve the nuclear problem, which is outlined in the following [RS80]. The nucleons are represented by a Slater determinant Φ, which can be written in terms of creation operators $c_\alpha^\dagger$ for nucleons in single particle states φ_α acting on the vacuum state $|0\rangle$ (A stands for the number of nucleons)

$$|\Phi(1\ldots A)\rangle = \prod_{\alpha=1}^{A} c_\alpha^\dagger |0\rangle. \tag{2.1}$$

The single–particle wave functions have to be orthogonal and the whole state is antisymmetrized due to the Pauli principle. The single–particle states α are eigenstates of a single–particle Hamiltonian, which has to be determined from the two–body potential. The two–body potential V, associated with the nuclear force, is expressed

in terms of antisymmetrized matrix elements

$$\langle\alpha\beta|\bar{V}|\gamma\delta\rangle = \langle\alpha\beta|V|\gamma\delta\rangle - \langle\alpha\beta|V|\delta\gamma\rangle. \tag{2.2}$$

Using these antisymmetrized matrix elements $\bar{V}$ we are able to construct the many-body Hamiltonian H in second quantization

$$H = \sum_{\alpha\beta}\langle\alpha|T|\beta\rangle\, c^\dagger_\alpha c_\beta + \frac{1}{4}\sum_{\alpha\beta\gamma\delta}\langle\alpha\beta|\bar{V}|\gamma\delta\rangle c^\dagger_\alpha c^\dagger_\beta c_\delta c_\gamma \tag{2.3}$$

with T the kinetic energy operator. Now we can denote the Hartree–Fock energy as a functional of the single–particle density matrix by virtue of Wick's theorem

$$\begin{aligned} E_{HF}[\rho] =& \langle\Phi|H|\Phi\rangle \\ =& \sum_{\alpha\beta}\langle\alpha|T|\beta\rangle\langle\Phi|c^\dagger_\alpha c_\beta|\Phi\rangle + \frac{1}{4}\sum_{\alpha\beta\gamma\delta}\langle\alpha\beta|\bar{V}|\gamma\delta\rangle\langle\Phi|c^\dagger_\alpha c^\dagger_\beta c_\delta c_\gamma|\Phi\rangle \\ =& \sum_{\alpha\beta}\langle\alpha|T|\beta\rangle\,\rho_{\beta\alpha} + \frac{1}{2}\sum_{\alpha\beta\gamma\delta}\rho_{\gamma\alpha}\langle\alpha\beta|\bar{V}|\gamma\delta\rangle\rho_{\delta\beta}. \end{aligned} \tag{2.4}$$

The Hartree–Fock basis $\{\varphi_\alpha\}$ is the basis in which the density matrix ρ is diagonal. In this basis the energy reads

$$E_{HF} = \sum_{\alpha=1}^{A}\langle\alpha|T|\alpha\rangle + \frac{1}{2}\sum_{\alpha\beta=1}^{A}\langle\alpha\beta|\bar{V}|\alpha\beta\rangle, \tag{2.5}$$

where the eigenvalues of the density matrix are 0 and 1. For eigenvalues between 0 and 1 the appropriate occupation scheme has to be employed.
Now our task is to determine the Hartree–Fock basis. The Hartree–Fock energy has to be minimized with respect to all product wave functions $|\Phi\rangle$ within the set of Slater determinants. With this requirement the variation of energy is written

$$\delta E = E[\rho+\delta\rho] - E[\rho] = \sum_{\alpha\alpha'} H^{HF}_{\alpha\alpha'}\,\delta\rho_{\alpha\alpha'} = 0, \tag{2.6}$$

where the hermitian matrix H is the matrix of the single–particle Hamiltonian

$$H^{HF}_{\alpha\alpha'} = \frac{\partial E_{HF}[\rho]}{\partial\rho_{\alpha\alpha'}} = (T+\Gamma)_{\alpha\alpha'}. \tag{2.7}$$

In this equation Γ is a self–consistent one–body field which depends on the density of the nucleus and averages over all two-body interactions

$$\Gamma_{\alpha\alpha'} = \sum_{\beta\beta'}\langle\alpha\beta'|\bar{V}|\alpha'\beta\rangle\rho_{\beta\beta'} \tag{2.8}$$

Due to the stationary condition for the energy (eq. 2.6) the equation

$$[H^{HF}, \rho] = [T + \Gamma[\rho], \rho] = 0 \tag{2.9}$$

holds for H^{HF} and the density matrix ρ. Hence the matrix elements of H^{HF} do not mix particle and hole states and from this equation we see that H^{HF} and ρ can be diagonalized simultaneously. Finally the equation (2.9) can be transformed to an eigenvalue problem

$$H^{HF}_{\alpha\alpha'} = \langle\alpha|T|\alpha'\rangle + \sum_{\beta=1}^{A}\langle\alpha\beta|\bar{V}|\alpha'\beta\rangle = \varepsilon_\alpha\delta_{\alpha\alpha'}, \tag{2.10}$$

from which we get the single–particle energies ε_α and the single–particle wave functions $\{\varphi_\alpha\}$ by transformation of the ansatz basis to the HF basis. These equations are nonlinear and can be solved by iterative diagonalization or some kind of gradient step method.

The ground state energy E_{HF} can be computed from equations (2.5) and (2.10) considering the A lowest single-particle states

$$E_{HF} = \sum_{\alpha=1}^{A}\varepsilon_\alpha - \frac{1}{2}\sum_{\alpha\beta=1}^{A}\langle\alpha\beta|\bar{V}|\alpha\beta\rangle. \tag{2.11}$$

The Hartree–Fock method conserves the symmetries of the initial density $\rho(0)$ of the ansatz wave set. Hence we have to start with a deformed ansatz if we are interested in deformed solutions.

In nuclear physics the Hartree–Fock method is widely used although it does not consider correlations and does not reproduce binding energies of both nuclear matter and finite nuclei if a so–called realistic nucleon–nucleon potential is plugged in the calculation. These NN potentials, which are fitted to reproduce the NN scattering data, are strongly repulsive for very short inter–nucleon distances and therefore one has to go beyond Hartree-Fock. A widely used extension of Hartree–Fock is the Brueckner–Hartree–Fock method e.g in [HKO95], where the antisymmetrized form of the Brueckner G–matrix is plugged into the Hartree–Fock method instead of the NN interaction $\bar{V}$. The G–matrix describes nucleon scattering in the medium and corresponds to the scattering matrix $\mathcal{T}$ which describes two–body scattering in free space and fulfills the Lippmann-Schwinger equation given in operator form

$$\mathcal{T} = V + V\frac{1}{E - H_0}\mathcal{T}, \tag{2.12}$$

where H_0 is the Hamiltonian for the non-interacting particles. Similarly the G-matrix satisfies the Bethe–Goldstone equation

$$G = V + V\frac{Q_F}{E - H_0}G, \tag{2.13}$$

where H_0 is now the single–particle Hamiltonian and Q_F a projection operator excluding all occupied states from the scattering process according to the Pauli principle. In this extended framework the Hartree–Fock method yields much better binding energies, but some deficiencies remain which are discussed later.

2.2 The Skyrme Interaction

The Skyrme interaction is a parametrization of an effective nuclear force and was originally proposed by Skyrme [Sk59]. Later on, Negele and Vautherin explored the connection between the ansatz for a Skyrme interaction and the Brueckner G–matrix [NV72, NV75]. In their work the density-matrix expansion of the G–matrix and the comparison with the Skyrme interaction gives reasonable parameters for the Skyrme force. The Skyrme interaction is of zero range and therefore it is easy to use in practical calculations. Moreover Vautherin and Brink were able to reproduce the binding energies and radii of almost all nuclei throughout the nuclear landscape with a reasonable choice of parameters [VB72]. In recent years, there are parametrizations available which are fitted not only to finite nuclei but also to an equation of state for neutron stars [CB$^+$97, CB$^+$98]. These parametrizations make the Skyrme interaction suitable for astrophysical applications.

The Skyrme interaction consists of a two–body and a three–body term

$$V = \sum_{\alpha<\beta} V^{(2)}(\alpha,\beta) + \sum_{\alpha<\beta<\gamma} V^{(3)}(\alpha,\beta,\gamma). \tag{2.14}$$

Chabanat et al. called the following widely used form of the Skyrme interaction the *standard* form [CB$^+$97, CB$^+$98]. First some quantities are introduced: the relative coordinate $\boldsymbol{r} = \boldsymbol{r}_1 - \boldsymbol{r}_2$, the center of mass coordinate of two particles $\boldsymbol{R} = \frac{1}{2}(\boldsymbol{r}_1 + \boldsymbol{r}_2)$, the relative momentum $\boldsymbol{p} = \frac{1}{2i}(\boldsymbol{\nabla}_1 - \boldsymbol{\nabla}_2)$ with its complex conjugate counterpart acting on the bra–state with momentum $\boldsymbol{p'}$, the two-body spin operator $\boldsymbol{\sigma} = \boldsymbol{\sigma}_1 + \boldsymbol{\sigma}_2$, and the spin exchange operator $P_\sigma = (1 + \boldsymbol{\sigma}_1 \cdot \boldsymbol{\sigma}_2)/2$. With the help of these quantities

we are able to express the two–body interaction as

$$\begin{aligned} V^{(2)}(\boldsymbol{r}_1,\boldsymbol{r}_2) = & t_0(1+x_0P_\sigma)\delta(\boldsymbol{r}) \\ & + \frac{1}{2}t_1(1+x_1P_\sigma)\left[\boldsymbol{p'}^2\delta(\boldsymbol{r})+\delta(\boldsymbol{r})\boldsymbol{p}^2\right] \\ & + t_2(1+x_2P_\sigma)\boldsymbol{p'}\cdot\delta(\boldsymbol{r})\boldsymbol{p} \\ & + iW_0\boldsymbol{\sigma}\cdot[\boldsymbol{p'}\times\delta(\boldsymbol{r})\boldsymbol{p}]\,, \end{aligned} \tag{2.15}$$

which contains a central term with the parameter t_0 and x_0, effective range terms depending on the parameters t_1, x_1, t_2, x_2, and the spin–orbit term with the spin–orbit strength parameter W_0. The three–body potential was originally given by

$$V^{(3)}(\boldsymbol{r}_1,\boldsymbol{r}_2,\boldsymbol{r}_3) = t_3\delta(\boldsymbol{r}_1-\boldsymbol{r}_2)\delta(\boldsymbol{r}_2-\boldsymbol{r}_3). \tag{2.16}$$

For spin saturated even–even nuclei the three–body term is equivalent to a density dependent two–body interaction [RS80]. This two–body interaction is often modified by introducing a density dependence in a power of α:

$$V^{(3')}(\boldsymbol{r}_1,\boldsymbol{r}_2) = \frac{1}{6}t_3(1+x_3P_\sigma)[\rho(\boldsymbol{R})]^\alpha\delta(\boldsymbol{r}) \tag{2.17}$$

For $\alpha = 1$ we get the original three–body interaction in equation (2.16). Besides the three–body force (2.16) both different and additional terms have been investigated [VB72]. However, it turned out that these modifications often provoke collapses in the equation of state of symmetric nuclear matter.

2.3 The Energy Functional

Skyrme interaction leads to a density functional theory (DFT) which is easy to use in practical applications. The idea of density functional theories is to derive an energy functional from the underlying interaction. This energy functional should only depend on various densities. The development of the density functional theory is outlined briefly.

The density functional theory was first developed for an electron gas. The first attempt has been made by Thomas and Fermi, as they expressed the kinetic energy in terms of the electron density assuming that the wave functions can be approximated locally by plane waves [Th27, Fe28]. In case of infinite nuclear matter we get first a correspondence of the Fermi momentum $p_{F,q}$ and the density ρ_q for nucleons with spin–degenerate states

$$\rho_q = 2\int\frac{d^3p}{(2\pi)^3}\,\eta_q(p), \tag{2.18}$$

where $q = p, n$ denotes the isospin quantum number and $\eta_q(p)$ is the appropriate occupation scheme. For zero temperature and without pairing the occupation factor η_q obeys the Hartree–Fock occupation

$$\eta_q(p) = \begin{cases} 1 & \text{for } p \leq p_{F,q}, \\ 0 & \text{for } p > p_{F,q}, \end{cases} \tag{2.19}$$

and hence equation (2.18) becomes

$$\rho_q = \frac{1}{3\pi^2} p_{F,q}^3. \tag{2.20}$$

Having fixed the Fermi momentum $p_{F,q}$ for a given density ρ_q by equation (2.18) the kinetic energy density τ_q is obtained by

$$\tau_q = 2 \int \frac{d^3p}{(2\pi)^3}\, p^2\, \eta_q(p). \tag{2.21}$$

In the Hartree–Fock occupation the kinetic energy density is easy to evaluate and we obtain the following formula

$$\tau_q = \frac{1}{5\pi^2} (3\pi^2 \rho_q)^{5/3}, \tag{2.22}$$

which shows the density dependence explicitly [RS80].

The next step was taken by Hohenberg and Kohn as they found that for slowly varying densities the variation of the energy functional leads to the correct ground state energy and ground state density [HK64]. This statement is referred to as the *Hohenberg–Kohn theorem*. Further they included electron correlations in the functional and stated that the functional is formally exact.

One year later Kohn and Sham made the step towards current density functional theory [KS65]. In addition to the previous approach they performed the variation of the density and obtained Hartree–Fock equations for the single–particle wave functions. The exchange and correlation parts of the interaction result in additional effective potential terms.

The density functional theory of Kohn and Sham is still applied to electron systems. In this context the theory is much easier to handle than for nuclear systems since the correlations are much weaker. The application of density functional theory for nuclear systems simplifies the calculations and so makes it possible to compute large systems. However, one should bear in mind that the theory has its limitations [SR07].

Nevertheless, the density functional theory provides a useful tool called the local density approximation (LDA). For example, the Thomas–Fermi approximation for nuclear matter constructs a functional based on the assumption that the energy density is the same in infinite nuclear matter and in finite systems. This is equivalent to the assumption that the wave functions can be approximated by plane waves. In section (2.2) the density–matrix expansion for the Brueckner G–matrix was discussed, wherein it was assumed that the G–matrix elements are the same for infinite nuclear matter and for finite nuclei. Even for relativistic calculations discussed in the next section this will be an important ingredient to get a reasonable effective field theory.

Now we come back to the Skyrme interaction and outline the derivation of the energy functional, what is quite straight forward for the Skyrme interaction. The total binding energy E of a nuclear system is calculated by

$$E = \langle \Phi | H | \Phi \rangle \tag{2.23}$$

with Φ a Slater determinant of the single–particle wave functions $\varphi^q_\alpha(\boldsymbol{r}, s)$. In the case of a Skyrme force the Hartree–Fock Hamiltonian is based on the Skyrme interaction from section (2.2) and the energy E becomes

$$E = \langle \Phi | T + V^{(2)} + V^{(3)} | \Phi \rangle \tag{2.24}$$

with T the kinetic energy operator, $V^{(2)}$ the two–body part, and $V^{(3)}$ the three–body part of the Skyrme interaction. Because the Skyrme force is of zero range the energy E can be evaluated by an integral over a Hamiltonian density $\mathcal{H}$

$$E[\Phi] = \int d^3r \; \mathcal{H}(\boldsymbol{r}), \tag{2.25}$$

what is outlined in [VB72]. The Hamiltonian density $\mathcal{H}$ depends on various densities which are the local matter density ρ, the kinetic energy density τ, and the spin–orbit density $\boldsymbol{J}$. They are defined in terms of the corresponding densities for protons and neutrons $\rho = \rho_p + \rho_n$, $\tau = \tau_p + \tau_n$, and $\boldsymbol{J} = \boldsymbol{J}_p + \boldsymbol{J}_n$. The local matter densities of neutrons and protons are given by

$$\rho_q(\boldsymbol{r}) = \sum_{\alpha, s} \; \eta^q_\alpha \, |\varphi^q_\alpha(\boldsymbol{r}, s)|^2, \tag{2.26}$$

where $\varphi^q_\alpha(\boldsymbol{r}, s)$ is the single–particle wave function with orbital, spin and isospin quantum numbers α, s, and q, respectively. The occupation factors η^q_α are determined by the Fermi energy $\varepsilon_{F,q}$ and the desired scheme of occupation described in

chapter 4. The kinetic energy and spin–orbit densities are defined by

$$\tau_q(\boldsymbol{r}) = \sum_{\alpha,s} \eta_\alpha^q \, |\boldsymbol{\nabla}\varphi_\alpha^q(\boldsymbol{r},s)|^2, \tag{2.27}$$

$$\boldsymbol{J}_q(\boldsymbol{r}) = -i \sum_{\alpha,s,s'} \eta_\alpha^q \, (\varphi_\alpha^q)^*(\boldsymbol{r},s') \; \boldsymbol{\nabla}\varphi_\alpha^q(\boldsymbol{r},s) \times \langle s'|\boldsymbol{\sigma}|s\rangle. \tag{2.28}$$

The gradient of the spin–orbit density $\boldsymbol{\nabla J} = \boldsymbol{\nabla J}_p + \boldsymbol{\nabla J}_n$ can be directly evaluated without first calculating $\boldsymbol{J}$:

$$\boldsymbol{\nabla J}_q(\boldsymbol{r}) = -i \sum_{\alpha,s,s'} \eta_\alpha^q \, \boldsymbol{\nabla}(\varphi_\alpha^q)^*(\boldsymbol{r},s') \; \times \boldsymbol{\nabla}\varphi_\alpha^q(\boldsymbol{r},s) \cdot \langle s'|\boldsymbol{\sigma}|s\rangle. \tag{2.29}$$

Then a lengthy but straightforward calculation according to Vautherin and Brink [VB72] gives the Hamiltonian density $\mathcal{H}$ which consists of the following parts [CB+98]:

$$\mathcal{H} = \mathcal{H}_K + \mathcal{H}_0 + \mathcal{H}_3 + \mathcal{H}_{\text{eff}} + \mathcal{H}_{\text{fin}} + \mathcal{H}_{\text{so}} + \mathcal{H}_{\text{sg}} + \mathcal{H}_{\text{Coul}}, \tag{2.30}$$

where $\mathcal{H}_K$ is the kinetic energy term, $\mathcal{H}_0$ a zero range term, $\mathcal{H}_3$ a density dependent term, $\mathcal{H}_{\text{eff}}$ an effective mass term, $\mathcal{H}_{\text{fin}}$ a finite range term, $\mathcal{H}_{\text{so}}$ a spin–orbit term, and $\mathcal{H}_{\text{sg}}$ a term due to the tensor coupling with spin and gradient. The time–odd part is omitted because it vanishes in time–independent problems of even–even systems [SR07]. Here are the explicit formulas for the parts of this functional:

$$\begin{aligned}
\mathcal{H}_K &= \frac{\hbar^2}{2m}\tau, \\
\mathcal{H}_0 &= \tfrac{1}{4}t_0\big[(2+x_0)\rho^2 - (2x_0+1)(\rho_p^2+\rho_n^2)\big], \\
\mathcal{H}_3 &= \tfrac{1}{24}t_3\rho^\alpha\big[(2+x_3)\rho^2 - (2x_3+1)(\rho_p^2+\rho_n^2)\big], \\
\mathcal{H}_{\text{eff}} &= \tfrac{1}{8}\big[t_1(2+x_1)+t_2(2+x_2)\big]\tau\rho \\
&\quad +\tfrac{1}{8}\big[t_2(2x_2+1)-t_1(2x_1+1)\big]\big[\tau_p\rho_p+\tau_n\rho_n\big], \\
\mathcal{H}_{\text{fin}} &= -\tfrac{1}{32}\big[3t_1(2+x_1)-t_2(2+x_2)\big]\rho\Delta\rho \\
&\quad +\tfrac{1}{32}\big[3t_1(2x_1+1)+t_2(2x_2+1)\big]\big[\rho_p\Delta\rho_p+\rho_n\Delta\rho_n\big], \\
\mathcal{H}_{\text{so}} &= -\tfrac{1}{2}W_0\big[\rho\,\boldsymbol{\nabla J}+\rho_p\,\boldsymbol{\nabla J}_p+\rho_n\,\boldsymbol{\nabla J}_n\big]. \\
\mathcal{H}_{\text{sg}} &= -\tfrac{1}{16}(t_1x_1+t_2x_2)\boldsymbol{J}^2+\tfrac{1}{16}(t_1-t_2)\big[\boldsymbol{J}_p^2+\boldsymbol{J}_n^2\big]
\end{aligned} \tag{2.31}$$

The coefficients t_i, x_i, W_0, and α are the parameters of the Skyrme interaction from section 2.2 and m the nucleon mass. The energy density of equation (2.30) contains furthermore the contribution of the Coulomb force, $\mathcal{H}_{\text{Coul}}$, which is calculated from the charge density ρ_C as

$$\mathcal{H}_{\text{Coul}}(\boldsymbol{r}) = \frac{e^2}{2}\rho_C(\boldsymbol{r}) \int d^3r' \, \frac{\rho_C(\boldsymbol{r'})}{|\boldsymbol{r}-\boldsymbol{r'}|} \; - \frac{3e^2}{4}\left(\frac{3}{\pi}\right)^{1/3} \rho_C^{4/3}. \tag{2.32}$$

Here the exchange part of the Coulomb term is calculated within the Slater approximation. Following Bonche et al. [BF+85] the charge density is replaced by the proton density ρ_p and whenever electrons are present the electron density ρ_e has to be subtracted

$$\rho_C(\boldsymbol{r}) = \rho_p(\boldsymbol{r}) - \rho_e(\boldsymbol{r}). \tag{2.33}$$

Further the center of mass recoil energy has been approximated as

$$E_{cm} = -\sum \frac{\boldsymbol{p}_\alpha^2}{2Am}. \tag{2.34}$$

In this work the spin–gradient term $\mathcal{H}_{\text{sg}}$ is left out. This term depends on the spin–orbit density $\boldsymbol{J}$ which is cumbersome to evaluate numerically in three dimensions and not very important.

For comparison asymmetric nuclear matter is considered by directly evaluating the energy functional (eq. 2.25), in which the kinetic energy density is obtained by equation (2.21) which is exact for infinite nuclear matter. The spin–orbit term in asymmetric nuclear matter does not contribute to the energy and the Coulomb interaction is neglected as usual in nuclear matter calculations. In fact the Coulomb energy vanishes in homogeneous (n, p, e) matter in a neutron star due to charge neutrality. The baryon energy density is then $\mathcal{E} = \mathcal{H}$ and the baryon energy per nucleon becomes $E/A = \mathcal{E}/\rho$. Further the chemical potential is obtained by

$$\mu_q = \frac{p_{F,q}^2}{2m_q^*} + U_q(p_{F,q}), \tag{2.35}$$

where m_q^* is the effective mass and U_q the single particle potential, which are both specified in the next section. It must be mentioned that the potential depends on the density and the kinetic energy density, which are both determined by the Fermi momentum.

2.4 Hartree-Fock Equations

In order to obtain the ground state of a nuclear system the energy E has to be minimized. Because nucleons are fermions and obey the Pauli principle a Slater determinant Φ composed of the single particle wave functions $\varphi_\alpha^q(\boldsymbol{r}, s)$ is an appropriate approximation and leads to Hartree–Fock equations. These conditions lead to the variational principle

$$\delta E[\Phi] = 0. \tag{2.36}$$

The variation of the energy functional E is carried out with the side condition that Φ is a Slater determinant. The single particle wave functions φ^q_α have to form an orthonormal basis due to the fact that they are eigenstates of a single–particle Hamiltonian. The normalization condition leads to Lagrange multipliers which are the single particle energies ε^q_α. Thus we end up with the following variation

$$\frac{\delta}{\delta\varphi^*_\alpha}\left\{E[\Phi]-\sum_{\alpha,s,q}\varepsilon^q_\alpha\left(\int d^3r\,|\varphi^q_\alpha(\boldsymbol{r},s)|^2-1\right)\right\}=0. \tag{2.37}$$

By inserting the energy functional (eq. 2.25) and integrating by parts the Hartree–Fock equations for the single particle energies are obtained [RS80]

$$\left\{-\boldsymbol{\nabla}\frac{\hbar^2}{2m^*_q(\boldsymbol{r})}\boldsymbol{\nabla}+U_q(\boldsymbol{r})-i\,\boldsymbol{W}_q(\boldsymbol{r})\cdot(\boldsymbol{\nabla}\times\boldsymbol{\sigma})\right\}\varphi^q_\alpha(\boldsymbol{r},s)=\varepsilon^q_\alpha\,\varphi^q_\alpha(\boldsymbol{r},s). \tag{2.38}$$

These equations contain an effective mass term $m^*(\boldsymbol{r})$, which depends on the $\mathcal{H}_{\text{eff}}$ part of the energy density functional

$$\begin{aligned}\frac{\hbar^2}{2m^*_q(\boldsymbol{r})}=&\frac{\hbar^2}{2m}+\tfrac{1}{8}[t_1(2+x_1)+t_2(2+x_2)]\,\rho(\boldsymbol{r})\\&+\tfrac{1}{8}[t_2(1+2x_2)-t_1(1+2x_1)]\,\rho_q(\boldsymbol{r}),\end{aligned} \tag{2.39}$$

a nuclear central Potential

$$\begin{aligned}U_q(\boldsymbol{r})=&\tfrac{1}{2}t_0\big[(2+x_0)\rho-(1+2x_0)\rho_q\big]\\&+\tfrac{1}{24}t_3(2+x_3)(2+\alpha)\rho^{\alpha+1}\\&-\tfrac{1}{24}t_3(2x_3+1)\big[2\rho^\alpha\rho_q+\alpha\rho^{\alpha-1}\big(\rho_p^2+\rho_n^2\big)\big]\\&+\tfrac{1}{8}\big[t_1(2+x_1)+t_2(2+x_2)\big]\,\tau\\&+\tfrac{1}{8}\big[t_2(2x_2+1)-t_1(2x_1+1)\big]\,\tau_q\\&+\tfrac{1}{16}\big[t_2(2+x_2)-3t_1(2+x_1)\big]\,\Delta\rho\\&+\tfrac{1}{16}\big[3t_1(2x_1+1)+t2(2x_2+1)\big]\,\Delta\rho_q\\&-\tfrac{1}{2}W_0\big[\boldsymbol{\nabla}\boldsymbol{J}+\boldsymbol{\nabla}\boldsymbol{J}_q\big]\\&+\delta_{q,p}\,V_{\text{Coul}}\end{aligned} \tag{2.40}$$

with the Coulomb field

$$V_{\text{Coul}}(\boldsymbol{r})=e^2\int d^3r'\,\frac{\rho_C(\boldsymbol{r}')}{|\boldsymbol{r}-\boldsymbol{r}'|}\;-e^2\left(\frac{3}{\pi}\right)^{1/3}\rho_C^{1/3}, \tag{2.41}$$

and a spin–orbit field:

$$\begin{aligned}\boldsymbol{W}_q(\boldsymbol{r}) = \tfrac{1}{2}\, W_0\, (\boldsymbol{\nabla}\rho + \boldsymbol{\nabla}\rho_q) \\ - \tfrac{1}{8}(t_1 x_1 + t_2 x_2)\boldsymbol{J} + \tfrac{1}{8}(t_1 - t_2)\boldsymbol{J}_q.\end{aligned} \tag{2.42}$$

The Hartree–Fock equations have to be solved self–consistently taking care that the wave functions remain orthonormal. For the triaxial approach we apply the *imaginary time step* method which is described in section 5.3.
The Hartree-Fock energy E_{HF} can be calculated by evaluating the energy functional for the Hartree–Fock basis. A different possibility is to calculate the Hartree–Fock energy using the single–particle energies ε_α. In this case we have to take into account the rearrangement energy E_r arising from the density dependence of the three–body potential and the Slater approximation for the Coulomb exchange part [VB72, LMK91]:

$$\begin{aligned}E_r = &- \int d^3r\, \tfrac{\alpha}{48} t_3 \rho^\alpha \left[(2+x_3)\rho^2 - (1+2x_3)(\rho_p^2 + \rho_n^2)\right] \\ &+ \frac{1}{4}\left(\frac{3}{\pi}\right)^{1/3} \int d^3r\, \rho_p^{4/3}.\end{aligned} \tag{2.43}$$

Altogether the Hartree–Fock ground state energy is obtained by

$$E_{HF} = \tfrac{1}{2}\Big(\sum_{\alpha\, q} t_\alpha^q + \varepsilon_\alpha^q\Big) + E_r. \tag{2.44}$$

Hence the final ground state energy in the Hartree–Fock approximation is computed by

$$E_0 = E_{HF} + E_{cm}. \tag{2.45}$$

Both methods for the energy calculation should give equal results. This provides a check of self-consistency.

Chapter 3

Relativistic Hartree–Fock

During the last years the description of nuclear properties in terms of effective interactions (like the Skyrme force) to be used in a Schrödinger equation has been challenged by the development of effective field theories which lead to a Dirac equation for the nucleons.
The relativistic treatment has some obvious advantages over the non–relativistic one. The first one is that the spin–orbit term which is essential in nuclear calculations is contained naturally (see eq. 3.113). Furthermore the strong interaction acting on the nucleons is described in terms of meson exchange, a theory which has also been applied to describe realistic NN–interaction. Finally, the saturation point of nuclear matter can be reproduced by the Dirac–Brueckner–Hartree–Fock approach, which is based on a realistic meson exchange interaction [BM90]. In non-relativistic calculations the saturation points are located on a so called "Coester line" and it is necessary to take three–body forces into account to get better results. But non-relativistic calculations do not reproduce the experimental saturation point even with three-body forces. Only the Dirac–Brueckner–Hartree–Fock approach with the Bonn potential did a good job so far as we see in figure 3.1.
In the relativistic Hartree–Fock approximation effective correlation effects are included by density dependent coupling. This gives a rather good description of binding energies and radii of finite nuclei. This density dependent coupling constants can be determined by a fit either to experimental data or to the self–energies of the Dirac–Brueckner–Hartree–Fock approach for assymetric nuclear matter. To be consistent with more involved theories for nuclear physics the second method is preferred. For the derivation of such density dependent coupling constants by a local density approximation the reader may consult the Ph.D. thesis of Fritz [Fr94] and

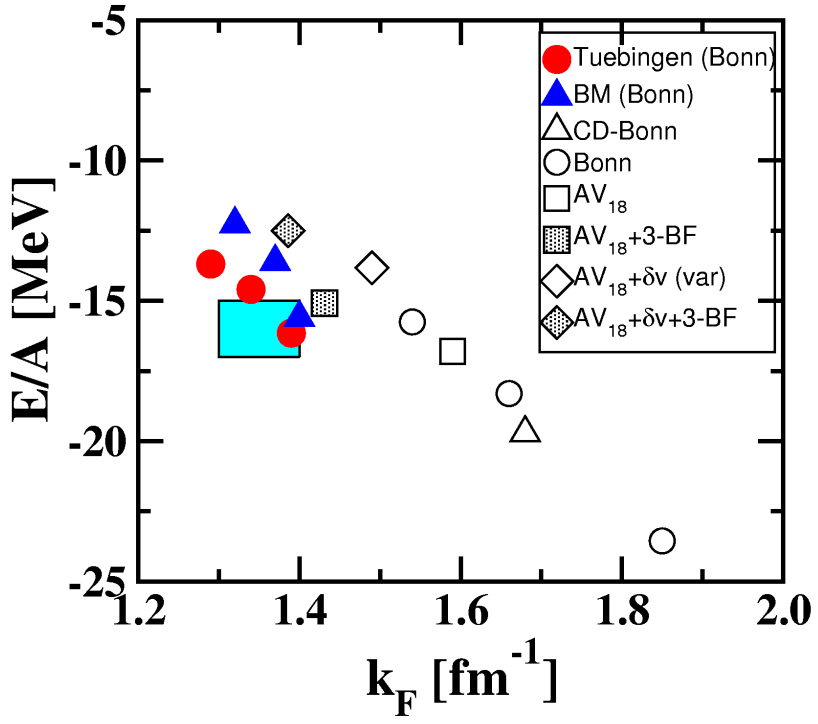

Figure 3.1: Saturation points for different NN–potentials and the Coester line. The red points are obtained from DBHF calculations.

Schiller [Sch00]. This section is an extension of a previous relativistic Hartree–Fock approach by Fritz and Müther [FM94].

3.1 The Lagrangian

The relativistic Hartree–Fock Approach is an effective Field theory. The strong force is modeled by meson exchange between the nucleons, where all species of particles are described by a quantum field. Due to simplicity the meson fields are approximated using classical fields. In order to have a covariant theory the approach starts from a Lagrangian density which is taken in the Hartree case from [HKL01] and in the Hartree–Fock case it is similar to [LGM06] and [BM$^+$87].

meson	J^P	I	m [MeV]
$\pi^{\pm,0}$	0^-	1	139.57 / 134.96
σ	0^+	0	550
δ	0^+	1	983
ω	1^-	0	782.6
ρ	1^-	1	769

Table 3.1: Properties of the mesons which model the strong interaction, which are spin J, parity P, isospin I and the experimental mass m. The mass of the σ–meson, which represents 2π–exchange processes, is not determined by an independent experiment, but adjusted to the NN–scattering data.

The different Lagrangian densities differ from each other in the mesons included and the various couplings to the nucleon field. The Lagrangian density presented here includes all mesons and couplings used in this work. In the actual application terms for unused mesons or couplings have to be omitted. The properties of the included mesons are summarized in Table 3.1, which are the scalar mesons σ and δ, the vector mesons ω and ρ, and the pion is included as pseudo–vector meson. The electromagnetic interaction is mediated by the photon γ. The Lagrangian density consists of three parts: the free baryon Lagrangian density $\mathcal{L}_B$, the free meson Lagrangian density $\mathcal{L}_M$ and the interaction Lagrangian density $\mathcal{L}_{\text{int}}$:

$$\mathcal{L} = \mathcal{L}_B + \mathcal{L}_M + \mathcal{L}_{\text{int}}, \tag{3.1}$$

which take on the explicit form

$$\begin{aligned}
\mathcal{L}_B &= \bar{\Psi}(\, i\gamma_\mu\partial^\mu - M)\Psi, \\
\mathcal{L}_M &= \tfrac{1}{2}\sum_{\iota=\sigma,\delta,\pi}\left(\partial_\mu\Phi_\iota\partial^\mu\Phi_\iota - m_\iota^2\Phi_\iota^2\right) \\
&\quad - \tfrac{1}{2}\sum_{\kappa=\omega,\rho,\gamma}\left(\tfrac{1}{2}F_{(\kappa)\mu\nu}\,F^{\mu\nu}_{(\kappa)} - m_\kappa^2 A_{(\kappa)\mu}A^\mu_{(\kappa)}\right), \\
\mathcal{L}_{\text{int}} &= -g_\sigma\bar{\Psi}\Phi_\sigma\Psi - g_\delta\bar{\Psi}\boldsymbol{\tau}\boldsymbol{\Phi}_\delta\Psi - \tfrac{f_\pi}{m_\pi}\bar{\Psi}\boldsymbol{\tau}\gamma_5\gamma_\mu[\partial^\mu\boldsymbol{\Phi}_\pi]\Psi \\
&\quad - g_\omega\bar{\Psi}\gamma_\mu A^\mu_{(\omega)}\Psi - g_\rho\bar{\Psi}\boldsymbol{\tau}\gamma_\mu\boldsymbol{A}^\mu_{(\rho)}\Psi + \tfrac{f_\rho}{2M}\bar{\Psi}\boldsymbol{\tau}\sigma_{\mu\nu}[\partial^\nu\boldsymbol{A}^\mu_{(\rho)}]\Psi \\
&\quad - e\bar{\Psi}\gamma_\mu\tfrac{1}{2}(1+\tau_3)A^\mu_{(\gamma)}\Psi,
\end{aligned} \tag{3.2}$$

with the field strength tensor $F_{(\kappa)\mu\nu} = \partial_\mu A_{(\kappa)\nu} - \partial_\nu A_{(\kappa)\mu}$ for the vector mesons. In the above Lagrangian density the nucleon field consisting of Dirac–spinors in isospin space is denoted by Ψ and the nucleon rest mass by M. The scalar meson fields are Φ_σ and $\boldsymbol{\Phi}_\delta$, the vector meson fields $A_{(\omega)}$ and $\boldsymbol{A}_{(\rho)}$, and the pseudo–vector pion field $\boldsymbol{\Phi}_\pi$. Bold symbols denote vectors in the isospin space acting between the two species of nucleons. The mesons have rest masses m_σ, m_ω, m_δ, m_ρ, and m_π and couple to the nucleons with the strength of the coupling constants g_σ, g_δ, g_ω , g_ρ, f_ρ, and f_π. The electromagnetic field $A_{(\gamma)}$ couples to the nucleons by the electron charge $e^2 = 4\pi\alpha$ where α is the fine structure constant. Notations are taken from [BD64]: $x = x^\mu$ and x_μ denote the contravariant and covariant vectors in space-time, γ^μ the Dirac γ matrices and $\boldsymbol{\tau}$ consists of the isospin Pauli matrices τ_k.

The density dependence of the baryon–meson vertices improves the capability of the model significantly since it enables the latter to assimilate the self–energies of a Dirac–Brueckner–Hartree–Fock calculation. This means that the coupling constants g_κ and f_κ, κ a meson, depend on a density $\rho(\bar{\Psi},\Psi)$ obtained from the nucleon field Ψ. In the literature we find a dependence on the scalar density or on the vector density. It turned out that the dependence on the zero component of the vector density, the baryon density $\rho = \mathrm{Tr}(\bar{\Psi}\gamma_0\Psi)$, is the most suitable one since it describes finite nuclei better and has a natural connection to the vertices in the DBHF calculations [HKL01].

The pion can be coupled either as pseudo–vector meson or as pseudo–scalar meson with the interaction term $-ig_\pi\bar{\Psi}\gamma_5\boldsymbol{\Phi}_\pi\Psi$. In the non–relativistic limit both variants lead to the same one–pion exchange potential for on-shell nucleons if the coupling constants satisfy $\frac{g_\pi}{2M} = \frac{f_\pi}{m_\pi}$. Because of the important contribution of the pion exchange in the Hartree–Fock approach one has to make a decision. From con-

siderations related to chiral symmetry and from an empirical point of view the pseudo–vector coupling is used. The tensor coupling for the ω–meson is related to the isoscalar anomalous magnetic moment of the nucleon which gives a quite small ratio of $f_\omega/g_\omega = -0.12$. Therefore no tensor coupling is incorporated for the ω–meson. In case of the tensor coupling for the ρ–meson the isovector anomalous magnetic moment of the nucleon gives a remarkable value of $f_\rho/g_\rho = 3.7$ or even larger if pion–nucleon scattering is considered [BM$^+$87].

3.2 Deriving the Dirac Hamiltonian

In quantum theories the energy of the system is obtained using the Hamiltonian formulation of the problem. Therefore we minimize the action for variations of the fields ϕ_κ included in the Lagrangian density (eq. 3.1)

$$\delta \int_{t_0}^{t_1} dt \int d^3x \, \mathcal{L}\big(\phi_\kappa(x), \partial_\mu \phi_\kappa(x), t\big) = 0 \tag{3.3}$$

where ϕ_κ stands for the nucleon field, the meson fields and the electromagnetic field. Finally the Euler–Lagrange field equations are obtained for each field ϕ_κ

$$\frac{\partial}{\partial x^\mu} \frac{\partial \mathcal{L}}{\partial(\partial_\mu \phi_\kappa)} - \frac{\partial \mathcal{L}}{\partial \phi_\kappa} = 0. \tag{3.4}$$

The variation for the fields or the adjoint fields lead to the same physical equations which are a Dirac equation for the nucleons and Klein–Gordan or Proca equations for the mesons and the electromagnetic field. The coupling constants are regarded as constant in the following derivation and afterwards the so called rearrangement terms are derived, which occur if density dependent coupling is considered.
First of all we obtain the Dirac equation for the nucleon field

$$(i\gamma_\mu \partial^\mu - M - \Sigma)\, \Psi = 0 \tag{3.5}$$

with the self–energy Σ generated by the interaction terms

$$\begin{aligned} \Sigma = \Big(& g_\sigma \Phi_\sigma + g_\delta \boldsymbol{\tau} \boldsymbol{\Phi}_\delta + \tfrac{f_\pi}{m_\pi} \boldsymbol{\tau} \gamma_5 \gamma_\mu [\partial^\mu \boldsymbol{\Phi}_\pi] + g_\omega \gamma_\mu A^\mu_{(\omega)} \\ & + g_\rho \boldsymbol{\tau} \gamma_\mu \boldsymbol{A}^\mu_{(\rho)} - \tfrac{f_\rho}{2M} \boldsymbol{\tau} \sigma_{\mu\nu} [\partial^\nu \boldsymbol{A}^\mu_{(\rho)}] + e\gamma_\mu \tfrac{1}{2}(1+\tau_3) A^\mu_{(\gamma)} \Big). \end{aligned} \tag{3.6}$$

Secondly the inhomogeneous Klein–Gordan equations are listed for the scalar mesons

σ and δ and the pseudo–vector pion meson

$$\begin{aligned}(\Box + m_\sigma^2)\Phi_\sigma &= -g_\sigma \bar{\Psi}\Psi \\ (\Box + m_\delta^2)\boldsymbol{\Phi}_\delta &= -g_\delta \bar{\Psi}\boldsymbol{\tau}\Psi \\ (\Box + m_\pi^2)\boldsymbol{\Phi}_\pi &= \partial^\mu \tfrac{f_\pi}{m_\pi}\bar{\Psi}\boldsymbol{\tau}\gamma_5\gamma_\mu\Psi. \end{aligned} \tag{3.7}$$

In case of the pion the derivative ∂^μ has been moved to the source terms of the field using integration by parts. Finally for any vector meson a Proca equation is obtained. Let's take the ω–meson as an example how to treat these kind of equations

$$\partial^\nu F_{(\omega)\mu\nu} - m_\omega^2 A_{(\omega)\mu} + \bar{\Psi} g_\omega \gamma_\mu \Psi = 0. \tag{3.8}$$

If the Proca equation is differentiated again by ∂^μ the antisymmetric Tensor vanishes

$$\partial^\mu \partial^\nu F_{(\omega)\mu\nu} = 0 \tag{3.9}$$

and the same is true for the nucleon current due to the continuity equation for the nucleons obtained from the Dirac equation (3.5)

$$\partial^\mu (\bar{\Psi}\gamma_\mu \Psi) = 0. \tag{3.10}$$

Hence differentiating the Proca equation leads to

$$\partial^\nu F_{(\omega)\mu\nu} = -\Box A_{(\omega)\mu} \tag{3.11}$$

what we can insert again in equation (3.8) and end up with Klein–Gordan equations also for the vector mesons

$$\begin{aligned}(\Box + m_\omega^2)A_{(\omega)\mu} &= g_\omega \bar{\Psi}\gamma_\mu\Psi \\ (\Box + m_\rho^2)\boldsymbol{A}_{(\rho)\mu} &= g_\rho \bar{\Psi}\boldsymbol{\tau}\gamma_\mu\Psi + \partial^\nu \tfrac{f_\rho}{2M}\bar{\Psi}\boldsymbol{\tau}\sigma_{\mu\nu}\Psi \\ \Box A_{(\gamma)\mu} &= e\bar{\Psi}\tfrac{1}{2}(1+\tau_3)\gamma_\mu\Psi \end{aligned} \tag{3.12}$$

In these equations the sign got positive compared to the scalar mesons. This is the reason why meson exchange contributions originating from vector mesons are repulsive while the contributions due to scalar mesons are attractive.

Our aim is now to express the self–energy Σ in the Dirac equation for the nucleons in terms of the nucleon field only. For this purpose the meson fields have to be integrated using the retarded Green function with forward propagation. This Green function satisfies

$$(\Box_x + m_\kappa^2)\, D_\kappa^R(x-y) = \delta^4(x-y) = \frac{1}{(2\pi)^4}\int e^{ik(x-y)} d^4k, \tag{3.13}$$

where κ is any meson. From now on derivatives and some operators will carry an index to assign the coordinate on which they are acting. This Green function can be evaluated by a Fourier transform into momentum space and we obtain [Br78]

$$D^R_\kappa(x^0-y^0,\boldsymbol{x}-\boldsymbol{y}) = \lim_{\varepsilon\to 0}\frac{1}{(2\pi)^4}\int \frac{e^{i[k^0(x^0-y^0)-\boldsymbol{k}(\boldsymbol{x}-\boldsymbol{y})]}}{m^2_\kappa - k^2 + i\varepsilon}dk^0 d^3k. \tag{3.14}$$

The shift of the singularity in the denominator towards the upper k^0-plane leads to a Green function for time–forward propagation by the Cauchy integral theorem for complex functions [BD64, BD65]. This integral can be evaluated analytically introducing $z = x - y$

$$D^R_\kappa(z) = \frac{1}{2\pi}\theta(z)\delta(z_\mu z^\mu) - \frac{m_\kappa}{4\pi}\theta(z)\frac{\theta(z_\mu z^\mu)}{\sqrt{z_\mu z^\mu}}J_1(m\sqrt{z_\mu z^\mu}) \tag{3.15}$$

where $\theta(z)$ is the unit step function sensitive to the time component

$$\theta(z) = \begin{cases} 0 & \text{if } z_0 < 0, \\ 1 & \text{if } z_0 \geq 0 \end{cases} \tag{3.16}$$

and J_1 denotes the Bessel function of integer order [Br78].
Now we can reshape the meson field equations into integral equations depending only on the nucleon fields

$$\begin{aligned}
\Phi_\sigma(x) &= -\int d^4y\, D^R_\sigma(x-y)\, g_\sigma(y)\bar\Psi(y)\Psi(y) \\
\boldsymbol{\Phi}_\delta(x) &= -\int d^4y\, D^R_\delta(x-y)\, g_\delta(y)\bar\Psi(y)\boldsymbol{\tau}\Psi(y) \\
\boldsymbol{\Phi}_\pi(x) &= \int d^4y\, D^R_\pi(x-y)\, [\partial^\mu \tfrac{f_\pi(y)}{m_\pi}\bar\Psi(y)\boldsymbol{\tau}\gamma_5\gamma_\mu\Psi(y)] \\
A_{(\omega)\mu}(x) &= \int d^4y\, D^R_\omega(x-y)\, g_\omega(y)\bar\Psi(y)\gamma_\mu\Psi(y) \\
\boldsymbol{A}_{(\rho)\mu}(x) &= \int d^4y\, D^R_\rho(x-y)\, \Big(g_\rho(y)\bar\Psi(y)\boldsymbol{\tau}\gamma_\mu\Psi(y) \\
&\qquad\qquad +[\partial^\nu \tfrac{f_\rho(y)}{2M}\bar\Psi(y)\boldsymbol{\tau}\sigma_{\mu\nu}\Psi(y)]\Big) \\
A_{(\gamma)\mu}(x) &= e\int d^4y\, D^R_\gamma(x-y)\, \bar\Psi\tfrac{1}{2}(1+\tau_3)\gamma_\mu\Psi.
\end{aligned} \tag{3.17}$$

Inserting these equations into the self–energy for the nucleons (3.6) the Dirac equation (3.5) turns to a non–linear equation for the nucleon field.
So far we neglected the density dependent coupling "constants". The functions for the various couplings are specified later together with the associated parameter set.

As a matter of fact we have to vary the Lagrangian density by

$$\frac{\delta\mathcal{L}}{\delta\bar{\Psi}} = \frac{\partial\mathcal{L}}{\partial\bar{\Psi}} + \frac{\partial\mathcal{L}}{\partial\rho}\frac{\delta\rho}{\delta\bar{\Psi}} \tag{3.18}$$

where the second expression generates the so called rearrangement contribution $\Sigma^{(r)}$ to the self–energies of the nucleon field. Actually a contribution to the zero component of the vector self–energy is created from the interaction Lagrangian density (3.1) and has to be added to the Dirac equation (3.5)

$$\left(i\gamma_\mu\partial^\mu - M - \Sigma\right)\Psi = 0 \longrightarrow \left(i\gamma_\mu\partial^\mu - M - (\Sigma + \Sigma^{(r)}\gamma_0)\right)\Psi = 0 \tag{3.19}$$

where the rearrangement self–energy contribution $\Sigma^{(r)}$ reads

$$\begin{aligned}\Sigma^{(r)} = \Big(&\frac{\partial g_\sigma}{\partial\rho}\bar{\Psi}\Phi_\sigma\Psi + \frac{\partial g_\delta}{\partial\rho}\bar{\Psi}\boldsymbol{\tau}\boldsymbol{\Phi}_\delta\Psi + \frac{1}{m_\pi}\frac{f_\pi}{\partial\rho}\bar{\Psi}\boldsymbol{\tau}\gamma_5\gamma_\mu[\partial^\mu\boldsymbol{\Phi}_\pi]\Psi \\ &+ \frac{\partial g_\omega}{\partial\rho}\bar{\Psi}\gamma_\mu A^\mu_{(\omega)}\Psi + \frac{\partial g_\rho}{\partial\rho}\bar{\Psi}\boldsymbol{\tau}\gamma_\mu\boldsymbol{A}^\mu_{(\rho)}\Psi - \frac{1}{2M}\frac{f_\rho}{\partial\rho}\bar{\Psi}\boldsymbol{\tau}\sigma_{\mu\nu}[\partial^\nu\boldsymbol{A}^\mu_{(\rho)}]\Psi\Big).\end{aligned} \tag{3.20}$$

Physically the rearrangement self–energy contribution accounts for static polarization effects in the nuclear medium [FLW95].
In order to derive the Hamiltonian from the Lagrangian density, the general Legendre transformation is performed and leads to the Hamiltonian density

$$\mathcal{H}(t) = \sum_{\kappa=N,\sigma,\delta,\omega,\pi,\rho} \Pi_\kappa(x)\,\partial^0\phi_\kappa(x) - \mathcal{L}\big(\phi_\kappa(x), \partial_\mu\phi_\kappa(x), t\big) \tag{3.21}$$

with the conjugate momentum of the nucleon and meson fields ϕ_κ

$$\Pi_\kappa = \frac{\partial\mathcal{L}}{\partial(\partial^0\phi_\kappa)}. \tag{3.22}$$

The Hamiltonian is obtained from the Hamiltonian density by integration

$$H = \int_{t=0} d^3x\,\mathcal{H}(t). \tag{3.23}$$

The result for the Hamiltonian density contains energy–momentum terms for the meson fields, e.g. for the σ–meson

$$\mathcal{H}(t) = \ldots + \frac{1}{2}\big(\Pi_\sigma^2 + (\nabla\Phi_\sigma)^2 + \frac{1}{2}m_\sigma^2\Phi_\sigma^2\big) + \ldots\ . \tag{3.24}$$

These expressions should be replaced in terms of the nucleon field again. Therefore we apply Gauss's divergence theorem on the spatial components

$$\int d^3x\,\nabla\big(\Phi_\sigma\,\nabla\Phi_\sigma\big) = \int d^3x\big((\nabla\Phi_\sigma)^2 + \Phi_\sigma\,\Delta\Phi_\sigma\big) = \int_S dS\,(\Phi_\sigma\nabla\Phi_\sigma) \tag{3.25}$$

where the integral over the surface S vanishes because fields shall be L^2 integrable in a Hilbert space. Further the conjugate momentum is connected to the energy of the meson field applying the energy operator $i\partial_t\Phi_\sigma$ and the Schroedinger formulation of the Klein–Gordan equation [Grn87]

$$\Pi_\sigma^2 = \Phi_\sigma \partial_t^2 \Phi_\sigma. \tag{3.26}$$

Altogether the expression (3.24) can be rewritten to the Greens function of the σ–meson and replaced by the corresponding interaction term using equation (3.7)

$$\tfrac{1}{2}\Phi_\sigma(\Box + m_\sigma^2)\Phi_\sigma = -\tfrac{1}{2} g_\sigma \bar{\Psi}\Phi_\sigma\Psi. \tag{3.27}$$

Similar equations are obtained for all the other mesons. Finally the meson fields only remain in the source terms and we get a factor of one half for the self–energy of the nucleons as expected. Replacing the meson fields by the integral equations (3.17) the general exact form of the Hamiltonian becomes

$$\begin{aligned} H = &\int_{t=0} d^3x\, \bar{\Psi}(-i\boldsymbol{\gamma}\cdot\boldsymbol{\nabla} + M)\Psi \\ &+ \frac{1}{2}\sum_{\kappa=\sigma,\delta,\pi,\omega,\rho,\gamma} \int_{t=0} d^3x\, d^4y\, \bar{\Psi}(x)\bar{\Psi}(y)\big[\Gamma_\kappa(x,y) D_\kappa^R(x-y)\big]\Psi(y)\Psi(x), \end{aligned} \tag{3.28}$$

where the interaction vertices $\Gamma_\kappa(x,y)$ are

$$\begin{aligned} \Gamma_\sigma(x,y) &= -g_\sigma(x) g_\sigma(y) \\ \Gamma_\omega(x,y) &= g_\omega(x)\gamma_\mu(x) g_\omega(y)\gamma^\mu(y) \\ \Gamma_\delta(x,y) &= -g_\delta(x)\boldsymbol{\tau}(x)\cdot g_\delta(y)\boldsymbol{\tau}(y) \\ \Gamma_\pi^{pv}(x,y) &= -\big[\tfrac{f_\pi}{m_\pi}\boldsymbol{\tau}\gamma_5\gamma_\mu\partial^\mu\big]_x \cdot \big[\tfrac{f_\pi}{m_\pi}\boldsymbol{\tau}\gamma_5\gamma_\nu\partial^\nu\big]_y \\ \Gamma_\rho^V(x,y) &= g_\rho(x)\boldsymbol{\tau}(x)\gamma_\mu(x)\cdot g_\rho(y)\boldsymbol{\tau}(y)\gamma^\mu(y) \\ \Gamma_\rho^T(x,y) &= \big[\tfrac{f_\rho}{2M}\boldsymbol{\tau}\sigma_{\mu\nu}\partial^\nu\big]_x \cdot \big[\tfrac{f_\rho}{2M}\boldsymbol{\tau}\sigma^{\mu\lambda}\partial_\lambda\big]_y \\ \Gamma_\rho^{VT}(x,y) &= \big[\tfrac{f_\rho}{2M}\boldsymbol{\tau}\sigma_{\mu\nu}\partial^\nu\big]_x \cdot \big[g_\rho\boldsymbol{\tau}\gamma^\mu\big]_y - \big[g_\rho\boldsymbol{\tau}\gamma_\mu\big]_x \cdot \big[\tfrac{f_\rho}{2M}\boldsymbol{\tau}\sigma^{\mu\nu}\partial_\nu\big]_y \\ \Gamma_\gamma(x,y) &= +\tfrac{e^2}{4}[\gamma_\mu(1+\tau_3)]_x\,[\gamma^\mu(1+\tau_3)]_y. \end{aligned} \tag{3.29}$$

Non–relativistic reductions of the pion and rho vertex functions lead to the NN potential which can be decomposed into a tensor and a central part [BM$^+$87]. For the pion the tensor part gives no contribution in the HF approximation applied to spin–saturated systems. The Fourier transform of the central part shows a repulsive contact interaction in addition to the attractive Yukawa potential. This contact

interaction is suppressed in many–body systems. It is argued that short–range correlations induced by strong repulsive components in the NN–interaction make this contact interaction "invisible". Consequently this δ–interaction is removed by adding

$$\delta\big[\Gamma_\pi^{pv}(x,y)D_\pi(x,y)\big] = \tfrac{1}{3}\big[\tfrac{f_\pi}{m_\pi}\boldsymbol{\tau}\gamma_5\boldsymbol{\gamma}\big]_x \cdot \big[\tfrac{f_\pi}{m_\pi}\boldsymbol{\tau}\gamma_5\boldsymbol{\gamma}\big]_y \delta(x-y) \tag{3.30}$$

to the pion exchange. For the ρ tensor potential the contact interaction is removed by adding

$$\delta\big[\Gamma_\rho^{T}(x,y)D_\rho(x,y)\big] = \tfrac{1}{3}\big[\tfrac{f_\rho}{2M}\boldsymbol{\tau}\sigma^{\mu k}\big]_x \big[\tfrac{f_\rho}{2M}\boldsymbol{\tau}\sigma_{\mu k}\big]_y \delta(x-y) \tag{3.31}$$

to the ρ tensor terms in the Dirac Hamiltonian.
The Hamilton operator H contains still the whole kinetic energy which is due to the center of mass motion and the relative motion among the nucleons

$$H = H_{cm} + H_{rel}. \tag{3.32}$$

Now we pay attention to the Hamiltonian for relative motion Hamiltonian H_{rel} being independent of Lorentz transformations. In section (3.3.4) the removal of center of mass contributions from the Hamiltonian will be discussed.
Unfortunately the Dirac equation $E\Psi = H\Psi$ cannot be solved exactly and has to be solved in an adequate approximation viz the Hartree–Fock approximation. There are two possibilities to obtain the Hartree–Fock equations from the exact Hamiltonian: to use the Dyson equation for the baryon propagator [HSe83] or to approximate the field operators for the nucleons to the Hartree–Fock level together with a self–consistent determination of the self–energy Σ. The approximate nucleon field Ψ_0 then satisfies the Dirac equation

$$(-i\gamma^\mu\partial_\mu + M + \Sigma + \Sigma^{(r)}\gamma_0)\Psi_0(x) = 0 \tag{3.33}$$

in coordinate representation and causes an effective Hamiltonian H_0. Minimizing the Energy $E_0 = \langle\Psi_0|H_0|\Psi_0\rangle$ with self–consistent self–energy Σ the equations for Σ equal the ones derived by the Dyson equation method [BM$^+$87]. The next step is to expand Ψ_0 on the set of stationary eigenstates of equation (3.33) and we obtain the following equations

$$\begin{aligned}
\Psi_0(x) &= \sum_\alpha \big[\psi_\alpha(\boldsymbol{x})\, e^{-iE_\alpha t}\, c_\alpha + \tilde{\psi}_\alpha(\boldsymbol{x})\, e^{iE'_\alpha t}\, d_\alpha^\dagger\big], \\
\Psi_0^\dagger(x) &= \sum_\alpha \big[\psi_\alpha^\dagger(\boldsymbol{x})\, e^{iE_\alpha t}\, c_\alpha^\dagger + \tilde{\psi}_\alpha^\dagger(\boldsymbol{x})\, e^{-iE'_\alpha t}\, d_\alpha\big]
\end{aligned} \tag{3.34}$$

with c_α, $c_\alpha^\dagger$, d_α, $d_\alpha^\dagger$ the creation and annihilation operators of a nucleon in a state α and $\psi_\alpha(\boldsymbol{x})$, $\tilde{\psi}_\alpha(\boldsymbol{x})$ the spatial coordinate representation of the positive and negative energy states. Since the interaction with anti–nucleons in the so called "Dirac-sea" is considered to be negligible, the "no-sea" approximation is imposed on the problem and the d_α, $d_\alpha^\dagger$ terms vanish.

This approximation coincides with the Dirac–Brueckner–Hartree–Fock calculations of van Dalen et al. for asymmetric nuclear matter [vD+07], which employ a realistic NN interaction of the Bonn type [Ml89]. From these calculations one can extract a local density approximation (LDA) of self–energies and gain a parametrization for the relativistic Hartree or Hartree–Fock calculation [FM94]. By means of the expansion (3.34) of the nucleon field we obtain the approximation of the Hamiltonian

$$\begin{aligned} H_0 = &\sum_{\alpha,\beta} c_\alpha^\dagger c_\beta \int_{x^0=0} d^3x\, \bar{\psi}_\alpha(\boldsymbol{x})(-i\boldsymbol{\gamma}\cdot\boldsymbol{\nabla} + M)\psi_\beta(\boldsymbol{x}) e^{i(E_\alpha - E_\beta)x^0} \\ &+ \frac{1}{2} \sum_{\kappa=\sigma,\delta,\pi,\omega,\rho,\gamma} \sum_{\alpha,\beta;\gamma,\delta} c_\alpha^\dagger c_\beta^\dagger c_\gamma c_\delta \int_{x^0=0} d^3x\, d^4y \\ &\bar{\psi}_\alpha(\boldsymbol{x})\bar{\psi}_\beta(\boldsymbol{y}) \left[\Gamma_\kappa(x,y) D_\kappa^R(x-y)\right] \psi_\gamma(\boldsymbol{y})\psi_\delta(\boldsymbol{x}) e^{i(E_\alpha - E_\delta)x^0} e^{i(E_\beta - E_\gamma)y^0}. \end{aligned} \tag{3.35}$$

The dependence on x_0 vanishes due to stationary evaluation, whereas the integration for y_0 can be performed together with the Green function $D_\kappa^R(x-y)$ applying extensive mathematical tables [GR65, Br78]. The result are meson propagators in Yukawa form

$$\int_{\mathbb{R},x_0=0} dy^0\, D_\kappa^R(x-y)\, e^{i(\epsilon_\beta - \epsilon_\gamma)y^0} = \frac{\exp(-\sqrt{m_\kappa^2 - (\epsilon_\beta - \epsilon_\gamma)^2}\,|\boldsymbol{x}-\boldsymbol{y}|)}{4\pi\,|\boldsymbol{x}-\boldsymbol{y}|}. \tag{3.36}$$

For vertices with momentum exchange the corresponding derivatives in coordinate space operate on the Green function as indicated by the brackets in the Dirac Hamiltonian (3.35). In this case the time component disappears and for the spatial components we get the same result with derivatives acting on it. For the electromagnetic field the mass of the exchanged photon is zero. Hence the meson propagator for three-dimensional integration in y reads

$$D_\kappa^R(\boldsymbol{x},\boldsymbol{y}) = \frac{\exp\left(-\sqrt{m_\kappa^2 - (\epsilon_\beta - \epsilon_\gamma)^2}\,|\boldsymbol{x}-\boldsymbol{y}|\right)}{4\pi\ |\boldsymbol{x}-\boldsymbol{y}|} \tag{3.37}$$

and the Hartree–Fock Hamiltonian H_0 becomes

$$\begin{aligned} H_0 = & \sum_{\alpha,\beta} c_\alpha^\dagger c_\beta \int d^3x\, \bar{\psi}_\alpha(\boldsymbol{x})(-i\boldsymbol{\gamma}\cdot\boldsymbol{\nabla} + M)\psi_\beta(\boldsymbol{x}) \\ & + \frac{1}{2} \sum_{\kappa=\sigma,\delta,\pi,\omega,\rho,\gamma} \sum_{\alpha,\beta;\gamma,\delta} c_\alpha^\dagger c_\beta^\dagger c_\gamma c_\delta \\ & \int d^3x\, d^3y\ \bar{\psi}_\alpha(\boldsymbol{x})\bar{\psi}_\beta(\boldsymbol{y}) \left[\Gamma_\kappa(x,y) D_\kappa^R(\boldsymbol{x},\boldsymbol{y})\right] \psi_\gamma(\boldsymbol{y})\psi_\delta(\boldsymbol{x}). \end{aligned} \tag{3.38}$$

An nuclear system containing A nucleons is considered as an A–body state, which is represented by a Slater determinant in the Hartree–Fock approximation.

$$|\Psi_0\rangle = \prod_{\alpha=1}^{A} c_\alpha^\dagger |0\rangle \tag{3.39}$$

Here A nucleons are created out of the vacuum with occupation probability zero or one. If pairing or thermal excitation is included in the approach, it is necessary to create more particles out of the vacuum considering the appropriate occupation scheme. Then the total Hartree–Fock binding energy is obtained by the expectation value

$$E_{HF} = \langle\Psi_0|H_0|\Psi_0\rangle - AM \tag{3.40}$$

where E_{HF} is minimized by the variational ansatz

$$\delta\Big[E_{HF} - \sum_\alpha \varepsilon_\alpha \int d^3x\, \psi_\alpha^\dagger(\boldsymbol{x})\psi_\alpha(\boldsymbol{x})\Big] = 0. \tag{3.41}$$

This variation employs the side condition that all nucleon states has to be orthogonal to each other, what is equivalent to the Pauli principle. The Lagrange multipliers act as single–particle energies which has to be determined decomposing the HF-Hamiltonian in kinetic energy, the local Hartree and the non–local Fock self–energies. In addition the rearrangement self–energy has to be considered

$$H^{HF} = T + \Sigma^H + \Sigma^F + \Sigma^{(r)}. \tag{3.42}$$

To simplify the the numerical task, retardation effects of the meson exchange are neglected, which are small compared to the meson masses. This is a good approximation for heavy meson exchange and also a fair one for the pion exchange. Subsequently the meson propagators appear in an energy independent form

$$D_\kappa(\boldsymbol{x},\boldsymbol{y}) = \frac{\exp(-m_\kappa|\boldsymbol{x}-\boldsymbol{y}|)}{4\pi\,|\boldsymbol{x}-\boldsymbol{y}|}. \tag{3.43}$$

We employ the widely used normalization for the single–particle wave functions ψ_α of the state $|\alpha\rangle$

$$\langle\alpha|\beta\rangle = \int d^3x\, \psi^\dagger_\alpha(\boldsymbol{x})\psi_\beta(\boldsymbol{x}) = \delta_{\alpha\beta}. \tag{3.44}$$

In this normalization the kinetic energy operator and the self–energy inherit a γ^0. Together with the occupation factors η_α for the state $|\alpha\rangle$ the self–energy components become

$$\begin{aligned}
T\psi_\alpha(\boldsymbol{x}) &= \gamma^0(-i\boldsymbol{\gamma}\boldsymbol{\nabla} + M)\psi_\alpha(\boldsymbol{x}) \\
\Sigma^H\psi_\alpha(\boldsymbol{x}) &= \gamma^0(\boldsymbol{x}) \sum_{\kappa=\sigma,\delta,\pi,\omega,\rho,\gamma} \\
&\quad \sum_\beta \eta_\beta \int d^3y\, \bar\psi_\beta(\boldsymbol{y})\left[\Gamma_\kappa(x,y)D_\kappa(\boldsymbol{x},\boldsymbol{y})\right]\psi_\beta(\boldsymbol{y})\,\psi_\alpha(\boldsymbol{x}) \\
\Sigma^F\psi_\alpha(\boldsymbol{x}) &= \gamma^0(\boldsymbol{x}) \sum_{\kappa=\sigma,\delta,\pi,\omega,\rho,\gamma} \\
&\quad \sum_\beta \eta_\beta \int d^3y\, \bar\psi_\beta(\boldsymbol{y})\left[\Gamma_\kappa(x,y)D_\kappa(\boldsymbol{x},\boldsymbol{y})\right]\psi_\alpha(\boldsymbol{y})\,\psi_\beta(\boldsymbol{x}) \\
\Sigma^{(r)}\psi_\alpha(\boldsymbol{x}) &= \sum_{\kappa=\sigma,\delta,\pi,\omega,\rho} \Big(\sum_{\gamma,\beta} \eta_\gamma\eta_\beta \int d^3y \\
&\quad \bar\psi_\gamma(\boldsymbol{x})\bar\psi_\beta(\boldsymbol{y})\Big[\frac{\partial\Gamma_\kappa}{\partial\rho_x}(x,y)D_\kappa(\boldsymbol{x},\boldsymbol{y})\Big]\psi_\beta(\boldsymbol{y})\,\psi_\gamma(\boldsymbol{x}) \\
&\quad \bar\psi_\gamma(\boldsymbol{x})\bar\psi_\beta(\boldsymbol{y})\Big[\frac{\partial\Gamma_\kappa}{\partial\rho_x}(x,y)D_\kappa(\boldsymbol{x},\boldsymbol{y})\Big]\psi_\gamma(\boldsymbol{y})\,\psi_\beta(\boldsymbol{x})\Big)\psi_\alpha(\boldsymbol{x}),
\end{aligned} \tag{3.45}$$

where the rearrangement self–energy contains contributions generated from the Hartree and the Fock self–energy terms. The various parts of the self–energy are treated in the sections (3.3) and (3.4).

The single–particle energy in Hartree–Fock approximation is calculated by

$$\varepsilon_\alpha = t_\alpha + v_\alpha + v^{(r)}_\alpha \tag{3.46}$$

with $t_\alpha = \langle\alpha|T|\alpha\rangle$, $v_\alpha = \langle\alpha|\Sigma^H + \Sigma^F|\alpha\rangle$ and $v^{(r)}_\alpha = \langle\alpha|\Sigma^{(r)}|\alpha\rangle$. The procedure how to obtain the single–particle energies from the self–consistent Dirac equation is addressed in section (3.3.5). Afterwards the Hartree–Fock binding energy E_{HF} can

be obtained in different ways

$$\begin{aligned} E_{HF} &= \sum_{\alpha} \eta_{\alpha}(t_{\alpha} + \tfrac{1}{2}v_{\alpha}) - AM \\ &= \frac{1}{2}\sum_{\alpha} \eta_{\alpha}(t_{\alpha} + \varepsilon_{\alpha} - v_{\alpha}^{(r)}) - AM \\ &= \sum_{\alpha} \eta_{\alpha}\varepsilon_{\alpha} - \sum_{\alpha} \eta_{\alpha}(v_{\alpha}^{(r)} + \tfrac{1}{2}v_{\alpha}) - AM. \end{aligned} \tag{3.47}$$

The rearrangement terms modify the single–particle energies but do not contribute to the total energy. Therefore they have to be subtracted if the single–particle energies are employed to obtain the Hartree–Fock energy.
Finally the total energy E combines the Hartree–Fock energy E_{HF} with the pairing energy E_{pair} and the center of mass correction E_{cm}

$$E = E_{HF} + E_{cm} + E_{pair}. \tag{3.48}$$

The center of mass correction is depicted in section 3.3.4 for different correction methods. For the pairing phenomenon without and with temperature dependence the reader is referred to chapter 4. Altogether we are able to describe nuclear physics in the relativistic Hartree–Fock approximation.

3.3 The Triaxial Approach

We choose the triaxial approach due to several reasons. First we want to explore the "Pasta" phases in the crust of neutron stars. A lot of calculations in spherical boxes have been done, e.g. [MMM04], which suffer from the restriction to spherical symmetry. The problems of this approach are apparent: the electrons and the neutron sea outside of the spherical box are neglected, and all spatial density distributions show fluctuations, what means that the density for plane waves in the box does not coincide with the homogeneous nuclear matter. These deficiencies can be cured by applying a triaxial approach which allows the coexistence of spherical and plane wave states.
The Dirac spinor ψ_{α} for the state $|\alpha\rangle$ in isospin space is decomposed into Pauli spinors φ_{α} for the upper component and χ_{α} for the lower component. Together with the isospinor $\chi_{\frac{1}{2}}(q_{\alpha})$ we denote the single–particle wave function in coordinate space

$$\langle \boldsymbol{x}|\alpha\rangle = \psi_{\alpha}(\boldsymbol{x}) = \begin{pmatrix} \varphi_{\alpha}(\boldsymbol{x}) \\ \chi_{\alpha}(\boldsymbol{x}) \end{pmatrix} \chi_{\frac{1}{2}}(q_{\alpha}). \tag{3.49}$$

This decomposition is convenient to evaluate the self–energies, but even essential for the solution of the Dirac equation. For consistence with the isospin matrix τ_3, the isospin quantum number q_α is chosen to be $+\frac{1}{2}$ for the protons and $-\frac{1}{2}$ for the neutrons.

In the following subsections, first the different components of the self–energy for the nucleons are evaluated, then the center of mass energy is discussed, and finally we pay attention to the numerical method to solve the Dirac equation.

3.3.1 Hartree Self–Energy

The Hartree contributions to the nucleon self–energy has to be evaluated from Σ^H in equation (3.45). It is striking that the sum over β can be interchanged with the integration over y. Hence the Hartree self-energy component for each meson κ takes on the form

$$\Sigma^H_\kappa \, \psi_\alpha(\boldsymbol{x}) = \gamma^0(\boldsymbol{x}) \int d^3y \sum_\beta \eta_\beta \, \bar{\psi}_\beta(\boldsymbol{y}) \big[\Gamma_\kappa(\boldsymbol{x},\boldsymbol{y}) D_\kappa(\boldsymbol{x},\boldsymbol{y})\big] \psi_\beta(\boldsymbol{y}) \, \psi_\alpha(\boldsymbol{x}). \tag{3.50}$$

In this manner a decomposition of the Hartree contribution to the self–energy into densities and meson fields is possible. The isopin factor for the isoscalar mesons σ and ω in the Hartree approximation of the Dirac Hamiltonian (3.38) gets

$$\langle \chi_{\frac{1}{2}}(q_\alpha) | \chi_{\frac{1}{2}}(q_\alpha) \rangle \cdot \langle \chi_{\frac{1}{2}}(q_\beta) | \chi_{\frac{1}{2}}(q_\beta) \rangle = 1 \tag{3.51}$$

and we obtain

$$\langle \chi_{\frac{1}{2}}(q_\alpha) | \boldsymbol{\tau}(\boldsymbol{x}) | \chi_{\frac{1}{2}}(q_\alpha) \rangle \cdot \langle \chi_{\frac{1}{2}}(q_\beta) | \boldsymbol{\tau}(\boldsymbol{y}) | \chi_{\frac{1}{2}}(q_\beta) \rangle = \begin{cases} 1 & \text{if } q_\alpha = q_\beta \\ -1 & \text{if } q_\alpha \neq q_\beta \end{cases} \tag{3.52}$$

for the isovector mesons δ and ρ. The pion exchange vanishes in the Hartree approximation due to parity conservation of the nucleon states. For the vector mesons there remain only the zero–components of the Hartree self–energy in even–even nuclear systems.

Now we turn to the densities with η_α the occupation numbers

$$\begin{aligned}
\rho^s(\boldsymbol{x}) &= \sum_\alpha \eta_\alpha\, \bar\psi_\alpha(\boldsymbol{x})\psi_\alpha(\boldsymbol{x}) \\
\rho_3^s(\boldsymbol{x}) &= \sum_\alpha \eta_\alpha\, \bar\psi_\alpha(\boldsymbol{x})\tau_3\psi_\alpha(\boldsymbol{x}) \\
\rho(\boldsymbol{x}) &= \sum_\alpha \eta_\alpha\, \bar\psi_\alpha(\boldsymbol{x})\gamma_0\psi_\alpha(\boldsymbol{x}) \\
\rho_3(\boldsymbol{x}) &= \sum_\alpha \eta_\alpha\, \bar\psi_\alpha(\boldsymbol{x})\gamma_0\tau_3\psi_\alpha(\boldsymbol{x}) \\
\boldsymbol{\rho}_3^t(\boldsymbol{x}) &= \sum_\alpha \eta_\alpha\, \bar\psi_\alpha(\boldsymbol{x})i\boldsymbol{\alpha}\tau_3\psi_\alpha(\boldsymbol{x}) \\
\rho^{(em)}(\boldsymbol{x}) &= \sum_\alpha \eta_\alpha\, \bar\psi_\alpha(\boldsymbol{x})\tfrac{1}{2}(1-\tau_3)\,\psi_\alpha(\boldsymbol{x}) \quad [-\rho_e(\boldsymbol{x})].
\end{aligned} \tag{3.53}$$

where ρ^s is the scalar density, ρ the baryon density, ρ_3^s the scalar isovector density, ρ_3 the vector isovector density, $\boldsymbol{\rho}_3^t$ the tensor isovector density and $\rho^{(em)}$ the charge density. The tensor isovector density is a spatial vector. This is due to the fact that the Hartree tensor self–energy contributes to momentum exchange as we will see soon. In case of electrons present in the nuclear environment, e.g. in the neutron star, it is necessary to subtract the electron density ρ_e from the charge density.
Applying these densities the field equations for the mesons can be solved. This can be either done by evaluating the integral equation or by solving the appropriate partial differential equation. The corresponding equations for the field ϕ_κ of a meson κ with source term ζ_κ are

$$\phi_\kappa(\boldsymbol{x}) = \int d^3y\, \zeta_\kappa(\boldsymbol{y}) D_\kappa(\boldsymbol{x},\boldsymbol{y}) \quad \Longleftrightarrow \quad (-\Delta + m_\kappa^2)\,\phi_\kappa(\boldsymbol{x}) = \zeta_\kappa(\boldsymbol{x}). \tag{3.54}$$

where the right hand side ζ_κ of the differential equation summarizes all dependencies on $\boldsymbol{y}$ of the integral equation. For numerical reasons we write down the meson field equations in the differential form. Neglecting the retardation effects the Klein-Gordan equations reduce to inhomogeneous Helmholtz equations with source terms

$$\begin{aligned}
(-\Delta + m_\sigma^2)\,\Phi_\sigma(\boldsymbol{x}) &= -g_\sigma(\boldsymbol{x})\,\rho^s(\boldsymbol{x}) \\
(-\Delta + m_\delta^2)\,\Phi_\delta(\boldsymbol{x}) &= -g_\delta(\boldsymbol{x})\,\rho_3^s(\boldsymbol{x}) \\
(-\Delta + m_\omega^2)\,A_0^{(\omega)}(\boldsymbol{x}) &= \quad g_\omega(\boldsymbol{x})\,\rho(\boldsymbol{x}) \\
(-\Delta + m_\rho^2)\,A_0^{(\rho)}(\boldsymbol{x}) &= \quad g_\rho(\boldsymbol{x})\,\rho_3(\boldsymbol{x}) + \boldsymbol{\nabla}\tfrac{f_\rho(\boldsymbol{x})}{2M}\boldsymbol{\rho}_3^t(\boldsymbol{x}) \\
-\Delta\, A_0^{(\gamma)}(\boldsymbol{x}) &= \quad e\,\rho^{(em)}(\boldsymbol{x}).
\end{aligned} \tag{3.55}$$

After working out the meson fields and the delta-tensor field

$$A_0^{(\delta\rho)}(\boldsymbol{x}) = -\tfrac{f_\rho(\boldsymbol{x})}{2M}\boldsymbol{\rho}_3^t(\boldsymbol{x}), \tag{3.56}$$

we can denote the Hartree self–energy contributions

$$\begin{aligned}
\Sigma_\sigma^H\psi_\alpha(\boldsymbol{x}) &= g_\sigma(\boldsymbol{x})\Phi_\sigma(\boldsymbol{x})\,\gamma^0\psi_\alpha(\boldsymbol{x}) \\
\Sigma_\delta^H\psi_\alpha(\boldsymbol{x}) &= g_\delta(\boldsymbol{x})\Phi_\delta(\boldsymbol{x})\,\tau_3\gamma^0\psi_\alpha(\boldsymbol{x}) \\
\Sigma_\omega^H\psi_\alpha(\boldsymbol{x}) &= g_\omega(\boldsymbol{x})A_0^{(\omega)}(\boldsymbol{x})\,\psi_\alpha(\boldsymbol{x}) \\
\Sigma_\rho^H\psi_\alpha(\boldsymbol{x}) &= g_\rho(\boldsymbol{x})A_0^{(\rho)}(\boldsymbol{x})\,\tau_3\psi_\alpha(\boldsymbol{x}) \\
&= +i\big[\tfrac{f_\rho(\boldsymbol{x})}{2M}\,(-\boldsymbol{\nabla}A_0^{(\rho)}(\boldsymbol{x}) + A_0^{(\delta\rho)}(\boldsymbol{x}))\big]\cdot\gamma^0\boldsymbol{\alpha}\tau_3\psi_\alpha(\boldsymbol{x}).
\end{aligned} \tag{3.57}$$

It is convenient to combine the different contributions to a scalar, time–like vector and space-like vector Hartree self–energy potential

$$\begin{aligned}
\Sigma_S^H(\boldsymbol{x}) &= g_\sigma(\boldsymbol{x})\Phi_\sigma(\boldsymbol{x}) + g_\delta(\boldsymbol{x})\Phi_\delta(\boldsymbol{x})\tau_3 \\
\Sigma_0^H(\boldsymbol{x}) &= g_\omega(\boldsymbol{x})A_0^{(\omega)}(\boldsymbol{x}) + g_\rho(\boldsymbol{x})A_0^{(\rho)}(\boldsymbol{x})\tau_3 + e\,\frac{1}{2}(1-\tau_3)A_0^{(\gamma)}(\boldsymbol{x}) \\
\boldsymbol{\Sigma}_T^H(\boldsymbol{x}) &= \tfrac{f_\rho(\boldsymbol{x})}{2M}\big(-\boldsymbol{\nabla}A_0^{(\rho)}(\boldsymbol{x}) + A_0^{(\delta\rho)}(\boldsymbol{x})\big)\tau_3.
\end{aligned} \tag{3.58}$$

Applying these definitions the single–particle Hartree self–energy can be evaluated by

$$v_\alpha^H = \langle\alpha|\Sigma^H|\alpha\rangle = \int d^3x\,\bar\psi_\alpha(\boldsymbol{x})\big(\Sigma_S^H(\boldsymbol{x}) + \gamma_0\Sigma_0^H(\boldsymbol{x}) + i\gamma_0\boldsymbol{\gamma}\cdot\boldsymbol{\Sigma}_T^H(\boldsymbol{x})\big)\psi_\alpha(\boldsymbol{x}). \tag{3.59}$$

And finally the total Hartree contribution of the self–energy for a nuclear system can be obtained replacing the sum over single–particle states by densities, which correspond to the meson fields:

$$\begin{aligned}
E_H &= \frac{1}{2}\sum_\alpha \eta_\alpha\, v_\alpha^H \\
&= \frac{1}{2}\int d^3x\,\Big[\, g_\sigma(\boldsymbol{x})\Phi_\sigma(\boldsymbol{x})\rho^s(\boldsymbol{x}) + g_\delta(\boldsymbol{x})\Phi_\delta(\boldsymbol{x})\rho_3^s(\boldsymbol{x}) + g_\omega(\boldsymbol{x})A_0^{(\omega)}(\boldsymbol{x})\rho(\boldsymbol{x}) \\
&\qquad + g_\rho(\boldsymbol{x})A_0^{(\rho)}(\boldsymbol{x})\rho_3(\boldsymbol{x}) + \tfrac{f_\rho(\boldsymbol{x})}{2M}[-\boldsymbol{\nabla}A_0^{(\rho)}(\boldsymbol{x}) + A_0^{(\delta\rho)}(\boldsymbol{x})]\boldsymbol{\rho}_3^t(\boldsymbol{x}) \\
&\qquad + e\,\frac{1}{2}(1-\tau_3)A_0^{(\gamma)}(\boldsymbol{x})\rho^{(em)}(\boldsymbol{x})\Big].
\end{aligned} \tag{3.60}$$

Altogether the Hartree self–energy contributions are transformed in a comfortable formalism ready to be implemented into the Dirac equation for the nucleons.

3.3.2 Fock Self–Energy

The general expression for the contributions of the various mesons κ to the Fock self–energy is obtained from Σ^F in equation (3.45)

$$\Sigma^F_\kappa\,\psi_\alpha(\boldsymbol{x}) = -\gamma^0(\boldsymbol{x})\sum_\beta \eta_\beta \int d^3y\;\bar{\psi}_\beta(\boldsymbol{y})\big[\Gamma_\kappa(\boldsymbol{x},\boldsymbol{y})D_\kappa(\boldsymbol{x},\boldsymbol{y})\big]\psi_\alpha(\boldsymbol{y})\,\psi_\beta(\boldsymbol{x}). \tag{3.61}$$

The isopin factor for the isoscalar mesons σ and ω in the Fock approximation of the Dirac Hamiltonian (3.38) becomes

$$\langle\chi_{\frac{1}{2}}(q_\alpha)|\chi_{\frac{1}{2}}(q_\beta)\rangle\cdot\langle\chi_{\frac{1}{2}}(q_\beta)|\chi_{\frac{1}{2}}(q_\alpha)\rangle = \delta_{q_\alpha q_\beta} \tag{3.62}$$

and for the isovector mesons δ, π and ρ we get

$$\langle\chi_{\frac{1}{2}}(q_\alpha)|\boldsymbol{\tau}(\boldsymbol{x})|\chi_{\frac{1}{2}}(q_\beta)\rangle\cdot\langle\chi_{\frac{1}{2}}(q_\beta)|\boldsymbol{\tau}(\boldsymbol{y})|\chi_{\frac{1}{2}}(q_\alpha)\rangle = 2-\delta_{q_\alpha q_\beta}. \tag{3.63}$$

The Fock terms are exchange integrals and therefore only the expression $(\Sigma^F_\kappa\,\psi_\alpha)(\boldsymbol{x})$ for a special single–particle wave function $\psi_\alpha(\boldsymbol{x})$ can be evaluated. The calculation in equation (3.61) has to be performed explicitly by a sum over the exchange integrals due to triaxial evaluation. However, these exchange integrals can be calculated in two different ways: as integration employing the Green function or by rewriting it to a differential equation similar to (3.54), as in the Hartree case. For numerical reasons we prefer this way although it is very unusual. In order to acquaint the reader to this method, it is outlined for the σ–meson. From equation (3.61) the exchange integral $I^\sigma_{\beta\alpha}(\boldsymbol{x})$ can be defined for the σ–meson

$$I^\sigma_{\beta\alpha}(\boldsymbol{x}) = -\int d^3y\, g_\sigma(\boldsymbol{y})\psi^\dagger_\beta(\boldsymbol{y})\gamma^0\psi_\alpha(\boldsymbol{y})\,\frac{\exp(-m_\sigma|\boldsymbol{x}-\boldsymbol{y}|)}{4\pi|\boldsymbol{x}-\boldsymbol{y}|} \tag{3.64}$$

and the σ–Fock term gets

$$(\Sigma^F_\sigma\psi_\alpha)(\boldsymbol{x}) = -g_\sigma(\boldsymbol{x})\sum_\beta \eta_\beta\,\delta_{q_\alpha q_\beta}\,I^\sigma_{\beta\alpha}(\boldsymbol{x})\,\gamma^0\psi_\beta(\boldsymbol{x}). \tag{3.65}$$

The above equations are just the usual method. Now we rewrite the exchange integral $I^\sigma_{\beta\alpha}(\boldsymbol{x})$ applying the correspondence of (3.54) to the partial differential equation

$$(-\Delta+m^2_\sigma)I^\sigma_{\beta\alpha}(\boldsymbol{x}) = -g_\sigma(\boldsymbol{x})\,\psi^\dagger_\beta(\boldsymbol{x})\gamma^0\psi_\alpha(\boldsymbol{x}), \tag{3.66}$$

where the source terms on the right hand side has to be exactly the expression in the integral depending on $\boldsymbol{y}$ besides the Green function which is accounted for by the differential operator.

The δ–meson is an isovector meson and hence we have to consider the isospin factor of $(2 - \delta_{q_\alpha q_\beta})$ according to (3.63). The exchange integral employs scalar coupling and is obtained by

$$(-\Delta + m_\delta^2) I^\delta_{\beta\alpha}(\boldsymbol{x}) = -g_\delta(\boldsymbol{x})\, \psi^\dagger_\beta(\boldsymbol{x}) \gamma^0 \psi_\alpha(\boldsymbol{x}) \tag{3.67}$$

and the δ Fock term gets

$$(\Sigma^F_\delta\, \psi_\alpha)(\boldsymbol{x}) = -g_\delta(\boldsymbol{x}) \sum_\beta \eta_\beta (2 - \delta_{q_\alpha q_\beta})\, I^\delta_{\beta\alpha}(\boldsymbol{x})\, \gamma^0 \psi_\beta(\boldsymbol{x}), \tag{3.68}$$

which is evaluated similar to the σ–meson besides the isospin factor. We get two different kinds of contributions: The terms with only protons or only neutrons get the factor 1 while the terms with different isospin are weighted twice as much. The δ–contribution gives an isospin dependence but it contributes also in case of equal proton and neutron densities, what has to be considered in a fit for parameters.
The π–meson is also an an isovector meson and considered with pseudo–vector coupling. Hence the exchange integral gets

$$(-\Delta + m_\pi^2) I^{(\pi)}_{\beta\alpha}(\boldsymbol{x}) = \partial_l \tfrac{f_\pi(\boldsymbol{x})}{m_\pi}\, \psi^\dagger_\beta(\boldsymbol{x})\, \gamma^0 \gamma_5 \gamma^l\, \psi_\alpha(\boldsymbol{x}), \tag{3.69}$$

and the π Fock term for pseudo–vector coupling reads

$$(\Sigma^F_\pi\, \psi_\alpha)(\boldsymbol{x}) = \frac{f_\pi(\boldsymbol{x})}{m_\pi} \sum_\beta \eta_\beta (2 - \delta_{q_\alpha q_\beta}) \left[\partial^k\, I^{(\pi)}_{\beta\alpha}(\boldsymbol{x})\right] \gamma^0 \gamma_5 \gamma_k\, \psi_\beta(\boldsymbol{x}), \tag{3.70}$$

where the zero vector component vanishes. Thus k and l run over the spatial indices only and $\gamma^0\gamma_5\gamma_k$ is the operator

$$\gamma^0 \gamma_5 \gamma_k = \begin{pmatrix} \sigma^k & 0 \\ 0 & \sigma^k \end{pmatrix} \tag{3.71}$$

with σ^k the Pauli spin matrices. The δ–term of the pion potential is evaluated together with the pseudo–vector Fock term. The exchange integral for the delta contribution collapses to a contact interaction due to the delta function in the vertex

$$\begin{aligned} I^{\delta(\pi)k}_{\beta\alpha}(\boldsymbol{x}) &= \frac{1}{3} \int d^3y\, \delta(\boldsymbol{x} - \boldsymbol{y})\, \frac{f_\pi(\boldsymbol{y})}{m_\pi} \psi^\dagger_\beta(\boldsymbol{y}) \left(\gamma^0\gamma_5\gamma^k\right)_y \psi_\alpha(\boldsymbol{y}) \\ &= \frac{1}{3}\, \frac{f_\pi(\boldsymbol{x})}{m_\pi} \psi^\dagger_\beta(\boldsymbol{x}) \gamma^0\gamma_5\gamma^k \psi_\alpha(\boldsymbol{x}). \end{aligned} \tag{3.72}$$

Finally we end up with the the same summation as for the usual pion contribution

$$(\Sigma^{F,\delta}_\pi \psi_\alpha)(\boldsymbol{x}) = \frac{f_\pi(\boldsymbol{x})}{m_\pi} \sum_\beta \eta_\beta (2 - \delta_{q_\alpha q_\beta})\, I^{\delta(\pi)k}_{\beta\alpha}(\boldsymbol{x})\, \gamma^0\gamma_5\gamma_k\, \psi_\beta(\boldsymbol{x}), \tag{3.73}$$

which simplifies the numerical calculation.
The Fock term for the ω–meson is guided by vector coupling. Hence we evaluate the exchange Integral by

$$(-\Delta + m_\omega^2) I_{\beta\alpha}^{(\omega)\mu}(\boldsymbol{x}) = g_\omega(\boldsymbol{x})\, \psi_\beta^\dagger(\boldsymbol{x}) \gamma^0 \gamma^\mu \psi_\alpha(\boldsymbol{x}). \tag{3.74}$$

From this expression we derive the ω–Fock term

$$(\Sigma_\omega^F\, \psi_\alpha)(\boldsymbol{x}) = -g_\omega(\boldsymbol{x}) \sum_\beta \eta_\beta \delta_{q_\alpha q_\beta}\, I_{\beta\alpha}^{(\omega)\mu}(\boldsymbol{x})\, \gamma^0 \gamma_\mu\, \psi_\beta(\boldsymbol{x}). \tag{3.75}$$

For $\mu = 0$ the expressions $\gamma^0\gamma^\mu$ and $\gamma^0\gamma_\mu$ are a unity operators and don't have to be considered. The space–like components are evaluated by the formulas

$$\gamma^0\gamma^k = \begin{pmatrix} 0 & \sigma^k \\ \sigma^k & 0 \end{pmatrix} \qquad \gamma^0\gamma_k = -\begin{pmatrix} 0 & \sigma^k \\ \sigma^k & 0 \end{pmatrix}. \tag{3.76}$$

Because ω is an isoscalar meson the same isospin law as for the σ–meson is valid.
For the ρ–meson there are available two different kinds of couplings: the vector and the tensor coupling. Some approaches include only the vector coupling and others both contributions. The exchange integral for vector coupling we get by

$$I_{\beta\alpha}^{(\rho,V)\mu}(\boldsymbol{x}) = g_\rho(\boldsymbol{x})\, \psi_\beta^\dagger(\boldsymbol{x}) \gamma^0 \gamma^\mu \psi_\alpha(\boldsymbol{x}), \tag{3.77}$$

whereas the tensor exchange is evaluated by

$$I_{\beta\alpha}^{(\rho,T)\mu}(\boldsymbol{x}) = -\partial_l \tfrac{f_\rho(\boldsymbol{x})}{2M}\, \psi_\beta^\dagger(\boldsymbol{x}) \gamma^0 \sigma^{\mu l} \psi_\alpha(\boldsymbol{x}). \tag{3.78}$$

The partial derivative acting on the propagator is moved to the source term by integration by parts what causes the negative sign. Since we have two different types of couplings we have to deal with two different contributions to the self–energy: the vector and the tensor coupling. First we denote the expression for the vector coupling

$$(\Sigma_\rho^{F,V}\, \psi_\alpha)(\boldsymbol{x}) = -g_\rho(\boldsymbol{x}) \sum_\beta \eta_\beta (2 - \delta_{q_\alpha q_\beta}) \left(I_{\beta\alpha}^{(\rho,V)\mu}(\boldsymbol{x}) - I_{\beta\alpha}^{(\rho,T)\mu}(\boldsymbol{x}) \right) \gamma^0 \gamma_\mu\, \psi_\beta(\boldsymbol{x}), \tag{3.79}$$

and secondly the tensor piece

$$(\Sigma_\rho^{F,T}\, \psi_\alpha)(\boldsymbol{x}) = -\tfrac{f_\rho(\boldsymbol{x})}{2M} \sum_\beta \eta_\beta (2 - \delta_{q_\alpha q_\beta})\, \partial^k \left(I_{\beta\alpha}^{(\rho,T)\mu}(\boldsymbol{x}) - I_{\beta\alpha}^{(\rho,V)\mu}(\boldsymbol{x}) \right) \gamma^0 \sigma_{\mu k}\, \psi_\beta(\boldsymbol{x}). \tag{3.80}$$

In addition the delta–tensor contribution has to be added to the tensor piece. The exchange part is evaluated similar to the pion delta–term and yields

$$I^{\delta T(\rho)\mu k}_{\beta\alpha}(\boldsymbol{x}) = \tfrac{1}{3}\,\tfrac{f_\rho(\boldsymbol{x})}{2M}\psi^\dagger_\beta(\boldsymbol{x})\gamma^0\sigma^{\mu k}\,\psi_\alpha(\boldsymbol{x}). \tag{3.81}$$

Hence the tensor part of the self–energy is modified by the contribution

$$(\Sigma^{F,\delta T}_\rho\,\psi_\alpha)(\boldsymbol{x}) = -\tfrac{f_\rho(\boldsymbol{x})}{2M}\sum_\beta \eta_\beta(2-\delta_{q_\alpha q_\beta})\,I^{\delta T(\rho)\mu k}_{\beta\alpha}(\boldsymbol{x})\,\gamma^0\sigma_{\mu k}\,\psi_\beta(\boldsymbol{x}) \tag{3.82}$$

removing the contact interaction. Let's denote some useful formulas for the evaluation of the tensor terms

$$\sigma^{0k} = i\alpha^k = i\begin{pmatrix} 0 & \sigma^k \\ \sigma^k & 0 \end{pmatrix}, \qquad\qquad \sigma^{ij} = \begin{pmatrix} \sigma^k & 0 \\ 0 & \sigma^k \end{pmatrix} \tag{3.83}$$

where (i,j,k) has to be a cyclic permutation in the second formula.
In case of the photon the exchange integral is evaluated by

$$-\Delta I^{(\gamma)\mu}_{\beta\alpha}(\boldsymbol{x}) = e^2\psi^\dagger_\beta(\boldsymbol{x})\tfrac{1}{2}(1-\tau_3)\gamma^0\gamma^\mu\,\psi_\beta(\boldsymbol{x}), \tag{3.84}$$

from which we obtain the electromagnetic self–energy of the protons

$$(\Sigma^F_\gamma\,\psi_\alpha)(\boldsymbol{x}) = -\sum_\beta \eta_\beta\,I^{(\gamma)\mu}_{\beta\alpha}(\boldsymbol{x})\,\tfrac{1}{2}(1-\tau_3)\gamma^0\gamma_\mu\psi_\beta(\boldsymbol{x}). \tag{3.85}$$

Summarizing all contributions from the various mesons κ we can denote the single–particle Fock potential

$$v^F_\alpha = \langle\alpha|\Sigma^F|\alpha\rangle = \sum_{\kappa=\sigma,\delta,\pi,\omega,\rho,\gamma}\int d^3x\,\psi^\dagger_\alpha(\boldsymbol{x})\big(\Sigma^F_\kappa\psi_\alpha\big)(\boldsymbol{x}). \tag{3.86}$$

And finally the total Fock self–energy for a nuclear system can obtained by

$$E_F = \frac{1}{2}\sum_\alpha \eta_\alpha\,v^F_\alpha \tag{3.87}$$

The evaluation of the Fock terms discussed in this section needs a lot of calculation time in the triaxial approach. But they are a step forward to improve the relativistic many-body calculation for finite nuclei.

3.3.3 Rearrangement Self–Energy

The rearrangement contributions to the nucleon self–energy have to be evaluated from $\Sigma^{(r)}$ in equation (3.45). Since we have already evaluated the Hartree and the Fock self–energies we can reduce the calculation to appropriate expressions and the rearrangement self–energy is divided into contributions from the Hartree and the Fock self–energies

$$\Sigma^{(r)}(\boldsymbol{x})\psi_\alpha(\boldsymbol{x}) = \Sigma^{(r)H}(\boldsymbol{x})\psi_\alpha(\boldsymbol{x}) + \Sigma^{(r)F}(\boldsymbol{x})\psi_\alpha(\boldsymbol{x}). \tag{3.88}$$

In the Hartree case the rearrangement self–energy contribution is expressed in terms of densities and meson fields as for the usual Hartree self–energy

$$\begin{aligned}\Sigma^{(r)H}(\boldsymbol{x}) = \Big(&\tfrac{\partial g_\sigma}{\partial\rho}(\boldsymbol{x})\Phi_\sigma(\boldsymbol{x})\rho^s(\boldsymbol{x}) + \tfrac{\partial g_\delta}{\partial\rho}(\boldsymbol{x})\Phi_\delta(\boldsymbol{x})\rho_3^s(\boldsymbol{x}) \\ &+ \tfrac{\partial g_\omega}{\partial\rho}(\boldsymbol{x})A_0^{(\omega)}(\boldsymbol{x})\rho(\boldsymbol{x}) + \tfrac{\partial g_\rho}{\partial\rho}(\boldsymbol{x})A_0^{(\rho)}(\boldsymbol{x})\rho_3(\boldsymbol{x}) \\ &+ \tfrac{1}{2M}\tfrac{\partial f_\rho}{\partial\rho}(\boldsymbol{x})[-\boldsymbol{\nabla}A_0^{(\rho)}(\boldsymbol{x}) + A_0^{(\delta\rho)}(\boldsymbol{x})]\cdot\boldsymbol{\rho}_3^t(\boldsymbol{x})\Big).\end{aligned} \tag{3.89}$$

The Fock rearrangement terms are more complicated, but they arise in the same way as in the Hartree case from the Fock self–energies. Based on the exchange integrals in subsection (3.3.2), we obtain for each meson κ the following contributions to the Fock rearrangement self–energy

$$\begin{aligned}
\Sigma_\sigma^{(r)F}(\boldsymbol{x}) &= -\tfrac{\partial g_\sigma}{\partial\rho}(\boldsymbol{x})\sum_{\gamma,\beta}\delta_{q_\gamma q_\beta}\eta_\gamma\eta_\beta\,\psi_\gamma^\dagger(\boldsymbol{x})I_{\beta\gamma}^{\sigma}(\boldsymbol{x})\,\gamma^0\psi_\beta(\boldsymbol{x}),\\
\Sigma_\delta^{(r)F}(\boldsymbol{x}) &= -\tfrac{\partial g_\delta}{\partial\rho}(\boldsymbol{x})\sum_{\gamma,\beta}(2-\delta_{q_\gamma q_\beta})\eta_\gamma\eta_\beta\,\psi_\gamma^\dagger(\boldsymbol{x})I_{\beta\gamma}^{\delta}(\boldsymbol{x})\,\gamma^0\psi_\beta(\boldsymbol{x}),\\
\Sigma_\pi^{(r)F}(\boldsymbol{x}) &= \tfrac{1}{m_\pi}\tfrac{\partial f_\pi}{\partial\rho}(\boldsymbol{x})\sum_{\gamma,\beta}(2-\delta_{q_\gamma q_\beta})\eta_\gamma\eta_\beta\,\psi_\gamma^\dagger(\boldsymbol{x})\left[\partial^k\,I_{\beta\gamma}^{(\pi)}(\boldsymbol{x})\right]\gamma^0\gamma_5\gamma_k\psi_\beta(\boldsymbol{x}),\\
\Sigma_\pi^{(r)F,\delta}(\boldsymbol{x}) &= \tfrac{1}{m_\pi}\tfrac{\partial f_\pi}{\partial\rho}(\boldsymbol{x})\sum_{\gamma,\beta}(2-\delta_{q_\gamma q_\beta})\eta_\gamma\eta_\beta\,\psi_\gamma^\dagger(\boldsymbol{x})I_{\beta\gamma}^{\delta(\pi)\,k}(\boldsymbol{x})\,\gamma^0\gamma_5\gamma_k\psi_\beta(\boldsymbol{x}),\\
\Sigma_\omega^{(r)F}(\boldsymbol{x}) &= -\tfrac{\partial g_\omega}{\partial\rho}(\boldsymbol{x})\sum_{\gamma,\beta}\delta_{q_\gamma q_\beta}\eta_\gamma\eta_\beta\,\psi_\gamma^\dagger(\boldsymbol{x})I_{\beta\gamma}^{(\omega)\mu}(\boldsymbol{x})\,\gamma^0\gamma_\mu\psi_\beta(\boldsymbol{x}),\\
\Sigma_\rho^{(r)F,V}(\boldsymbol{x}) &= -\tfrac{\partial g_\rho}{\partial\rho}(\boldsymbol{x})\sum_{\gamma,\beta}(2-\delta_{q_\gamma q_\beta})\eta_\gamma\eta_\beta\\
&\qquad\psi_\gamma^\dagger(\boldsymbol{x})\big(I_{\beta\gamma}^{(\rho,V)\mu}(\boldsymbol{x}) - I_{\beta\gamma}^{(\rho,T)\mu}(\boldsymbol{x})\big)\,\gamma^0\gamma_\mu\psi_\beta(\boldsymbol{x}),
\end{aligned}$$

$$\begin{aligned}
\Sigma_{\rho}^{(r)F,T}(\boldsymbol{x}) &= -\tfrac{1}{2M}\tfrac{\partial f_\rho}{\partial \rho}(\boldsymbol{x})\sum_{\gamma,\beta}\eta_\gamma\eta_\beta(2-\delta_{q_\gamma q_\beta}) \\
&\qquad \psi_\gamma^\dagger(\boldsymbol{x})\left[\partial^k\big(I_{\beta\gamma}^{(\rho,T)\mu}(\boldsymbol{x})-I_{\beta\gamma}^{(\rho,V)\mu}(\boldsymbol{x})\big)\right]\gamma^0\sigma_{\mu k}\,\psi_\beta(\boldsymbol{x}), \\
\Sigma_{\rho}^{(r)F,\delta T}(\boldsymbol{x}) &= -\tfrac{1}{2M}\tfrac{\partial f_\rho}{\partial \rho}(\boldsymbol{x})\sum_{\gamma\beta}\eta_\gamma\eta_\beta(2-\delta_{q_\gamma q_\beta}) \\
&\qquad \psi_\gamma^\dagger(\boldsymbol{x})I_{\beta\gamma}^{\delta T(\rho)\mu k}(\boldsymbol{x})\,\gamma^0\sigma_{\mu k}\psi_\beta(\boldsymbol{x}).
\end{aligned} \tag{3.90}$$

The numerical evaluation is done together with the Fock self–energy, which results in an exchange of the coupling constants with their derivatives and an additional sum over the single–particle wave functions. In order to get the Fock rearrangement self–energy we sum up contributions from all mesons

$$\begin{aligned}
\Sigma^{(r)F}(\boldsymbol{x}) = &\Sigma_\sigma^{(r)F}(\boldsymbol{x})+\Sigma_\delta^{(r)F}(\boldsymbol{x})+\Sigma_\pi^{(r)F}(\boldsymbol{x})+\Sigma_\pi^{(r)F,\delta}(\boldsymbol{x}) \\
&+\Sigma_\omega^{(r)F}(\boldsymbol{x})+\Sigma_\rho^{(r)F,V}(\boldsymbol{x})+\Sigma_\rho^{(r)F,T}(\boldsymbol{x})+\Sigma_\rho^{(r)F,\delta T}(\boldsymbol{x}).
\end{aligned} \tag{3.91}$$

After all we can denote the rearrangement single–particle potential

$$v_\alpha^{(r)} = \langle\alpha|\Sigma^{(r)}|\alpha\rangle = \int d^3x\,\psi_\alpha^\dagger(\boldsymbol{x})\big(\Sigma^{(r)H}(\boldsymbol{x})+\Sigma^{(r)F}(\boldsymbol{x})\big)\psi_\alpha(\boldsymbol{x}) \tag{3.92}$$

from which we obtain the rearrangement energy

$$E_R = \sum_\alpha \eta_\alpha v_\alpha^{(r)} = \int d^3x\,\Sigma^{(r)}(\boldsymbol{x})\rho(\boldsymbol{x}). \tag{3.93}$$

The rearrangement energy does not contribute to the Hartree–Fock energy but has to be subtracted if the sum of the single–particle energy is employed for the calculation of the total binding energy. The rearrangement self–energy contribution is important to get appropriate single–particle energies and wave functions.

3.3.4 The Center of Mass Energy

The origin of the center of mass energy is the quantum mechanical effect that fixing the center of the nucleus to the center of our coordinate system leads to an expectation value for the sequence of the center of mass momentum, which is different from zero. This leads to a center of mass energy of

$$E_{cm} = -\frac{1}{2AM}\langle \boldsymbol{P}_{cm}^2\rangle, \tag{3.94}$$

with $\boldsymbol{P}_{cm}$ the center of mass momentum of the nucleus. This energy has to be removed in order to get the energy levels of the nucleonic states and the total binding

energy without spurious center of mass contributions. There are several approaches to this problem but even in relativistic approaches the non–relativistic kinetic energy of the center of mass motion is considered. As the whole nucleus usually has a big mass and therefore moves slow enough, this yields a good approximation even in relativistic approaches.

In a simple harmonic oscillator model one obtains the center of mass correction [HKL01]

$$E_{cm} = -\frac{3}{4}\hbar\omega \tag{3.95}$$

with $\hbar\omega = 41\,A^{-1/3}$ MeV. Of course, this formula gives only a correction to the binding energy, whereas the single–particle energies are not modified.

More realistically we turn to (3.94). The evaluation of the expectation value $\langle \boldsymbol{P}_{cm}^2 \rangle$ leads to a two–body operator acting on the nucleon field

$$\boldsymbol{P}_{cm}^2 = \sum_{\alpha\beta} \boldsymbol{p}_\alpha \cdot \boldsymbol{p}_\beta = \sum_{\alpha\alpha'} \boldsymbol{p}_{\alpha\alpha'}^2 c_\alpha^\dagger c_{\alpha'} + \sum_{\alpha\beta\alpha'\beta'} \boldsymbol{p}_{\alpha\alpha'} \cdot \boldsymbol{p}_{\beta\beta'} c_\alpha^\dagger c_\beta^\dagger c_{\beta'} c_{\alpha'}. \tag{3.96}$$

Taking care of the normal occupation factors η_α and the anomalous occupation factors ζ_α (see equations 4.19 and 4.58), we obtain for the center of mass momentum with respect to the single–particle wave functions

$$\langle \boldsymbol{P}_{cm}^2 \rangle = \sum_\alpha \eta_\alpha \langle \alpha | \boldsymbol{p}_\alpha^2 | \alpha \rangle - \sum_{\alpha\beta} (\eta_\alpha \eta_\beta + \zeta_\alpha \zeta_\beta) \, \langle \beta | \boldsymbol{p}_\alpha | \alpha \rangle \cdot \langle \alpha | \boldsymbol{p}_\beta | \beta \rangle. \tag{3.97}$$

This operator can be employed in the one–body approximation or fully. An additional option is the calculation before or after the variation. The calculation after variation naturally does not modify the single–particle states and it is often used for simplicity. For example in the Skyrme calculation with the SLy4 parameter set the one–body approximation is calculated after variation. In the similar SLy6 set the full center of mass operator is included in the self–consistent variation [CB$^+$98]. In the relativistic mean–field calculations in the Hartree case we included only the harmonic oscillator approximation to be consistent with the fit of the parameter set of Hofmann et al. [HKL01]. In the relativistic Hartree–Fock approach there is a parameter set of Long et al. [LGM06] which includes the full center of mass operator after the variation.

The center of mass energy in three dimensional approaches is evaluated as follows for the relativistic framework. The one-body part gets

$$\Sigma_{cm}^{(1)} \, \psi_\alpha(\boldsymbol{x}) = \tfrac{1}{2AM} \, \Delta\psi_\alpha(\boldsymbol{x}), \tag{3.98}$$

which is just a modification of the kinetic energy. The two–body part has a similar structure as the Fock self–energy and is thus added to the latter. First the exchange Integral is calculated

$$\boldsymbol{I}_{\beta\alpha} = \int dx^3\, \psi^\dagger_\beta(\boldsymbol{x}) \boldsymbol{\nabla} \psi_\alpha(\boldsymbol{x}), \tag{3.99}$$

which is the exchange momentum besides a factor of $-i$ and has to be projected on all other nucleons

$$\Sigma^{(2)}_{cm}\psi_\alpha(\boldsymbol{x}) = -\tfrac{1}{2AM} \sum_\beta (\eta_\beta + \zeta_\alpha\zeta_\beta/\eta_\alpha)\, \boldsymbol{I}_{\beta\alpha} \cdot \boldsymbol{\nabla}\psi_\beta(\boldsymbol{x}), \tag{3.100}$$

where the sum over β runs over protons p and neutrons n. These two contributions can be included into the variation or calculated a posteriori by

$$E_{cm} = \sum_\alpha \int dx^3\, \psi^\dagger_\alpha(\boldsymbol{x}) \left(\Sigma^{(1)}_{cm}\, \psi_\alpha(\boldsymbol{x}) + \Sigma^{(2)}_{cm}\psi_\alpha(\boldsymbol{x})\right). \tag{3.101}$$

Finally, it has to be mentioned that all approaches give different center of mass energies and the most reliable seems to be the full approach. Note, however, that even this full approach represents an approximation only. Actually one should project the Slater determinant on a state with momentum zero and perform a variation after projection [SR91].

3.3.5 Solving the Dirac Equation

Similar to the nuclear problem employing Skyrme forces we apply the variational principle

$$\frac{\delta}{\delta\psi^\dagger_\alpha}\left\{E[\psi] - \sum_\alpha \varepsilon_\alpha \left(\int d^3x\, |\psi_\alpha(x)|^2 - 1\right)\right\} = 0 \tag{3.102}$$

to the Dirac Hamiltonian in Hartree–Fock approximation (eq. 3.38) and obtain the Dirac equation for the nucleons with the self–energies

$$\begin{aligned}\varepsilon_\alpha\psi_\alpha(\boldsymbol{x}) = \Big(&\boldsymbol{\alpha p} + \beta\left[M + \Sigma^H_S(\boldsymbol{x})\right] \\ &+ \Sigma^H_0(\boldsymbol{x}) + \Sigma^{(r)}(\boldsymbol{x}) + i\beta\boldsymbol{\alpha}\boldsymbol{\Sigma}^H_T(\boldsymbol{x})\Big)\,\psi_\alpha(\boldsymbol{x}) + (\Sigma^F\psi_\alpha)(\boldsymbol{x}).\end{aligned} \tag{3.103}$$

In order to perform the Hartree approach the Fock terms are simply to ignored.
For the solution of the spherical symmetric problem the Fock self–energy contributions are projected on the Dirac spinor to get back a Potential term (compare [Fr94], [BM$^+$87]). However, the Fock terms are only valid for the one special wave function ψ_α, for which the exchange integrals has been calculated. It is possible to calculate

an operator matrix for the Fock self–energy, but this has to be done incorporating all states into the calculation and not only one Dirac spinor at one spatial point. In the present code the plain Fock terms without projection has been included because of better numerical accuracy.

Now we turn to the procedure for solving the Dirac equation in the Hartree–Fock approximation. In the following we take advantage of the Pauli spinor representation introduced in equation (3.49) to decompose the Dirac equation. It is convenient to have the eigenvalues without rest mass, so the eigenvalues are shifted by

$$\varepsilon_\alpha \rightarrow \varepsilon_\alpha - M. \tag{3.104}$$

and we obtain the following equations

$$\begin{aligned}
\varepsilon_\alpha\varphi_\alpha(\boldsymbol{x}) &= \boldsymbol{\sigma}\big[\boldsymbol{p} + i\,\boldsymbol{\Sigma}_T^H(\boldsymbol{x})\big]\chi_\alpha(\boldsymbol{x}) \\
&\quad + \big[\Sigma_S^H(\boldsymbol{x}) + \Sigma_0^H(\boldsymbol{x}) + \Sigma^{(r)}(\boldsymbol{x})\big]\varphi_\alpha(\boldsymbol{x}) + (\Sigma^F\varphi_\alpha)(\boldsymbol{x}) \qquad (3.105)\\
\varepsilon_\alpha\chi_\alpha(\boldsymbol{x}) &= \boldsymbol{\sigma}\big[\boldsymbol{p} - i\,\boldsymbol{\Sigma}_T^H(\boldsymbol{x})\big]\varphi_\alpha(\boldsymbol{x}) \\
&\quad + \big[-2M - \Sigma_S^H(\boldsymbol{x}) + \Sigma_0^H(\boldsymbol{x}) + \Sigma^{(r)}(\boldsymbol{x})\big]\chi_\alpha(\boldsymbol{x}) \\
&\quad + (\Sigma^F\chi_\alpha)(\boldsymbol{x}). \qquad (3.106)
\end{aligned}$$

In these equations $(\Sigma^F\varphi_\alpha)$ and $(\Sigma^F\chi_\alpha)$ comply with the Fock self–energy for the whole Dirac spinor $(\Sigma^F\psi_\alpha)$. Now we define a potential U for the lower and upper component, which is actually the Hartree potential together with the rearrangement self–energy

$$\begin{aligned}
U_\varphi(\boldsymbol{x}) &= \Sigma_S^H(\boldsymbol{x}) + \Sigma_0^H(\boldsymbol{x}) + \Sigma^{(r)}(\boldsymbol{x}) \qquad (3.107)\\
U_\chi(\boldsymbol{x}) &= -2M - \Sigma_S^H(\boldsymbol{x}) + \Sigma_0^H(\boldsymbol{x}) + \Sigma^{(r)}(\boldsymbol{x}). \qquad (3.108)
\end{aligned}$$

The Reader should bear in mind that the scalar Hartree self–energy Σ_S^H is negative and therefore the scalar and vector Hartree self–energies cancel each other in the potential for the upper component to a large extend, which results in a nuclear potential, which is weak as compared to the scalar and vector contributions. For the lower component, the scalar and vector Hartree self–energies sum up and give rise to a large spin–orbit splitting.

By virtue of the following term, similar to an effective mass term

$$\mathcal{B}_\alpha(\boldsymbol{x}) = \frac{1}{\varepsilon_\alpha - U_\chi(\boldsymbol{x})} = \frac{1}{2M + \varepsilon_\alpha + \Sigma_S^H(\boldsymbol{x}) - \Sigma_0^H(\boldsymbol{x}) - \Sigma^{(r)}(\boldsymbol{x})}, \tag{3.109}$$

we obtain an "effective Schroedinger equation" by inserting the equation for the lower component

$$\chi_\alpha(\boldsymbol{x}) = \mathcal{B}_\alpha(\boldsymbol{x}) \Big(\boldsymbol{\sigma} \big[\boldsymbol{p} - i\, \boldsymbol{\Sigma}_T^H(\boldsymbol{x}) \big] \varphi_\alpha(\boldsymbol{x}) + \ (\Sigma^F \chi_\alpha)(\boldsymbol{x}) \Big) \tag{3.110}$$

into the one for the upper component

$$\begin{aligned} \varepsilon_\alpha \varphi_\alpha(\boldsymbol{x}) = & \boldsymbol{\sigma} \big[\boldsymbol{p} + i \boldsymbol{\Sigma}_T^H(\boldsymbol{x}) \big] \mathcal{B}_\alpha(\boldsymbol{x}) \Big(\boldsymbol{\sigma} \big[\boldsymbol{p} - i \boldsymbol{\Sigma}_T^H(\boldsymbol{x}) \big] \varphi_\alpha(\boldsymbol{x}) + (\Sigma^F \chi_\alpha)(\boldsymbol{x}) \Big) \\ & + U_\varphi(\boldsymbol{x})\, \varphi_\alpha(\boldsymbol{x}) + (\Sigma^F \varphi_\alpha)(\boldsymbol{x}). \end{aligned} \tag{3.111}$$

This "effective Schroedinger equation" is not a non–relativistic reduction of the problem but nothing else than a method to reduce numerical errors in the iterative procedure. Reinhard et. al. applied this method in [RR$^+$88, Rhd89] to spherical nuclei. In the triaxial treatment however, the spin–orbit term has to be treated in a different way. With the help of the formula

$$\boldsymbol{\sigma} \boldsymbol{A}\, \boldsymbol{\sigma} \boldsymbol{B} = \boldsymbol{A}\boldsymbol{B} + i \boldsymbol{\sigma}\, (\boldsymbol{A} \times \boldsymbol{B}) \tag{3.112}$$

for operators $\boldsymbol{A}$ and $\boldsymbol{B}$ commuting with $\boldsymbol{\sigma}$ we obtain

$$\begin{aligned} & \boldsymbol{\sigma} \big[\boldsymbol{p} + i \boldsymbol{\Sigma}_T^H(\boldsymbol{x}) \big] \mathcal{B}_\alpha(\boldsymbol{x})\, \boldsymbol{\sigma} \big[\boldsymbol{p} - i \boldsymbol{\Sigma}_T^H(\boldsymbol{x}) \big] \varphi_\alpha(\boldsymbol{x}) \\ & \qquad = - \big[\boldsymbol{\nabla} - \boldsymbol{\Sigma}_T^H(\boldsymbol{x}) \big] \mathcal{B}_\alpha(\boldsymbol{x}) \big[\boldsymbol{\nabla} + \boldsymbol{\Sigma}_T^H(\boldsymbol{x}) \big] \\ & \qquad\quad - i \big[(\boldsymbol{\nabla} - \boldsymbol{\Sigma}_T^H(\boldsymbol{x})) \mathcal{B}_\alpha(\boldsymbol{x}) \big] \cdot \big[(\boldsymbol{\nabla} + \boldsymbol{\Sigma}_T^H(\boldsymbol{x})) \times \boldsymbol{\sigma} \big] \varphi_\alpha(\boldsymbol{x}), \end{aligned} \tag{3.113}$$

which is a sum of the non–relativistic kinetic energy and the Hartree spin–orbit interaction. A further modification yields the "effective Hamiltonian" ready for implementation

$$\begin{aligned} H_{\varphi,\alpha}\, \varphi_\alpha(\boldsymbol{x}) = & - \mathcal{B}_\alpha(\boldsymbol{x}) \Delta \varphi_\alpha(\boldsymbol{x}) - [\boldsymbol{\nabla} \mathcal{B}_\alpha(\boldsymbol{x})] \cdot \big[\boldsymbol{\nabla} + \boldsymbol{\Sigma}_T^H(\boldsymbol{x}) \big] \varphi_\alpha(\boldsymbol{x}) \\ & + \mathcal{B}_\alpha(\boldsymbol{x}) \big[|\boldsymbol{\Sigma}_T^H(\boldsymbol{x})|^2 - (\boldsymbol{\nabla} \boldsymbol{\Sigma}_T^H(\boldsymbol{x})) \big] \varphi_\alpha(\boldsymbol{x}) \\ & - i \big[(\boldsymbol{\nabla} - \boldsymbol{\Sigma}_T^H(\boldsymbol{x})) \mathcal{B}_\alpha(\boldsymbol{x}) \big] \cdot \big[(\boldsymbol{\nabla} + \boldsymbol{\Sigma}_T^H(\boldsymbol{x})) \times \boldsymbol{\sigma} \big] \varphi_\alpha(\boldsymbol{x}) \\ & - i \boldsymbol{\sigma} \boldsymbol{\nabla} \big[\mathcal{B}_\alpha(\boldsymbol{x}) (\Sigma^F \chi_\alpha)(\boldsymbol{x}) \big] \\ & + U_\varphi(\boldsymbol{x}) \varphi_\alpha(\boldsymbol{x}) + (\Sigma^F \varphi_\alpha)(\boldsymbol{x}), \end{aligned} \tag{3.114}$$

where the lower component is taken from the previous result and regarded as constant. In order to calculate the eigenvalue we can't use the "effective Hamiltonian" like a Hamiltonian because we have to take into account the lower component by equation (3.110). Rewriting this equation using the definition of the "effective mass" (eq. 3.109) we get the following expression

$$[\varepsilon_\alpha - U_\varphi(\boldsymbol{x})]\, \chi_\alpha(\boldsymbol{x}) = \boldsymbol{\sigma} \big[\boldsymbol{p} - i\, \boldsymbol{\Sigma}_T^H(\boldsymbol{x}) \big] \varphi_\alpha(\boldsymbol{x}) + \ (\Sigma^F \chi_\alpha)(\boldsymbol{x}). \tag{3.115}$$

Hence the next approximation to the eigenvalue $\varepsilon_\alpha^{(n+1)}$ obeys

$$\varepsilon_\alpha^{(n+1)} \begin{pmatrix} \varphi_\alpha(\boldsymbol{x}) \\ \chi_\alpha(\boldsymbol{x}) \end{pmatrix} = \begin{pmatrix} H_{\varphi,\alpha}\,\varphi_\alpha(\boldsymbol{x}) \\ \big[\varepsilon_\alpha^{(n)} - U_\chi(\boldsymbol{x})\big]\chi_\alpha(\boldsymbol{x}) + U_\chi(\boldsymbol{x})\chi_\alpha(\boldsymbol{x}) \end{pmatrix} = \begin{pmatrix} H_{\varphi,\alpha}\,\varphi_\alpha(\boldsymbol{x}) \\ \varepsilon_\alpha^{(n)}\chi_\alpha(\boldsymbol{x}) \end{pmatrix}, \tag{3.116}$$

and it turns out that the whole new information of the lower component is contained in the Pauli spinor. The actual calculation is performed by the integral

$$\varepsilon_\alpha^{(n+1)} = \int d^3x \left(\varphi_\alpha^\dagger(\boldsymbol{x}) H_{\varphi,\alpha}\,\varphi_\alpha(\boldsymbol{x}) + \varepsilon^{(n)}\chi_\alpha^\dagger(\boldsymbol{x})\chi_\alpha(\boldsymbol{x})\right). \tag{3.117}$$

The energy is obtained from the Dirac Hamiltonian in Hartree–Fock approximation (eq. 3.47)

$$E_{HF} = \sum_\alpha \eta_\alpha\,\varepsilon_\alpha - (E_R + E_H + E_F). \tag{3.118}$$

For the variation of the wave functions we employ the imaginary time step method described in section 5.3 in the following manner: First we operate on the upper component by the imaginary time step

$$\varphi_\alpha^{(n+1)}(\boldsymbol{x}) = \exp(-\lambda H_{\varphi,\alpha})\,\varphi_\alpha^{(n)}(\boldsymbol{x}), \tag{3.119}$$

then the next approximation for the lower component is calculated by

$$\chi_\alpha^{(n+1)}(\boldsymbol{x}) = \mathcal{B}_\alpha(\boldsymbol{x})\left(\boldsymbol{\sigma}\big[-i(\boldsymbol{\nabla} + \boldsymbol{\Sigma}_T^H(\boldsymbol{x})\big]\varphi_\alpha^{(n+1)}(\boldsymbol{x}) + (\Sigma^F\chi_\alpha)^{(n)}(\boldsymbol{x})\right), \tag{3.120}$$

and finally both components are orthonormalized together via the Gram–Schmidt–method.

The calculation of powers of Fock terms in the imaginary time step is very time consuming, and the construction of potential terms like in the spherical calculation by the projection of the Fock terms on the wave function [Fr94] leads to an unstable algorithm. From the mathematical point of view it is clear that an integral operator like the Fock self–energy is linear in the wave functions but a more complicated object than a simple multiplication operator. For the latter repeated operation is easy to evaluate whereas for the Fock terms the whole exchange integral evaluation has to be repeated several times. Hence the iterative procedure for the full Hartree–Fock problem is truncated to first order, what still provides satisfactory convergence. For the calculation of a density dependent relativistic Hartree approach the imaginary time step method works excellent and the fast evaluation of the self–energies opens the door to astrophysical application.

3.4 Asymmetric Nuclear Matter

For comparison with the triaxial approach, asymmetric nuclear matter is calculated. In this section the relativistic Hartree–Fock approach for asymmetric nuclear matter is introduced. The derivation follows mainly [BM+87, FM94, LGM06] and is extended to asymmetric matter.

The self–energy Σ can be written quite generally in nuclear matter as

$$\boldsymbol{\Sigma}(\boldsymbol{p}) = \Sigma_S(p) + \gamma_0\Sigma_0(p) + \boldsymbol{\gamma}\cdot\hat{\boldsymbol{p}}\boldsymbol{\Sigma}_V(p), \tag{3.121}$$

where $\hat{\boldsymbol{p}}$ is the unit vector along $\boldsymbol{p}$. The tensor part $\gamma_0\boldsymbol{\gamma}\cdot\hat{\boldsymbol{p}}$ vanishes in the Hartree–Fock approximation for nuclear matter. All components of the self–energy Σ are functions of the four momentum $p = (E(p), \boldsymbol{p})$. The Dirac spinors $u(p, s, q)$ with spin s and isospin q are solutions of the following Dirac equation:

$$[\boldsymbol{\gamma}\cdot\boldsymbol{p}^*_q + M^*_q]u(p, s, q) = \gamma_0 E^*_q u(p, s, q), \tag{3.122}$$

where starred quantities are defined by

$$\begin{aligned} \boldsymbol{p}^*_{\boldsymbol{q}} &= \boldsymbol{p} + \hat{\boldsymbol{p}}\Sigma_{V,q}(p) \\ M^*_q &= M + \Sigma_{S,q}(p), \\ E^*_q &= E(p) - \Sigma_{0,q}(p), \end{aligned} \tag{3.123}$$

(3.124)

and the on-shell condition reads

$$E^{*2}_q = \boldsymbol{p}^{*2}_{\boldsymbol{q}} + M^{*2}_q. \tag{3.125}$$

The positive energy solutions of the Dirac equation (3.122) are

$$u(p, s, q) = \left(\frac{E^*_q + M^*_q}{2E^*_q}\right)^{1/2} \begin{pmatrix} 1 \\ \frac{\boldsymbol{\sigma}\cdot\boldsymbol{p}^*_{\boldsymbol{q}}}{E^*_q + M^*_q} \end{pmatrix} \chi_{1/2}(s)\chi_{1/2}(q). \tag{3.126}$$

The spinors $\chi_{1/2}(s)$ and $\chi_{1/2}(q)$ denote spin and isospin projection. The Dirac spinors $u(p, s, q)$ are normalized by

$$u^\dagger(p, s, q)u(p, s, q) = 1. \tag{3.127}$$

By defining the nucleon field Ψ_0 in terms of plane waves in the "no–sea" approximation

$$\begin{aligned} \Psi_0(x) &= \sum_{p,s,q} u(p, s, q)e^{-ipx}c_{p,s,q} \\ \Psi^\dagger_0(x) &= \sum_{p,s,q} u(p, s, q)e^{ipx}c^\dagger_{p,s,q}, \end{aligned} \tag{3.128}$$

we obtain the Hamiltonian H_0 defined in equation (3.38) for nuclear matter

$$H_0 = T + \sum_{\kappa=\sigma,\delta,\pi,\omega,\rho} V_\kappa, \tag{3.129}$$

where we ignore as usual the photon contribution γ. The kinetic energy T gets

$$T = \sum_{p_1,p_2} \sum_{\alpha,\beta} c^\dagger_{p_1,\alpha} c_{p_2,\beta}\, \bar{u}(p_1,\alpha)(\boldsymbol{\gamma}\cdot\boldsymbol{p} + M)u(p_2,\beta), \tag{3.130}$$

and the two-body interaction V_κ takes for different mesons κ the form

$$\begin{aligned} V_\kappa = \frac{1}{2}\sum_{p_1,p_2} \sum_{\alpha,\beta;\gamma,\delta} & c^\dagger_{\gamma,p_1+k} c^\dagger_{\delta,p_2-k} c_{\beta,p_1} c_{\alpha,p_2} \\ & \bar{u}(p_1+k,\gamma)\bar{u}(p_2-k,\delta)\Gamma_\kappa(1,2)\frac{1}{m_\kappa^2+\boldsymbol{k}^2}u(p_2,\beta)u(p_1,\alpha), \end{aligned} \tag{3.131}$$

which includes the energy independent meson propagator D_κ in compliance with the meson propagator for spatial representation (3.43). In the above formulas the spin and isospin quantum numbers are summarized in Greek indices and $k = p_2 - p_1$ is the intermediate momentum. The interaction vertices are the same as in coordinate representation (3.29) identifying the particle numbers with x and y coordinates. The vertices depending on momentum exchange are listed below:

$$\begin{aligned} \Gamma^{pv}_\pi(1,2) &= -\left[\tfrac{f_\pi}{m_\pi}\boldsymbol{\tau}\ \not{k}\gamma_5\right]_1 \cdot \left[\tfrac{f_\pi}{m_\pi}\boldsymbol{\tau}\ \not{k}\gamma_5\right]_2 \\ \Gamma^T_\rho(1,2) &= \left[\tfrac{f_\rho}{2M}\boldsymbol{\tau} k_\nu \sigma^{\mu\nu}\right]_1 \cdot \left[\tfrac{f_\rho}{2M}\boldsymbol{\tau} k^\lambda \sigma_{\mu\lambda}\right]_2 \\ \Gamma^{VT}_\rho(1,2) &= i\Big(\left[g_\rho \boldsymbol{\tau}\gamma_\mu\right]_2 \cdot \left[\tfrac{f_\rho}{2M}\boldsymbol{\tau}\sigma^{\mu\nu}k_\nu\right]_1 - \left[\tfrac{f_\rho}{2M}\boldsymbol{\tau}\sigma^{\mu\nu}q_\nu\right]_2 \cdot \left[g_\rho\boldsymbol{\tau}\gamma_\mu\right]_1\Big). \end{aligned} \tag{3.132}$$

The $\delta(\boldsymbol{r})$ contributions for the pion and the ρ–tensor term are removed by subtracting

$$\delta[\Gamma_{\pi,\rho}(1,2)] = \frac{1}{4\pi k^2}\int d\Omega_k\, \Gamma_{\pi,\rho}(1,2). \tag{3.133}$$

The energy density in a given Volume D is obtained from the Hamiltonian by

$$\epsilon = \frac{1}{D}\langle\Psi_0|H_0|\Psi_0\rangle = \langle T\rangle + \langle V\rangle. \tag{3.134}$$

To evaluate the kinetic energy density $\langle T\rangle$ and the potential energy density $\langle V\rangle$ we introduce the projection operator onto the positive energy states,

$$\Lambda^*_+ = \frac{\not{p}^* + M^*}{2M^*}. \tag{3.135}$$

From standard trace techniques the kinetic energy density is obtained

$$\langle T\rangle = \frac{1}{\pi^2}\sum_q \int \eta_q(p)\, p^2\, dp\, (p\hat{P}_q + M\hat{M}_q), \tag{3.136}$$

where $\hat{P}$, $\hat{M}$ and the normalization are defined as

$$\begin{aligned}
\hat{P}_q(p) &= \frac{p^*_q}{E^*_q} = \tfrac{1}{2}\sum_s \bar{u}(\boldsymbol{p},s,q)\,\boldsymbol{\gamma}\cdot\hat{\boldsymbol{p}}\,u(\boldsymbol{p},s,q),\\
\hat{M}_q(p) &= \frac{M^*_q}{E^*_q} = \tfrac{1}{2}\sum_s \bar{u}(\boldsymbol{p},s,q)\,u(\boldsymbol{p},s,q),\\
1 &= \tfrac{1}{2}\sum_s \bar{u}(\boldsymbol{p},s,q)\,\gamma_0\,u(\boldsymbol{p},s,q),
\end{aligned} \tag{3.137}$$

and $\eta_q(p)$ is the occupation factor depending on the momentum p for the isospin projection q.

The potential energy density $\langle V\rangle$ can be decomposed into the Hartree $\langle V^H\rangle$ and the Fock contributions $\langle V^F\rangle$. The Hartree energy density can be reduced to the following expression by introducing the scalar isoscalar, scalar isovector, vector isoscalar, and vector isovector densities

$$\langle V^H\rangle = -\frac{1}{2}\left(\frac{g_\sigma}{m_\sigma}\right)^2(\rho^s)^2 - \frac{1}{2}\left(\frac{g_\delta}{m_\delta}\right)^2(\rho^s_3)^2 + \frac{1}{2}\left(\frac{g_\omega}{m_\omega}\right)^2\rho^2 + \frac{1}{2}\left(\frac{g_\rho}{m_\rho}\right)^2\rho^2_3, \tag{3.138}$$

where the scalar and vector densities for protons or neutrons ($q = p, n$) are evaluated by

$$\begin{aligned}
\rho^s_q &= \frac{1}{\pi^2}\int \eta_q(p)\,p^2\,dp\,\hat{M}_q(p),\\
\rho_q &= \frac{1}{\pi^2}\int \eta_q(p)\,p^2\,dp,
\end{aligned} \tag{3.139}$$

from which we obtain all densities

$$\begin{aligned}
\rho^s &= \rho^s_p + \rho^s_n,\\
\rho^s_3 &= \rho^s_p - \rho^s_n,\\
\rho^s &= \rho^s_p + \rho^s_n,\\
\rho_3 &= \rho_p - \rho_n.
\end{aligned} \tag{3.140}$$

All mesons contribute to the Fock potential energy density and it is evaluated by the expression

$$\begin{aligned}
\langle V^F\rangle =& \frac{1}{2}\sum_{q,q'}\frac{1}{(2\pi)^4}\int \eta_q(p)\,p\,dp\int \eta_{q'}(p')\,p'\,dp'\\
&\Big[\sum_\kappa f_{q,q'}A_\kappa(p,p') + \hat{M}_q(p)\hat{M}_{q'}(p')\sum_\kappa f_{q,q'}B_\kappa(p,p')\\
&+ \hat{P}_q(p)\hat{P}_{q'}(p')\sum_\kappa f_{q,q'}C_\kappa(p,p') + \hat{P}_q(p)\hat{M}_{q'}(p')f_{q,q'}D(p,p')\Big].
\end{aligned} \tag{3.141}$$

κ	A_κ	B_κ	C_κ
σ	$g_\sigma^2\theta_\sigma$	$g_\sigma^2\theta_\sigma$	$-2g_\sigma^2\theta_\sigma$
δ	$g_\delta^2\theta_\delta$	$g_\delta^2\theta_\delta$	$-2g_\delta^2\theta_\delta$
π	$-\left(\frac{f_\pi}{m_\pi}\right)^2 m_\pi^2\theta_\pi$	$-\left(\frac{f_\pi}{m_\pi}\right)^2 m_\pi^2\theta_\pi$	$2\left(\frac{f_\pi}{m_\pi}\right)^2[(p^2+p'^2)\phi_\pi - pp'\theta_\pi]$
ω	$2g_\omega^2\theta_\omega$	$-4g_\omega^2\theta_\omega$	$-4g_\omega^2\theta_\omega$
ρ_V	$2g_\rho^2\theta_\rho$	$-4g_\rho^2\theta_\rho$	$-4g_\rho^2\theta_\rho$
ρ_T	$-\left(\frac{f_\rho}{2M}\right)^2 m_\rho^2\theta_\rho$	$-3\left(\frac{f_\rho}{2M}\right)^2 m_\rho^2\theta_\rho$	$4\left(\frac{f_\rho}{2M}\right)^2[(p^2+p'^2-m_\rho/2)\phi_\rho - pp'\theta_\rho]$
ρ_{VT}	$D = 12\frac{f_\rho g_\rho}{2M}(p\theta_\rho - 2p'\phi_\rho)$		

Table 3.2: The functions A_κ, B_κ, C_κ and D.

The various quantities A, B, C, D account for the contributions from the various mesons κ projected on the hatted operators (3.137), whereas the factor $f_{q,q'}$ denotes the isospin factor for the Fock terms which is

$$f_{q,q'} = \begin{cases} \delta_{q,q'} & \text{for } \sigma, \omega, \\ 2 - \delta_{q,q'} & \text{for } \delta, \pi, \rho. \end{cases} \tag{3.142}$$

The expression D comes from cross vector–tensor ρ–N coupling. The functions A, B, C, D are specified in Table 3.2 and depend on the following expressions

$$\begin{aligned} \theta_\kappa(p,p') &= \ln\left[\frac{m_\kappa^2 + (p+p')^2}{m_\kappa^2 + (p-p')^2}\right], \\ \phi_\kappa(p,p') &= \frac{p^2 + p'^2 + m_\kappa^2}{4pp'}\theta_\kappa(p,p') - 1. \end{aligned} \tag{3.143}$$

These expressions account for the removal of the zero–range interactions for the pion and the ρ–meson. From the variation of the potential energy density with respect to the Dirac spinors

$$\Sigma_q(p)u(p,s,q) = \frac{\delta}{\delta\bar{u}(p,s,q)}\big[\langle V^H\rangle + \langle V^F\rangle\big], \tag{3.144}$$

the self–energy is obtained, which consists of the general parts

$$\begin{aligned} \Sigma_{S,q}(p) &= \Sigma_{S,q}^H + \Sigma_{S,q}^F(p) \\ \Sigma_{0,q}(p) &= \Sigma_{0,q}^H + \Sigma_{0,q}^F(p) + \Sigma_R \\ \Sigma_{V,q}(p) &= \Sigma_{V,q}^F(p). \end{aligned} \tag{3.145}$$

The Hartree and Fock self–energy contributions reads

$$
\begin{aligned}
\Sigma^{H}_{S,q} &= -\frac{1}{2}\left(\frac{g_\sigma}{m_\sigma}\right)^2\rho^s - \frac{1}{2}\left(\frac{g_\delta}{m_\delta}\right)^2\rho^s_3\tau_3, \\
\Sigma^{F}_{S,q}(p) &= \frac{1}{2}\sum_{q'}\frac{1}{(4\pi)^2}\frac{1}{p}\int \eta_{q'}(p')\,p'\,dp' \\
&\qquad \Big[\hat{M}_{q'}(p')\sum_\kappa f_{q,q'}B_\kappa(p,p') + \tfrac{1}{2}\hat{P}_{q'}(p')f_{q,q'}D(p,p')\Big], \\
\Sigma^{H}_{0,q} &= \frac{1}{2}\left(\frac{g_\omega}{m_\omega}\right)^2\rho + \frac{1}{2}\left(\frac{g_\rho}{m_\rho}\right)^2\rho_3\tau_3, \\
\Sigma^{F}_{0,q}(p) &= \frac{1}{2}\sum_{q'}\frac{1}{(4\pi)^2}\frac{1}{p}\int \eta_{q'}(p')\,p'\,dp'\sum_\kappa f_{q,q'}A_\kappa(p,p'), \\
\Sigma^{F}_{V,q}(p) &= \frac{1}{2}\sum_{q'}\frac{1}{(4\pi)^2}\frac{1}{p}\int \eta_{q'}(p')\,p'\,dp' \\
&\qquad \Big[\hat{P}_{q'}(p')\sum_\kappa f_{q,q'}C_\kappa(p,p') + \tfrac{1}{2}\hat{M}_{q'}(p')f_{q,q'}D(p,p')\Big]. \qquad (3.146)
\end{aligned}
$$

The rearrangement self–energy contribution is an additional term from the variational principle and arises from the density dependence of the coupling constants

$$
\begin{aligned}
\Sigma^{H}_{R} &= -\frac{1}{2}\frac{\partial g_\sigma}{\partial\rho}\frac{g_\sigma}{m^2_\sigma}(\rho^s)^2 - \frac{1}{2}\frac{\partial g_\delta}{\partial\rho}\frac{g_\delta}{m^2_\delta}(\rho^s_3)^2 + \frac{1}{2}\frac{\partial g_\omega}{\partial\rho}\frac{g_\omega}{m^2_\omega}\rho^2 + \frac{1}{2}\left(\frac{g_\rho}{m_\rho}\right)^2\rho^2_3, \\
\Sigma^{F}_{R} &= \frac{\partial g_\sigma}{\partial\rho}\frac{1}{g_\sigma}\sum_q\frac{1}{\pi^2}\int \eta_q(p)\,p^2dp\left[\hat{M}_q(p)\Sigma^{\sigma,F}_{S,q}(p) + \Sigma^{\sigma,F}_{0,q}(p) + \hat{P}_q(p)\Sigma^{\sigma,F}_{V,q}(p)\right] \\
&\quad + \frac{\partial g_\delta}{\partial\rho}\frac{1}{g_\delta}\sum_q\frac{1}{\pi^2}\int \eta_q(p)\,p^2dp\left[\hat{M}_q(p)\Sigma^{\delta,F}_{S,q}(p) + \Sigma^{\delta,F}_{0,q}(p) + \hat{P}_q(p)\Sigma^{\delta,F}_{V,q}(p)\right] \\
&\quad + \frac{\partial f_\pi}{\partial\rho}\frac{1}{f_\pi}\sum_q\frac{1}{\pi^2}\int \eta_q(p)\,p^2dp\left[\hat{M}_q(p)\Sigma^{\pi,F}_{S,q}(p) + \Sigma^{\pi,F}_{0,q}(p) + \hat{P}_q(p)\Sigma^{\pi,F}_{V,q}(p)\right] \\
&\quad + \frac{\partial g_\omega}{\partial\rho}\frac{1}{g_\omega}\sum_q\frac{1}{\pi^2}\int \eta_q(p)\,p^2dp\left[\hat{M}_q(p)\Sigma^{\omega,F}_{S,q}(p) + \Sigma^{\omega,F}_{0,q}(p) + \hat{P}_q(p)\Sigma^{\omega,F}_{V,q}(p)\right] \\
&\quad + \frac{\partial g_\rho}{\partial\rho}\frac{1}{g_\rho}\sum_q\frac{1}{\pi^2}\int \eta_q(p)\,p^2dp\left[\hat{M}_q(p)\Sigma^{\rho_V,F}_{S,q}(p) + \Sigma^{\rho_V,F}_{0,q}(p) + \hat{P}_q(p)\Sigma^{\rho_V,F}_{V,q}(p)\right] \\
&\quad + \frac{\partial f_\rho}{\partial\rho}\frac{1}{f_\rho}\sum_q\frac{1}{\pi^2}\int \eta_q(p)\,p^2dp\left[\hat{M}_q(p)\Sigma^{\rho_T,F}_{S,q}(p) + \Sigma^{\rho_T,F}_{0,q}(p) + \hat{P}_q(p)\Sigma^{\rho_T,F}_{V,q}(p)\right] \\
&\quad + \left(\frac{\partial g_\rho}{\partial\rho}\frac{1}{g_\rho} + \frac{\partial f_\rho}{\partial\rho}\frac{1}{f_\rho}\right)\sum_q\frac{1}{\pi^2}\int \eta_q(p)\,p^2dp\left[\hat{M}_q(p)\Sigma^{\rho_{VT},F}_{S,q}(p) + \hat{P}_q(p)\Sigma^{\rho_{VT},F}_{V,q}(p)\right], \qquad (3.147)
\end{aligned}
$$

where $\Sigma^{\kappa,F}_{S,q}(q)$ $\Sigma^{\kappa,F}_{0,q}(q)$ and $\Sigma^{\kappa,F}_{V,q}(q)$ are the self–energy contributions from the meson

κ, which are obtained by restricting the Fock self-energy terms in equation (3.146) to the specified meson.

The calculation has to be performed self–consistently. From the self–energy contributions the starred and hatted functions are obtained. These have to be inserted into the self–energy calculation and after sufficient iterations a stable result is obtained. Finally the single–particle energy $E_q(p)$ can be determined from the self–energies by

$$E_q(p) = E_q^*(p) + \Sigma_{0,q}(p), \tag{3.148}$$

from which we obtain the chemical potential μ_q by inserting the Fermi momentum $p_{F,q}$

$$\mu_q = E_q^*(p_{F,q}) + \Sigma_{0,q}(p_{F,q}). \tag{3.149}$$

The kinetic energy part E_q^* already contains the contributions of the scalar and space–like vector self–energy.

Chapter 4

Pairing

Various properties of a neutron star are very sensitive to the occurrence of pairing correlations. For example the superfluidity of nuclear matter influences the rotation of the star and the neutrino opacity. Therefore possible effects of pairing are included in all calculations. In this chapter, first the BCS approach is introduced following [RS80], then we pay attention to the application together with the Hartree–Fock approach and finally pairing in connection with finite temperature is discussed.

4.1 The Standard BCS Approach

The approach got its name from Bardeen, Cooper and Schrieffer, who determined the ground state of a superconductor [BCS57]. The BCS wave function for an even–even nucleus is represented in the following way

$$|\mathrm{BCS}\rangle = \prod_{\alpha>0}(u_\alpha + v_\alpha c_\alpha^\dagger c_{\bar{\alpha}}^\dagger)|0\rangle, \tag{4.1}$$

where the u_α and v_α are variational parameters and denote the occupation properties of the paired state $(\alpha, \bar{\alpha})$. The states α and $\bar{\alpha}$ are conjugated, e.g. the conjugate state is the time–reversed one. By normalization of the BCS state the parameters u_α and v_α have to obey

$$|u|^2 + |v|^2 = 1. \tag{4.2}$$

Then a many–body Hamiltonian is introduced

$$H = \sum_{\alpha_1\alpha_2 \gtrless 0} \langle\alpha_1|T|\alpha_2\rangle c_{\alpha_1}^\dagger c_{\alpha_2} + \frac{1}{4}\sum_{\alpha_1\alpha_2\alpha_3\alpha_4 \gtrless 0} \langle\alpha_1\alpha_2|\bar{V}|\alpha_3\alpha_4\rangle c_{\alpha_1}^\dagger c_{\alpha_2}^\dagger c_{\alpha_4} c_{\alpha_3}. \tag{4.3}$$

The parameters u_α and v_α in the BCS ansatz 4.1 have to be determined by minimizing the energy while keeping the particle number at the desired value N

$$\langle \mathrm{BCS}|\hat{N}|\mathrm{BCS}\rangle = 2\sum_{\alpha>0} v_\alpha^2 = N. \tag{4.4}$$

Therefore a Lagrange multiplier λ is introduced and the variational Hamiltonian gets

$$H' = H - \lambda\hat{N}. \tag{4.5}$$

Since λ accounts for the variation of the particle number N its physical meaning is the Fermi energy ε_F or the chemical potential μ. For the calculation of energy in connection with H' the term λN has to be added. Unfortunately the particle number is not conserved any more but has an uncertainty of

$$(\Delta N)^2 = 4\sum_{\alpha>0} u_\alpha^2 v_\alpha^2. \tag{4.6}$$

To remove this uncertainty of the particle number, projection techniques are necessary, which are too cumbersome in the present application [CMF78, Sm04].
Applying the BCS state the expectation value of H' is evaluated by

$$\begin{aligned}\langle \mathrm{BCS}|H'|\mathrm{BCS}\rangle = &\sum_{\alpha \gtrless 0}\Big\{\big(\langle\alpha|T|\alpha\rangle - \lambda\big)v_\alpha^2 + \frac{1}{2}\sum_{\alpha' \gtrless 0}\langle\alpha\alpha'|\bar{V}|\alpha\alpha'\rangle v_\alpha^2 v_{\alpha'}^2\Big\}\\ &+ \sum_{\alpha\alpha'>0}\langle\alpha\bar{\alpha}|\bar{V}|\alpha'\bar{\alpha}'\rangle u_\alpha v_\alpha u_{\alpha'} v_{\alpha'}.\end{aligned} \tag{4.7}$$

The variation of the above expectation value yields the BCS equations

$$2\tilde{\varepsilon}_\alpha u_\alpha v_\alpha + \Delta_\alpha(v_\alpha^2 - u_\alpha^2) = 0, \qquad \alpha > 0 \tag{4.8}$$

with the modified single–particle energies

$$\tilde{\varepsilon}_\alpha = \frac{1}{2}\Big(\langle\alpha|T|\alpha\rangle + \langle\bar{\alpha}|T|\bar{\alpha}\rangle + \sum_{\alpha' \gtrless 0}\big(\langle\alpha\alpha'|\bar{V}|\alpha\alpha'\rangle + \langle\bar{\alpha}\alpha'|\bar{V}|\bar{\alpha}\alpha'\rangle\big)v_{\alpha'}^2\Big) - \lambda \tag{4.9}$$

and the pairing gap

$$\Delta_\alpha = -\sum_{\alpha'>0}\langle\alpha\bar{\alpha}|\bar{V}|\alpha'\bar{\alpha}'\rangle u_{\alpha'} v_{\alpha'}. \tag{4.10}$$

The normalization condition (4.8) and the BCS equations (4.8) lead to formulas for u_α and v_α

$$\begin{aligned} v_\alpha^2 &= \frac{1}{2}\left(1 - \frac{\tilde{\varepsilon}_\alpha}{E_\alpha}\right)\\ u_\alpha^2 &= \frac{1}{2}\left(1 + \frac{\tilde{\varepsilon}_\alpha}{E_\alpha}\right), \end{aligned} \tag{4.11}$$

where E_α identifies the quasi–particle energy

$$E_\alpha = \sqrt{\tilde{\varepsilon}_\alpha^2 + \Delta_\alpha^2}. \tag{4.12}$$

Together with the particle number condition (4.4) the BCS equations (4.9), (4.10) and (4.11) can be solved by a self–consistent iteration. Inserting (4.11) into (4.10) yields the gap equation

$$\Delta_\alpha = -\frac{1}{2}\sum_{\alpha'>0}\langle\alpha\bar{\alpha}|\bar{V}|\alpha'\bar{\alpha}'\rangle\frac{\Delta_{\alpha'}}{E_{\alpha'}}, \tag{4.13}$$

which is often employed to evaluate the the paring gap Δ_α.
A generalization of the BCS approach is the Hartree–Fock–Bogoliubov framework which solves the gap equation and the Hartree–Fock equation simultaneously. However, if time reversal invariance together with a monopole pairing force is applied, the coupled Hartree–Fock plus BCS equations already solve the full Hartree–Fock–Bogoliubov problem. This is actually the case in our calculations since we deal with even–even nuclear systems and a zero range pairing force derived from NN potentials.

4.2 The Pairing Application

Special attention was focused on isopin $T = 1$ pairing for nucleon pairs with total momentum equal to zero in ${}^1S_0$ partial wave like in an earlier approach in a spherical box [MMM04]. Using the standard BCS approach the pairing gap Δ for a pair of nucleons with momenta k and $-k$ is obtained by solving the gap equation (4.13) in nuclear matter [KM+03]

$$\Delta(k) = -\frac{2}{\pi}\int_0^\infty dk' k'^2\, V(k,k')\frac{\Delta(k')}{2\sqrt{(\varepsilon(k')-\varepsilon_F)^2+\Delta(k')^2}}. \tag{4.14}$$

Here $V(k,k')$ denotes the matrix elements of the NN interaction in the ${}^1S_0$ partial wave, $\varepsilon(k)$ the single particle energy for a nucleon with momentum k and ε_F the Fermi energy.
Instead of using the matrix elements of a realistic NN interaction, which is fit to the scattering data, we have decided to use a density dependent zero range effective interaction, which was proposed by Bertsch and Esbensen [BE91]:

$$V(\mathbf{r}_1,\mathbf{r}_2) = V_0\left(1-\eta\left(\frac{\rho(\mathbf{r}_1)}{\rho_0}\right)^\kappa\right)\delta(\mathbf{r}_1-\mathbf{r}_2). \tag{4.15}$$

Garrido et al. derived in [GS+99] parameters for such effective interactions from realistic NN interactions. They found the effective pairing force parameters $V_0 = 481\text{MeV fm}^3$, $\eta = 0.7$ and $\kappa = 0.45$. The saturation density of nuclear matter is denoted by $\rho_0 = 0.16$. The integral in the gap equation (4.14) needs to be truncated by a cut–off parameter which is $\varepsilon_c = 60$ MeV.

For simplicity the isospin quantum number is omitted in the following description of pairing for the spatial representation and in asymmetric nuclear matter. The occupation probabilities η_α for the waves of Skyrme or relativistic Hartree-Fock are evaluated by

$$v_\alpha^2 = \frac{1}{2}\Big(1 - \frac{\varepsilon_\alpha - \varepsilon_F}{E_\alpha}\Big), \tag{4.16}$$

$$u_\alpha^2 = \frac{1}{2}\Big(1 + \frac{\varepsilon_\alpha - \varepsilon_F}{E_\alpha}\Big), \tag{4.17}$$

with the quasi–particle energies

$$E_\alpha = \sqrt{(\varepsilon_\alpha - \varepsilon_F)^2 + \Delta_\alpha^2}, \tag{4.18}$$

in which the state depending pairing gap Δ_α, the single particle energy ε_α and the Fermi energy ε_F enters.

It is convenient to define the normal and anomalous occupation factors for the single particle states which are in the standard BCS approach

$$\eta_\alpha = v_\alpha^2, \qquad \zeta_\alpha = u_\alpha v_\alpha. \tag{4.19}$$

From this occupation factors and the single–particle wave function ψ_α we can obtain the anomalous density

$$\chi(\mathbf{r}) = \tfrac{1}{2}\sum_\alpha \zeta_\alpha \left|\psi_\alpha(\mathbf{r})\right|^2. \tag{4.20}$$

The summation has to be truncated by the energy cut–off ε_c. For large cut–off energies a sharp cut is used, while in finite nuclei often a smooth cut–off guided by the factor

$$f_{c,\alpha} = \frac{1}{1 + \exp[(\varepsilon_\alpha - (\varepsilon_F + \varepsilon_c))/\Delta\varepsilon]} \tag{4.21}$$

is used in connection with a low cut–off energy $\varepsilon_c = 5MeV$ and the smear out range $\Delta\varepsilon = \varepsilon_c/10$ [SR07]. For a zero range pairing interaction as the one of (4.15) a local gap function can be defined

$$\Delta(\mathbf{r}) = -V(\mathbf{r})\,\chi(\mathbf{r}), \tag{4.22}$$

from which the state–dependent pairing gaps are calculated

$$\Delta_\alpha = \int d^3\mathbf{r}\ \Delta(\mathbf{r})\ |\psi_\alpha(\mathbf{r})|^2\,. \tag{4.23}$$

The BCS–equations has to be solved in a self–consistent procedure fixing the Fermi energy ε_F by the particle number condition for N nucleons:

$$N = \sum_\alpha \eta_\alpha. \tag{4.24}$$

Finally the the pairing energy E_{pair} is obtained from the state depending pairing gaps

$$E_{pair} = \frac{1}{2}\sum_{\alpha,q} \Delta_\alpha \zeta_\alpha, \tag{4.25}$$

where the sum is taken over both isospin projections $q = p, n$.
In asymmetric nuclear matter the pairing description is similar to that in [FT$^+$00] and the gap equation employing the pairing force (4.15) is solved in momentum space together with the parameters mentioned above.
The gap equation reduces for a density dependent pairing force to

$$\Delta(k_F) = -V(k_F) \int_0^{k_c} \frac{d^3k}{(2\pi)^3}\,\frac{\Delta(k_F)}{2E(k)} \tag{4.26}$$

with the quasi–particle Energy

$$E(k) = \sqrt{(\varepsilon(k) - \varepsilon_F)^2 + \Delta(k_F)^2}. \tag{4.27}$$

The cut–off momentum k_c corresponds to ε_c via the appropriate energy-momentum relation and the Fermi momentum k_F to the density. The single particle energy relative to the Fermi level is evaluated by

$$\tilde{\varepsilon}(k) = \varepsilon(k) - \varepsilon_F, \tag{4.28}$$

where $\varepsilon(k)$ specifies the single particle energy in nuclear matter depending on the momentum k and ε_F the corresponding Fermi energy. We introduce the anomalous density χ as

$$\chi = \int_0^{k_c} \frac{d^3k}{(2\pi)^3}\,\zeta(k), \tag{4.29}$$

with the anomalous occupation factor ζ, which is evaluated using the appropriate energy-momentum relation. The correspondence $\Delta(k_F) = u(k)v(k)E(k)$ obtained from the definition of the occupation factors leads the paring gap

$$\Delta(k_F) = -V(k_F)\,\chi. \tag{4.30}$$

And finally we obtain the pairing energy per particle by

$$\frac{E_{\text{pair}}}{N} = -\frac{3}{8}\frac{\Delta^2(k_F)}{\varepsilon_F}. \tag{4.31}$$

The parameters of the pairing force in equation (4.15) were originally derived by assuming a Gogny force [GS+99]. Adjusting slightly the parameter V_0 the pairing results of Garrido et al. can be reproduced in connection with the present Skyrme and relativistic Hartree–Fock approaches.

4.3 Pairing and Finite Temperature

The general framework for pairing effects together with finite temperature in the mean–field is the finite temperature Hartree–Fock–Bogoliubov approach. In the following the derivation of this approach is outlined according to [Gdm81, DA03]. The theory is based on a Hamiltonian

$$H = \sum_{\alpha\beta}\langle\alpha|\mathcal{T}|\beta\rangle\, c^\dagger_\alpha c_\beta + \frac{1}{4}\sum_{\alpha\beta\gamma\delta}\langle\alpha\beta|\bar{V}|\gamma\delta\rangle c^\dagger_\alpha c^\dagger_\beta c_\delta c_\gamma, \tag{4.32}$$

where $\mathcal{T}$ is the kinetic energy operator and $\bar{V}$ the antisymmetrized matrix elements of a two–body interaction. The quasi–particle creation $\alpha^\dagger_\alpha$ and annihilation α_α operators are obtained from the single-particle operators $c^\dagger_\alpha$ and c_α by the Bogoliubov transformation which is given in matrix form by

$$\begin{pmatrix}\alpha^\dagger \\ \alpha\end{pmatrix} = \begin{pmatrix}U & V \\ V^* & U^*\end{pmatrix}\begin{pmatrix}c^\dagger \\ c\end{pmatrix}, \tag{4.33}$$

where the transformation matrices U and V have the properties

$$UU^\dagger + VV^\dagger = \mathbb{1}, \qquad UV^T + VU^T = 0, \tag{4.34}$$

with $\mathbb{1}$ the unit matrix and ^{T} the transposing operation. Rewriting the Hamiltonian in terms of quasi–particles and truncating it to second order the Hartree–Fock–Bogoliubov Hamiltonian is obtained

$$H - \mu\hat{N} \approx H_{HFB} = E_0 + \sum_\alpha E_\alpha \alpha^\dagger_\alpha \alpha_\alpha. \tag{4.35}$$

In this equation μ is the chemical potential, $\hat{N}$ the particle number operator, E_α the quasi–particle energies and E_0 the ground state energy of the quasi–particle vacuum

$$\alpha_\alpha|0\rangle = 0. \tag{4.36}$$

The Hartree–Fock–Bogoliubov approach is now considered in thermal equilibrium. Therefore we have to minimize the grand potential Ω:

$$\Omega = E - TS - \mu N \tag{4.37}$$

with the total energy E, the entropy S and particle number N. The grand partition function Z takes the form

$$Z = \mathrm{Tr}[e^{-\beta(H-\mu\hat{N}}] \tag{4.38}$$

where $\beta = T^{-1}$ denotes the inverse temperature. The variation of the grand potential implies the so–called density operator $\mathcal{D}$

$$\mathcal{D} = Z^{-1}e^{-\beta(H-\mu\hat{N})} \tag{4.39}$$

which has the properties

$$\mathrm{Tr}\mathcal{D} = 1, \qquad \frac{\delta\Omega}{\delta\mathcal{D}} = 0. \tag{4.40}$$

Expectation values of any operator O have to be evaluated applying the density operator $\mathcal{D}$

$$\langle O\rangle = \mathrm{Tr}(\mathcal{D}O), \tag{4.41}$$

which averages over the grand canonical ensemble. Therefore the exact Hamiltonian in the density operator $\mathcal{D}$ is replaced by the HFB Hamiltonian (4.35). The HFB approximation of the density operator factorizes and reads

$$\mathcal{D}_{HFB} = \prod_{\alpha}[n_\alpha\alpha_\alpha^\dagger\alpha_\alpha + (1-n_\alpha)\alpha_\alpha^\dagger\alpha_\alpha] \tag{4.42}$$

where n_α denotes the quasi–particle occupation number for finite temperature

$$n_\alpha = \langle\alpha_\alpha^\dagger\alpha_\alpha\rangle = \frac{1}{e^{\beta E_\alpha}+1}. \tag{4.43}$$

The occupation of quasi–particles is guided by the Fermi–Dirac distribution as usual for independent particle approximations. A more elaborate approach in the Brueckner–Hartree–Fock framework going beyond mean–field can be found in [RPRM06]. The next step is to derive the FT–HFB equations. The generalized particle density matrix R is related to the generalized quasi–particle density matrix Q by the Bogoliubov transformation as

$$R = \mathcal{U}^\dagger Q\mathcal{U} \tag{4.44}$$

with the matrices

$$R = \begin{pmatrix} \rho & \tau \\ -\tau^* & 1-\rho^* \end{pmatrix}, \qquad Q = \begin{pmatrix} q & t \\ -t^* & 1-q^* \end{pmatrix} = \begin{pmatrix} n & 0 \\ 0 & 1-n \end{pmatrix}, \tag{4.45}$$

with the transformation matrix

$$\mathcal{U} = \begin{pmatrix} U & V \\ V^* & U^* \end{pmatrix}, \qquad \mathcal{U}\mathcal{U}^\dagger = \mathbb{1}. \tag{4.46}$$

The matrix elements of the single–particle density matrix ρ and the pairing tensor τ within the FT-HFB approximation are evaluated as

$$\rho_{\alpha\beta} = \langle c^\dagger_\alpha c_\beta \rangle, \qquad \tau_{\alpha\beta} = \langle c_\alpha c_\beta \rangle, \tag{4.47}$$

while those of the quasi–particle matrix q are given in terms of the quasi–particle occupation number since

$$q_{\alpha\beta} = \langle \alpha^\dagger_\alpha \alpha_\beta \rangle = \delta_{\alpha\beta} n_\alpha, \qquad t_{\alpha\beta} = \langle \alpha_\alpha \alpha_\beta \rangle = 0, \tag{4.48}$$

which follows from the HFB approximation. Using the inverse Bogoliubov transformation, the particle densities are obtained as

$$\rho = U^T n U^* + V^\dagger (1-n) V, \qquad \tau = U^T n V^* + V^\dagger (1-n) U. \tag{4.49}$$

By minimizing the grand potential Ω, Goodman has derived in [Gdm81] the FT-HFB equations in the following form

$$\begin{pmatrix} \mathcal{H} & \Delta \\ -\Delta^* & -\mathcal{H}^* \end{pmatrix} \begin{pmatrix} U_\alpha \\ V_\alpha \end{pmatrix} = E_\alpha \begin{pmatrix} U_\alpha \\ V_\alpha \end{pmatrix}, \tag{4.50}$$

where

$$\mathcal{H} = \mathcal{T} - \mu + \Gamma, \qquad \Gamma_{\alpha\beta} = \sum_{\gamma\delta} \langle \alpha\gamma | V | \beta\delta \rangle \rho_{\delta\gamma}, \qquad \Delta_{\alpha\beta} = \frac{1}{2} \sum_{\gamma\delta} \langle \alpha\beta | V | \gamma\delta \rangle \tau_{\gamma\delta}. \tag{4.51}$$

The total energy E, the entropy S and particle number N are given as

$$E = \mathrm{Tr}[(\mathcal{T} + \frac{1}{2}\Gamma)\rho + \frac{1}{2}\Delta\tau^\dagger], \tag{4.52}$$

$$S = -\sum_\alpha [n_\alpha \ln(n_\alpha) + (1-n_\alpha)\ln(1-n_\alpha)], \tag{4.53}$$

$$N = \mathrm{Tr}\rho, \tag{4.54}$$

from which the grand potential Ω is evaluated.

In case of time–reversal symmetry together with a monopole pairing force the FT–HFB equations become diagonal and reduce to FT–BCS equations with the gap equation

$$\Delta_\alpha = -\frac{1}{2}\sum_{\alpha'>0}\langle\alpha\bar{\alpha}|\bar{V}|\alpha'\bar{\alpha}'\rangle(1-2n_{\alpha'})\frac{\Delta_{\alpha'}}{2E_{\alpha'}}, \tag{4.55}$$

where $|\bar{\alpha}\rangle$ denotes the time–reversed state of $|\alpha\rangle$. The quantities u_α, v_α and the quasi–particle energy E_α are the same as in the BCS formalism and hence the relation between occupation factors, pairing gap and quasi–particle energy

$$u_\alpha v_\alpha = \frac{\Delta_\alpha}{2E_\alpha} \tag{4.56}$$

has been used to derive the above gap equation. From the gap equation (4.55) and equation (4.56) the normal and anomalous occupation factors of the Hartree–Fock single particle states can be obtained

$$\eta_\alpha = (1-2n_\alpha)v_\alpha^2 + n_\alpha, \tag{4.57}$$

$$\zeta_\alpha = (1-2n_\alpha)\,u_\alpha v_\alpha. \tag{4.58}$$

Plugging this modified occupation factors into the procedures of section 4.2 instead of those in eq. (4.19) we obtain the self–consistent solution of the FT–BCS equations, which combines the pairing and finite temperature approaches.

Chapter 5

Numerical Procedure

In this chapter we want to take special attention to the numerical details of the triaxial Skyrme Hartree–Fock and relativistic Hartree–Fock calculations. The relativistic code is a further development of the non–relativistic one for the Skyrme calculation and hence the methods are similar. In section 5.1 the discretization of the wave functions and the treatment of differential operators are introduced. Adjacent the integration of the Coulomb field and the meson fields is described in section 5.2. And finally in section 5.3 we pay attention to the *imaginary time step* method, which solves the Hartee–Fock equations.

5.1 Discretization

Various different methods have been developed to solve the Hartree–Fock equations numerically. Frequently the single particle wave functions are expanded in a basis like e.g. the eigenfunctions of an appropriate harmonic oscillator. Then the Hamiltonian is computed as matrix which has to be diagonalized, what is adequate for describing the wave functions for single-particle states, which are deeply bound. For the description of weakly bound or unbound single–particle states, however, an other method should be used since a lot of harmonic oscillator shells have to be considered. This can be cured by employing the eigenstates of a spherical box with an appropriate radius R [MMM04], which can also be considered as a Wigner–Seitz cell for describing periodic systems. These eigenstates are the Bessel functions representing spherical plane waves. Such a spherical box, however, is not suitable for the description of deformed nuclei and nuclear structures as they are expected for the pasta phase in the crust of neutron stars. This, as well as the problems with the boundary

conditions in a spherical WS cell call for a Cartesian WS cell.

In such a Cartesian WS cell some groups used the harmonic oscillator basis expansion method similar to the spherical calculations. In spherical symmetry this is a good method, but in strongly deformed nuclei the states are mixing and a high amount of oscillator shells has to be taken into account. Hence we choose another method: The wave functions are discretized on a spatial mesh. As for a basis expansion the relevant quantities are the oscillator parameter and the number of shells included, for a mesh only the so–called mesh size Δx provides a momentum space truncation. Furthermore the accuracy rises with a smaller mesh size Δx, which denotes the distance between the mesh points in each direction. The obvious disadvantage of a mesh discretization is the huge amount of mesh points, which has to be considered. Therefore one has to compromise the mesh size Δx.

Here a rectangular three–dimensional mesh is used with the same mesh size $\Delta x = 1.0$ fm in each direction. This choice saves calculation time but makes it necessary to use improved numeric algorithms. The momentum space truncation gets $\pi/\Delta x \approx 3.14\ \mathrm{fm}^{-1}$, which is a sufficiently large to handle wave functions up to saturation density and even larger (see e.g. [MHe02]). The box sizes vary from 2×10 fm to 2×16 fm. Applying this technique the wave functions are able to adapt to any kind of nuclear shape with the same accuracy and in addition the whole space of a neutron star can be covered by repeated cells.

The abscissae of the mesh points are $\frac{1}{2}(2n+1)\Delta x$. Such meshs have already been used in time dependent Hartree-Fock approaches and for the study of triaxial deformations ([BF$^+$85] and references therein). Because we intend to model a Wigner–Seitz cell taken out of the crust of a neutron star we impose periodic boundary conditions on the wave functions to get a smooth connection to neighboring cells. This discretization can be used also for finite nuclei, since the densities drop at the boundary to zero and for a sufficiently large box size the mirroring at the boundary has no effect. To save calculation power and memory only the positive coordinates in each direction are calculated and the other values are obtained by appropriate mirroring. This method does not restrict the triaxial deformations.

As initial set of wave functions harmonic oscillator and plane wave functions can be used. It has to be mentioned that some applications require an additional potential for the first few steps, for instance a Wood Saxon potential, to activate the variation. Because HF calculations are conserving initial symmetries [RS80], the ansatz has to be deformed to a nontrivial triaxial shape. In order to get good eigenstates the wave

functions have to satisfy the parity of the eigenstates in three dimensions, especially the eigenstates of orbital angular momentum and spin. According to Serot and Walecka [SW86], the single particle angular momentum operator is defined as

$$\boldsymbol{J} = \boldsymbol{L} + \boldsymbol{S} = \boldsymbol{x} \times \boldsymbol{p} + \tfrac{1}{2}\boldsymbol{\Sigma}. \tag{5.1}$$

Another operator K based on the angular momentum is defined by

$$K = \gamma^0[\boldsymbol{\Sigma} \cdot \boldsymbol{J} - \tfrac{1}{2}] = \gamma^0[\boldsymbol{\Sigma} \cdot \boldsymbol{L} + 1], \tag{5.2}$$

which commutes with the Hamiltonian. With the help of the eigenvalues $(-\kappa)$ of K the spin spherical harmonics reads

$$\Phi_{\kappa m}(\theta, \phi) = \sum_{m_l m_s} \langle l m_l \tfrac{1}{2} m_s | l \tfrac{1}{2} j m \rangle \, Y_{l m_l}(\theta, \phi) \, \chi_{1/2}(m_s), \tag{5.3}$$

where the correspondence between different quantum numbers is given by

$$j = |\kappa| - \tfrac{1}{2}, \qquad l = \begin{cases} \kappa, & \kappa > 0, \\ -(\kappa + 1), & \kappa < 0. \end{cases} \tag{5.4}$$

As already mentioned above, the initial wave set has to have the same parity and mirror properties as the spherical harmonics. Actually the initial harmonic oscillator wave set is chosen to be proportional to the spherical harmonics $Y_{l m_l}(\theta, \phi) \, \chi_{1/2}(m_s)$ in the Skyrme Hartree–Fock code. With this choice a fast convergence is obtained and in case of spherical symmetry they get proportional to the above form by the variation process. In the relativistic Hartree–Fock code the harmonic oscillator ansatz is of the form

$$\psi_\alpha(\boldsymbol{x}) = \psi_{n \kappa m q_\alpha} = \begin{pmatrix} \varphi_{n\kappa}(r, \theta, \phi) \, \Phi_{\kappa m}(\theta, \phi) \\ i \, \chi_{n\kappa}(r, \theta, \phi) \, \Phi_{-\kappa m}(\theta, \phi) \end{pmatrix} \chi_{1/2}(q_\alpha), \tag{5.5}$$

where $\varphi_{n\kappa}$ is a deformed harmonic oscillator wave function and $\chi_{n\kappa}$ is initialized from the upper component by equation (3.120) in the Gram–Schmidt orthonormalization. To decrease the numerical effort we assume two symmetries like in [BF+85]:

- parity

$$\hat{P}\varphi_\alpha(\boldsymbol{r}, s) = \varphi_\alpha(-\boldsymbol{r}, s) = p_\alpha \varphi_\alpha(\boldsymbol{r}, s), \qquad p_\alpha = \pm 1; \tag{5.6}$$

- z–signature

$$\begin{aligned} \exp\{i\pi(\hat{J}_z - \tfrac{1}{2})\}\varphi_\alpha(x, y, z, s) &= \sigma \varphi_\alpha(-x, -y, z, s) \\ &= \lambda_\alpha \varphi_\alpha(x, y, z, s), \qquad \lambda_\alpha = \pm 1. \end{aligned} \tag{5.7}$$

	x=0	y=0	z=0
Re $\varphi_\alpha(\mathbf{r}, +\frac{1}{2})$	$+$	$+$	p_k
Im $\varphi_\alpha(\mathbf{r}, +\frac{1}{2})$	$-$	$-$	p_k
Re $\varphi_\alpha(\mathbf{r}, -\frac{1}{2})$	$-$	$+$	$-p_k$
Im $\varphi_\alpha(\mathbf{r}, -\frac{1}{2})$	$+$	$-$	$-p_k$

Table 5.1: Parity properties of the Pauli spinors with respect to the coordinate planes for the triaxial Skyrme Hartree–Fock approach.

These symmetries still allow triaxial deformations and reduce the calculation to the positive coordinates in each direction. As additional symmetry time–reversal–invariance is assumed for the time–reversed pairs φ_α, and $\varphi_{\bar{\alpha}}$:

$$\varphi_{\bar{\alpha}}(\boldsymbol{r}, s) = (\hat{T}\varphi_\alpha)(\boldsymbol{r}, s) = \sigma\varphi^*_\alpha(\boldsymbol{r}, -s). \tag{5.8}$$

Summarizing these symmetries it is sufficient to solve the HF equations for one wave function of the time–reversed pairs. We choose the positive z–signature orbital in the Skyrme and relativistic Hartree calculations.

From the eigenstates of angular momentum and spin we obtain in connection with the symmetries the mirroring conditions in each direction, which are summarized in the Table 5.1 for the Skyrme Hartree–Fock and in Table 5.2 for the relativistic Hartree–Fock approach. In the triaxial relativistic Hartree–Fock code time reversal symmetry has to be dropped to get the vector currents in the Fock self–energy contributions. Here we include both, the positive and negative z–signature orbitals. The discretized spinors in the code are handled by complex functions. Different parity properties for real and imaginary part as they are found for the $x = 0$ and $y = 0$ plane are referred to by the parity of the real part and the complex conjugation operation.

The iteration is performed with accurate numerical methods. The numerical approximation for nabla ∇ and Laplace operators Δ were improved to 11–point precision. Further it improves precision if expressions with two ∇ operators are converted by partial integration into expressions with Laplace operator, since the latter can be performed numerically without first evaluating first derivatives.

The usual discretization of differential operators is to use the differential quotient

	positive z–signature			negative z-signature		
	$x=0$	$y=0$	$z=0$	$x=0$	$y=0$	$z=0$
Re $\varphi_\alpha(\boldsymbol{x},+\frac{1}{2})$	$+$	$+$	p_α	$-$	$+$	$-p_\alpha$
Im $\varphi_\alpha(\boldsymbol{x},+\frac{1}{2})$	$-$	$-$	p_α	$+$	$-$	$-p_\alpha$
Re $\varphi_\alpha(\boldsymbol{x},-\frac{1}{2})$	$-$	$+$	$-p_\alpha$	$+$	$+$	p_α
Im $\varphi_\alpha(\boldsymbol{x},-\frac{1}{2})$	$+$	$-$	$-p_\alpha$	$-$	$-$	p_α
Re $\chi_\alpha(\boldsymbol{x},+\frac{1}{2})$	$-$	$-$	$-p_\alpha$	$+$	$-$	p_α
Im $\chi_\alpha(\boldsymbol{x},+\frac{1}{2})$	$+$	$+$	$-p_\alpha$	$-$	$+$	p_α
Re $\chi_\alpha(\boldsymbol{x},-\frac{1}{2})$	$+$	$-$	p_α	$-$	$-$	$-p_\alpha$
Im $\chi_\alpha(\boldsymbol{x},-\frac{1}{2})$	$-$	$+$	p_α	$+$	$+$	$-p_\alpha$

Table 5.2: Parity properties of the Dirac spinor with respect to the coordinate planes for the triaxial relativistic approach.

on the mesh for approximation:

$$\frac{\partial}{\partial x} f(x_i) \approx \left(\frac{\partial}{\partial x}\right)_{\text{num}} f(x_i) = \frac{1}{2\Delta x}\left(f_{i+1} - f_{i-1}\right). \tag{5.9}$$

This method has some disadvantages which are crucial in 3D–calculations. In order to enhance precision one has to shrink the mesh size what means an increase of mesh points to the third power. The same occurs with calculation time and hence this is an unacceptable method. However, if the error of this operator is analyzed for functions with $f(x) = x^n$, one finds that it is exact up to second order. The idea is now to combine formulas of type (5.9) in a way that the error terms cancel out up to a certain $n_0 \in \mathbb{N}$. The ansatz for the numerical approximation of the derivatives on an equidistant mesh with the points x_i and $f_i = f(x_i)$ is for the first derivative

$$\frac{\partial}{\partial x} f(x_i) \approx \left(\frac{\partial}{\partial x}\right)_{\text{num}} f(x_i) = \sum_{j=1}^{N} a_j \frac{1}{2j\Delta x}\left(f_{i+j} - f_{i-j}\right), \tag{5.10}$$

with $N = 5$ for an 11–point formula and a_j the coefficients of the formula. Requiring that the numerical approximation formula provides an exact result up to a certain power $n_0 \in \mathbb{N}$ we obtain a linear equation. Inserting the result in the ansatz we

finally obtain

$$\left(\frac{\partial}{\partial x}\right)_{\text{num}} f(x_i) \tag{5.11}$$
$$= \frac{1}{\Delta x}\Big(\tfrac{1}{19860}(11f_{i+5} - 4500f_{i+2} + 16350f_{i+1} - 16350f_{i-1} + 4500f_{i-2} - 11f_{i-5}) + \tfrac{1}{55608}(-445f_{i+4} + 2950f_{i+3} - 2950f_{i-3} + 445f_{i-4})\Big).$$

For the second derivative used in the Laplacian the ansatz is

$$\frac{\partial^2}{\partial x^2} f(x_i) \approx \left(\frac{\partial^2}{\partial x^2}\right)_{\text{num}} f(x_i) = \sum_{j=1}^{N} a_j \, \frac{1}{(j\,\Delta x)^2} \, \left(f_{i+j} - 2f_i + f_{i-j}\right). \tag{5.12}$$

and the numerical approximation formula gets

$$\left(\frac{\partial^2}{\partial x^2}\right)_{\text{num}} f(x_i) \tag{5.13}$$
$$= \frac{1}{(\Delta x)^2}\Big(\tfrac{1}{49650}(11f_{i+5} - 11250f_{i+2} + 81750f_{i+1} + 81750f_{i-1} - 11250f_{i-2} + 11f_{i-5}) - \tfrac{1729639}{595800}f_i + \tfrac{1}{333648}(-1335f_{i+4} + 11800f_{i+3} + 11800f_{i-3} - 1335f_{i-4})\Big).$$

For application the boundary conditions has to be considered. This is done by mirroring the functions according to parity rules. This numerical derivative operators are applied to all kind of functions which are evaluated in the code.

5.2 Field equations

In this section we pay special attention to the Coulomb field and the meson fields. Let us turn first to the Coulomb field. In case of the Wigner Seitz cell calculations charge neutrality is assumed and electrons are taken into account as relativistic Fermi gas, which contributes to the charge density $\rho_C(\boldsymbol{r}) = \rho_p(\boldsymbol{r}) - \rho_e(\boldsymbol{r})$. For the calculation of finite nulcei the electrons are not taken into account and the electron charge density gets zero.

There are different methods to solve the Poisson equation

$$-\Delta V_C(\boldsymbol{r}) = 4\pi e^2 \rho_C(\boldsymbol{r}). \tag{5.14}$$

It turned out that the numerically most accurate and stable method is the integration applying the Green's function for this problem

$$V_C(\boldsymbol{r}) = e^2 \int_V dr'^3\, \rho_C(\boldsymbol{r'})\, \frac{1}{|\boldsymbol{r} - \boldsymbol{r'}|}. \tag{5.15}$$

Unfortunately, this integral has lots of singularities, but it can be rewritten. First, the Green's function is written as [Vau73]:

$$\frac{1}{|\boldsymbol{r} - \boldsymbol{r'}|} = \tfrac{1}{2}\, \Delta_{\boldsymbol{r'}} |\boldsymbol{r} - \boldsymbol{r'}|. \tag{5.16}$$

Then the integral is transformed by Green's theorem for scalar functions f and g defined on a Volume V with closed surface $A = \partial V$ [Jac75]:

$$\int_V dV\, (f\, \Delta g) - \int_V dV\, (g\, \Delta f) = \oint_{A=\partial V} \boldsymbol{dA} \cdot (f\, \boldsymbol{\nabla} g - g\, \boldsymbol{\nabla} f). \tag{5.17}$$

Identifying and $f = \rho_C(\boldsymbol{r'})$ and $g = \frac{1}{2}|\boldsymbol{r} - \boldsymbol{r'}|$ the final result gets

$$\begin{aligned} V_C(\boldsymbol{r}) = {} & \frac{1}{2} e^2 \int_V dr'^3\, \Delta \rho_C(\boldsymbol{r'})\, |\boldsymbol{r} - \boldsymbol{r'}| \\ & + \frac{1}{2} e^2 \oint_{A=\partial V} \boldsymbol{dA} \cdot \left(\rho_C(\boldsymbol{r'})\, \boldsymbol{\nabla}_{\boldsymbol{r'}} |\boldsymbol{r} - \boldsymbol{r'}| \; - \; |\boldsymbol{r} - \boldsymbol{r'}|\, \boldsymbol{\nabla}_{\boldsymbol{r'}} \rho_C(\boldsymbol{r'}) \right), \end{aligned} \tag{5.18}$$

which has no singularities. Altogether the result of this transformation behaves very well in numerical calculations and the numerical result is practically the same as the exact one. For finite nuclei it is possible to drop the boundary integrals, a feature which has been used already by Vautherin in axial symmetric calculations [Vau73]. The charge screening effect is included in the code by modifying the electron single particle energy ε_e with the Coulomb field V_C:

$$\varepsilon_e(p, \boldsymbol{r}) = \sqrt{m_e^2 + p^2} - V_C(\boldsymbol{r}), \tag{5.19}$$

where m_e denotes the electron mass and p the momentum. The occupation probability including thermal effects reads

$$n(p, \boldsymbol{r}) = \frac{1}{1 + \exp[\beta(\varepsilon_e(p, \boldsymbol{r}) - \mu_e)]}, \tag{5.20}$$

from which the electron density is obtained by an integral in momentum space

$$\rho_e(\boldsymbol{r}) = 2 \int \frac{d^3p}{(2\pi)^3}\, n(p, \boldsymbol{r}). \tag{5.21}$$

The electron chemical potential μ_e is determined by searching the root of the electron number condition

$$N_e = \int d^3r\, \rho_e(\boldsymbol{r}), \tag{5.22}$$

what provides concurrently the screened electron density ρ_e in a self–consistent iteration guided by the equations (5.19- 5.22). For zero temperature the charge screening has been investigated by Maruyama et al. in [MT$^+$05].

The meson fields are obtained by solving the Helmholtz equations for the various mesons with periodic boundary conditions (see e.g. equation (3.54)). A finite difference scheme is applied, for which the discretization of the Helmholtz equation gets a linear equation with a sparse matrix containing the boundary conditions. There are several reasons why the numerical solution of the Helmholtz equation is much faster than the integration over an exponential function and a denominator containing lots of singularities. The first one is that the integration over the discretized space has to be repeated for every calculated point, while the partial differential equation is solved at once for the whole space. Note that in our problem the number of necessary iterations for the differential equation are much less than the amount of mesh points. The second reason is that the squared meson masses which occur in the differential operator enhance the convergence of the discretized Helmholtz equations significantly since the main interference between the mesh points is restricted to some fm distance. Additional reasons arise from the integrals which should be solved instead: the singularities require additional mesh points or interpolation techniques. Testing both methods numerically has confirmed that solving the Helmholtz equation is faster and more precise than evaluating the corresponding integrals.

In this work the *conjugate gradient iterator* is applied, which has the advantage that there is no operator matrix needed but only the operation of the differential operator on the meson field. This saves a lot of memory, in fact there have only to be saved 4 vectors for some functions represented on the mesh. The method is used with diagonal preconditioning which provides a solution already within seconds. It has to be mentioned that calculation times of usual methods like the Gauss–Seidel algorithm are totally out of range; such algorithms need more time for the evaluation of a meson field than one all over Hartree–Fock step lasts.

The conjugate gradient method has been developed to solve linear equations [HSt52, Rcg71] and is now applied to a whole variety of numerical problems for example to finite element solver for elliptic boundary value problems on an adaptive mesh with

hierarchical basis preconditioning, which provides a very fast algorithm [Yse86]. The main idea of the conjugate gradient step is to solve the linear equation $Ax - b = 0$ with the linear operator A and a right hand side vector b by searching the minimum of the quadratic form

$$q(x) = \tfrac{1}{2} x^T A x - b^T x. \tag{5.23}$$

In order to search the solution numerically one can use an iteration scheme following the gradient of the quadratic form, which is done in the gradient method. Then it was discovered that the iteration is accelerated if one searches not straight in gradient direction but in the hyperplane perpendicular to all previous directions. Theoretically the conjugate gradient step converges in less or equal steps than the dimension of the vector space. In practical applications the machine errors require a restart after a certain amount of steps.

5.3 Imaginary Time Step

Davies et al. presented in [DF+80] an efficient method for the Hartree–Fock problem discretized on a mesh, the *imaginary time step method* which we want to outline briefly. The origin for the name of this method is the analogy to the time–dependent Hartree–Fock (TDHF) method which solves the equations

$$i\hbar \frac{\partial \varphi_\alpha}{\partial t} = H(t)\varphi_\alpha(t), \qquad \alpha = 1, \ldots, A \tag{5.24}$$

for an orthonormal set of N wave functions $\{\varphi_\alpha\}$, and a Hamiltonian H which depends on the time t as it depends on on the wave functions $\varphi_\alpha(t)$ via densities or self–energy terms in a self–consistent way. These equations are discretized in time introducing a time step Δt, with $t_n = n\,\Delta t$. Then the time evolution of the set of wave functions $\{\varphi_\alpha\}$ may be approximated by the iterative procedure

$$|\varphi_\alpha^{(n+1)}\rangle = \exp\left(-\frac{i}{\hbar}\Delta t\, H^{(n+\frac{1}{2})}\right)|\varphi_\alpha^{(n)}\rangle, \qquad \alpha = 1, \ldots, A, \tag{5.25}$$

in which $\varphi_\alpha^{(n)}$ represents the wave function φ_α at the time t_n and $H^{(n+\frac{1}{2})}$ denotes the numerical approximation to the Hamiltonian $H(t)$ at the time $(n+\frac{1}{2})\Delta t$. The idea of Davies et al. was to replace the time step Δt by the imaginary quantity $-i\Delta t$ which leads to a decrease of the HF energy. Introducing the positive parameter $\lambda = \Delta t/\hbar$ the procedure for the imaginary time step gets

$$|\tilde{\varphi}_\alpha^{(n+1)}\rangle = \exp\left(-\lambda\, H^{(n+\frac{1}{2})}\right)|\varphi_\alpha^{(n)}\rangle, \qquad \alpha = 1, \ldots, A, \tag{5.26}$$

where $\{\tilde{\varphi}_\alpha^{(n+1)}\}$ is not any more an orthonormal set of wave functions since the imaginary time operator $\exp\big(-\lambda\, H^{(n+\frac{1}{2})}\big)$ is not unitary. Applying the Gram–Schmidt orthonormalization method $\mathcal{O}$ we get the orthonormal set $\{\varphi_\alpha^{(n+1)}\}$ by

$$|\varphi_\alpha^{(n+1)}\rangle = \mathcal{O}|\tilde{\varphi}_\alpha^{(n+1)}\rangle \qquad \alpha = 1, \ldots, A, \tag{5.27}$$

which converges to the lowest N eigenfunctions of the Hamiltonian H.
In practical application the Hamiltonian $H^{(n+\frac{1}{2})}$ is replaced by the Hamiltonian $H^{(n)}$ of the n–th step, which makes the calculation fast keeping the algorithm stable. After this replacement, we get the following operation on the wave functions

$$\varphi_\alpha^{(n+1)} = \mathcal{O}\left(\exp\big(-\lambda\, H^{(n)}\big)\ \varphi_\alpha^{(n)}\right) \qquad \alpha = 1, \ldots, A. \tag{5.28}$$

For numerical application one has to truncate the exponential series to a certain order and evaluate the powers of the Hamiltonian, which is done by repeated action on the wave functions. In earlier HF calculations the gradient method was used with the operation $\mathcal{O}(1 - \lambda H)$ on the wave functions [RS80]. If we truncate the exponential series in the imaginary time step beyond the first order one obtains an improvement of the gradient method. Davies et al. recommended a truncation to 4th or 5th order for ^{40}Ca together with a time step $\Delta t = 4.0 \times 10^{-24}\,$s and a mesh size of 1.0 fm.
In our calculations we used the same mesh size as Davies et al. but the convergence got worse due to a high amount of wave functions, strong deformations, the inclusion of pairing properties and the solution of β–equilibrium. Hence we truncated the exponential operator at 9th order and the time step Δt was set to $2.0 \times 10^{-24}\,$s to have some reserve. For the check of convergence the mean square deviation of the single particle energies for A Nucleons with the occupation probability η_α is calculated by

$$\Delta H^{(n)} = \left(\frac{1}{N}\sum_{\alpha=1}^{A} \eta_\alpha \left(\langle\varphi_\alpha^{(n)}|H^{(n)^2}|\varphi_\alpha^{(n)}\rangle - \langle\varphi_\alpha^{(n)}|H^{(n)}|\varphi_\alpha^{(n)}\rangle^2\right)\right)^{\frac{1}{2}}, \tag{5.29}$$

where N is the average number of particles. This square deviation provides a better criterion for convergence as calculating energy differences. In the code both criterions are used simultaneously.
Before the pairing gap can be evaluated by the appropriate integral equation, the Fermi energy $E_{F,q}$ has to be fixed by requiring that the particle number is obtained

	SkyrmeIII	SLy4
t_0 (MeV fm^3)	-1128.75	-2488.91
t_1 (MeV fm^5)	395.00	486.82
t_2 (MeV fm^5)	-95.00	-546.39
t_3 (MeV fm$^{3+3\alpha}$)	14000.00	13777.0
x_0	0.45	0.834
x_1	0.00	-0.344
x_2	0.00	-1.000
x_3	1.00	1.354
α	1.0	1/6
W_0 (MeV fm^5)	120.0	123.0

Table 5.3: Parameters of the Skyrme forces SkyrmeIII and SLy4

by summing up the occupation probabilities. This means we have to search for the root of the function

$$f(E_{F,q}) = N_q - \sum_\alpha \eta_\alpha(E_{F,q}) \stackrel{!}{=} 0, \tag{5.30}$$

where N_q is the particle number of the particle species with isospin q. For this task the bisection algorithm with damping is used to get a save convergence.

The main step in the paring iteration is to solve the gap equation (4.13), or in case of non–zero temperature (4.55). This equation is an integral equation which can be solved using a self–consistent algorithm. The fixpoint theorem of Banach states that the iteration is stable if the norm of the integral operator is limited by one, which is the case in this application. The only concern is that there exists the trivial solution zero. The iterative process is prevented to converge to this solution by limiting the gap Δ_α to the termination error $\Delta_\alpha \geq \epsilon$. Keeping the pairing gap at this very small value has no effect in the practical application. The imaginary time step and the pairing iteration are performed concurrently.

The high efficiency of the imaginary time step can be attributed to the direct variation of the wave functions on the mesh. This is particularly important because the densities we are dealing with require to consider about 1500 nucleons. In addition for the pairing properties we need some additional shells, so we decided to take into account 1300 wave functions which correspond to 2600 nucleons.

We tested the Skyrme Hartree–Fock program for the parameter set Skyrme III with

M	m_σ	m_ω	m_ρ	g_σ	g_ω	g_ρ
938.9 MeV	520 MeV	783 MeV	770 MeV	10.4814	13.8144	4.04244

Table 5.4: Parameters for the linear model of Horowitz and Serot L–HS for relativistic Hartee.

the results in [BF+85] and found that the overall accuracy is slightly improved. Additional tests has been run with the parameter set SLy4 [CB+98]. Both parameter sets are summarized in Table 5.3.

For the relativistic calculation the numerical methods are essentially the same as in the case of Skyrme Hartree–Fock. Instead of the density functional meson fields have to be evaluated by the *conjugate gradient method* as outlined in section 5.2. Further the *imaginary time step* is extended to the lower component as already described in subsection 3.3.5.

In the test runs we used the parameter set for the linear model of Horowitz and Serot from [HSe81] cited as L–HS in [Rhd89]. The parameters are summarized in Table 5.4 where the ρ meson coupling is reduced by the factor of $\frac{1}{2}$, which is contained in the the original interaction Lagrangian.

In the density dependent relativistic Hartree code including the δ meson the parametrization in [HKL01] was employed for testing, since it is derived from Dirac–Brueckner–Hartree–Fock (DBHF) calculations. The DBHF calculation of van Dalen et al. [vD+07] provides a good equation of state [KB+06], therefore a new parameter set was extracted together with van Dalen et al. from these DBHF calculations by a local density approximation of the mesonic self-energy contributions. The density dependence of the coupling constants is modeled by

$$g_\kappa(\rho) = a_\kappa + \left[b_\kappa + d_\kappa x^3\right] \exp(-c_\kappa x) \tag{5.31}$$

where $x = \rho/\rho_0$, and ρ_0 is the parameter for the saturation density of symmetric nuclear matter. For the ω meson an additional correction was introduced to get better results for finite nuclei:

$$g_{\omega,cor}(\rho) = g_\omega(\rho) - a_{cor} \exp\Big(- \Big[\frac{\rho - b_{cor}}{c_{cor}}\Big]^2\Big). \tag{5.32}$$

This new parameter set is summarized in Table 5.5 and is ready to use for an equation of state for neutron stars and supernovae.

The relativistic Hartree–Fock code has been tested first with the different parametrizations from [BM+87], which allow the gradual inclusion of the various mesons. Then

M	m_σ	m_ω	m_δ	m_ρ	a_σ	b_σ
939 MeV	550 MeV	782.6 MeV	983 MeV	769 MeV	7.7868	2.58637
c_σ	d_σ	a_ω	b_ω	c_ω	a_δ	b_δ
2.32431	3.11504	9.73684	2.26377	7.05897	2.68849	6.7193
c_δ	d_δ	a_ρ	b_ρ	c_ρ	a_{cor}	b_{cor}
0.503759	0.403927	4.56919	5.45085	1.20926	0.014	0.16
c_{cor}	ρ_0					
0.035	0.16					

Table 5.5: Parameter set from DBHF by van Dalen et. al. for the density dependent relativistic Hartee approach.

the density dependence has been tested applying the set PKO1 from Long et. al. in [LGM06] which is used for the calculation of some exotic drip-line nuclei. The density dependent couplings for the σ and ω are modeled by

$$g_\kappa(\rho) = g_\kappa(\rho_0)h_\kappa(x), \qquad \text{for } \kappa = \sigma, \omega \tag{5.33}$$

where

$$h_\kappa(x) = a_\kappa \frac{1 + b_\kappa(x + d_\kappa)^2}{1 + c_\kappa(x + d_\kappa)^2} \tag{5.34}$$

is a function of x which is already defined above. For g_ρ and f_π an exponential density dependence is introduced

$$g_\rho(\rho) = g_\rho(0)\exp(-a_\rho x), \tag{5.35}$$

$$f_\pi(\rho) = f_\pi(0)\exp(-a_\pi x). \tag{5.36}$$

The parametrization PKO1 is obtained by a fit to experimental data and is summarized in Table 5.6.

The overall numerical procedure provides also a good convergence in relativistic calculations. In the imaginary time step the step Δt for $\lambda = \Delta t/\hbar$ could be set to 4.0×10^{-24} s for the L–HS parameter set, which is even larger compared to the corresponding Skyrme calculations. For the more elaborate models this time step has to be reduced again to the value used in the Skyrme code with comparable convergence. The numerical results show good agreement with the results cited together with the various parameter sets.

M	m_σ	m_ω	m_ρ	m_π
938.9 MeV	525.769084 MeV	783.0 MeV	769.0 MeV	138.0 MeV
$g_\sigma(\rho_0)$	$g_\omega(\rho_0)$	$g_\rho(0)$	$f_\pi(0)$	a_ρ
8.833239	10.729933	2.629000	1.000000	0.076760
a_π	ρ_0	a_σ	b_σ	c_σ
1.231976	0.151989	1.384494	1.513190	2.296615
d_σ	a_ω	b_ω	c_ω	d_ω
0.380974	1.403347	2.008719	3.046686	0.330770

Table 5.6: Parameter set PKO1 for the density dependent relativistic Hartee–Fock approach.

Chapter 6

Results and Discussion

6.1 The Parametrization from DBHF

The goal of a microscopic nuclear structure calculation, like in the Dirac–Brueckner–Hartree–Fock approach, is to predict the properties of nuclear matter and finite nuclei from a realistic interaction without any readjustment of parameters. The problem of such an approach is on the one side that such calculations are difficult to perform in particular for finite nuclei, and on the other side that they do not precisely reproduce the bulk properties of nuclear systems. A different approach is to derive a parametrization for a simple mean–field Hamiltonian from such DBHF calculations. Employing a slight readjustment of a parametrization one can even get a good description of finite nuclei.

In this section we would like to develop an approach, which is based on the properties of DBHF calculations and leads to an equation of state covering a very broad range as e.g. [ST$^+$98a, ST$^+$98b]. Since the DBHF approach of van Dalen et al. based on the Bonn A potential [vD$^+$07] passes almost all constraints for an equation of state in [KB$^+$06], it was decided to extract a parametrization for a density dependent relativistic Hartree approach to which is referred as density dependent relativistic mean–field model (DDRMF). Such a model provides both the possibility of fast calculations for asymmetric nuclear matter and the application in the density region of non-homogeneous nuclear matter as it is found in the crust of neutron stars. An additional point is that the DBHF approach was the only one which passed simultaneously the gravitational binding and the mass-radius test what implies that it can reproduce neutron stars with $M \approx 2.0 M_\odot$.

The method of extracting a parametrization from the DBHF approach has already been confirmed and developed by Fritz, Schiller and Müther [FM94, Sch00]. Fritz investigated both possibilities of a parametrization, The local density approximation for the Dirac spinors and the local density approximation for the Brueckner G–matrix, respectively. He found that the results for closed shell nuclei are comparable for both approximations what confirms that the method is a reasonable one. Various approaches were developed to determine the Dirac structure of the nucleon self energy Σ with the Dirac–Brueckner–Hartree–Fock theory. A simple approach was suggested by Brockmann and Machleidt [BM90]. The scalar and time–like vector self energies Σ^S and Σ^0 can be determined from the single particle energy by assuming that the commanding components of this self–energies do not depend on the momentum of the nucleons. In case of symmetric nuclear matter this method works well but there arise problems applying it to pure neutron matter [UM97].
Schiller developed the second possibility to a systematic way of including the properties of the Brueckner G–matrix into a relativistic Hartree or Hartree–Fock approach by a projection method. The antisymmetrized G–matrix elements are analyzed by projecting the nucleon self–energy on a complete set of bilinear covariant operators, which correspond to the interaction vertices of the various mesons. This projection leads to an effective density dependent nucleon–nucleon interaction [Sch00].
The theory of the DDRMF model is the reduction of the relativistic Hartree–Fock theory described in chapter 3 to the Hartree level. The included exchange bosons are the σ, δ, ω and ρ mesons. The inclusion of the δ–meson accounts for the different effective masses for protons and neutrons. In addition this meson is important for astrophysical applications since the dense asymmetric matter gets softer, which means that the pressure rises more shallowly for larger densities.
The effective coupling functions g_κ are given for each meson κ by

$$\left(\frac{g_\kappa(\rho,\beta)}{m_\kappa}\right)^2 = -\frac{1}{2}\frac{\Sigma_\kappa^{DBHF}}{\rho_\kappa}, \tag{6.1}$$

with Σ_κ the self–energy generated by the meson κ and ρ_κ the corresponding density according to the Hartree self–energy in section 3.4. The coupling functions depend weakly on the asymmetry parameter $\beta = \frac{\rho_n - \rho_p}{\rho}$.
The density dependent coupling functions can be directly used in the density dependent relativistic Hartree theory for infinite nuclear matter. Schiller found that the isospin dependence of the coupling functions obtained by the projection method is weak [Sch00]. Hence the isospin dependence is dropped for the coupling functions in

equation 6.1. The isoscalar σ and ω coupling functions are extracted from symmetric nuclear matter data of the DBHF calculation in [vD+07], while the isovector δ and ρ coupling functions are extracted from pure neutron matter data of this DBHF calculation. It turned out that smooth coupling functions are necessary for a stable calculation of binding energies in case of finite nuclei. Thus the parametrized functions 5.31 have been fitted to equation 6.1.

The effective mass M_q^* introduced in section 3.4 plays an important role in relativistic approaches, since it contains the scalar self–energy and accounts for the splitting of the proton and neutron effective masses by δ–meson exchange. In DDRMF the effective masses are given by

$$M_q^* = M - \left(\frac{g_\sigma(\rho)}{m_\sigma}\right)^2 \rho^s - \left(\frac{g_\delta(\rho)}{m_\delta}\right)^2 \rho_3^s \tau_3. \tag{6.2}$$

However, the DBHF self–energy is explicitly momentum dependent, e.g. due to contributions originating from Fock terms. For the comparison we always consider the self-energies at the corresponding Fermi momentum. The spatial contribution of the vector self energy Σ_V does not vanish in the DBHF theory, but disappears in the DDRMF model. Hence the spatial Σ_V component has to be included in a proper way. First, the effective mass has to be compared within both theories

$$\tilde{M}_q^* = \frac{M + \Sigma_{S,q}(p_{F,q})}{1 + \Sigma_{V,q}(p_{F,q})} = M + \Sigma_{S,q}^{DDRMF}, \tag{6.3}$$

what leads to the renormalized scalar self energy component

$$\Sigma_{S,q}^{DDRMF} = \frac{\Sigma_{S,q}(k_{F,q}) - M\Sigma_{V,q}(p_{F,q})}{1 + \Sigma_{V,q}(p_F)}. \tag{6.4}$$

Similarly, by comparing the DBHF energy density with the one of the DDRMF theory (restriction to the Hartree part of eq. (3.134)) the following expression for the renormalized time–like vector component is obtained

$$\Sigma_{0,q}^{DDRMF} = \Sigma_{0,q}(p_{F,q}) - \Sigma_{V,q}(p_{F,q}) \frac{1/\pi^2 \int_0^{p_{F,q}} dp\, p^2 E_q^*(p)}{\rho_q}. \tag{6.5}$$

With the help of these renormalized scalar and vector self–energies the renormalized coupling functions are obtained by equation 6.1. The coupling functions has been parametrized using the ansatz of equation (5.31). It was confirmed that this type of coupling functions leads to a minimal error in the fit of the self-energies.

Efforts have been made to insert the explicit momentum dependence of the DBHF binding energy into the RMF model by a Taylor expansion of the self–energy in

terms of the momentum [HKL01]. However, this leads to a slight deviation of the energy functional. Since the momentum dependence is weak in DBHF approaches, such additional terms are neglected.

Applying such a DDRMF model to finite nuclei without any correction, Fritz and Müther observed that one obtains less binding energy than the experimental value [FM94]. Since the parametrization should fit to both nuclear matter and finite nuclei, the intriguing task was to adjust a suitable correction. Such a correction has been imposed on the ω–meson coupling function by adding an additional term which was introduced in equation 5.32.

The values obtained for the parametrization of the coupling functions and the correction of the ω–meson are summarized in Table 5.5.

		^{16}O	^{40}Ca	^{48}Ca	^{90}Zr	^{208}Pb
E/A	[MeV]	-8.35	-8.73	-8.73	-8.74	-7.87
E/A exp.	[MeV]	-7.98	-8.55	-8.67	-8.71	-7.87
r_c	[fm]	2.78	3.44	3.45	4.17	5.31
r_c exp.	[fm]	2.74	3.48	3.47	4.27	5.50

Table 6.1: Results for closed shell nuclei applying the DDRMF parametrization from DBHF results. Experimental values are taken from [HKL01].

The results for closed shell nuclei are summarized in Table 6.1 and compared to experimental results. Special care was taken to the reproduction of the binding energy for the lead nucleus. The lighter nuclei are a little too much bound but the binding energies for heavy nuclei are well reproduced. The charge radii r_c show a good agreement for the lighter nuclei, whereas for the heavy nuclei the radii are a little too small. Too less binding as well as small radii are well known problems of parametrizations obtained from DBHF, which we eliminated as far as possible. The overall properties for closed shell nuclei in the DDRH model are similar compared to the approach in [HKL01].

The binding energy of symmetric nuclear matter and pure neutron matter obtained from the DBHF calculations and the renormalized DDRMF model are compared in Fig. 6.1. In case of symmetric nuclear matter small deviations occur at very small densities and at densities larger than 0.3 fm^{-3}. The binding energy of pure neutron matter is reproduced well, however, a slight decrease can bee seen.

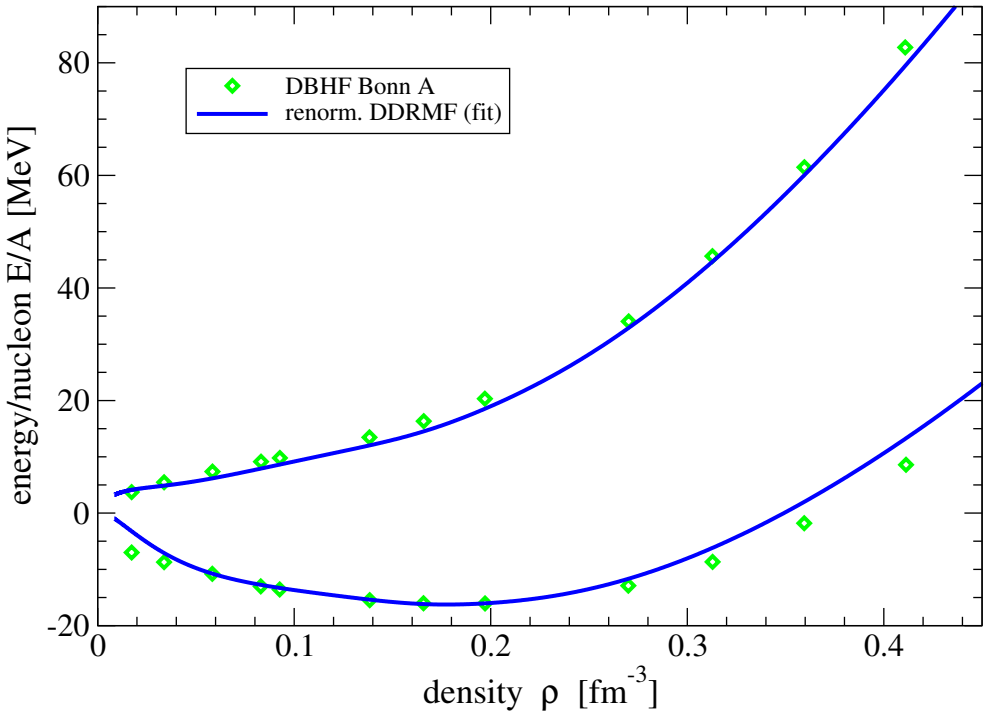

Figure 6.1: Comparison of binding energy for symmetric nuclear matter and pure neutron matter obtained from DBHF calculations and from the renormalized DDRMF model.

		DBHF	DDRMF
ρ_{sat}	fm^{-3}	0.181	0.178
E/A	[MeV]	-16.15	-16.25
K	[MeV]	230	337
a_s	[MeV]	34.36	32.11

Table 6.2: Nuclear matter properties obtained in the different models. The DDRMF model includes the correction from renormalization.

In Table 6.2 the nuclear matter properties of the DBHF calculations are compared to those of the DDRMF model. Due to the fitting process the nuclear matter properties changed slightly around the saturation point. The saturation density shifted to a slightly lower value so it is even closer to the experimental value. The binding energy per nucleon E/A of symmetric nuclear matter is fairly well reproduced but the compression modulus K is rising during the fit procedure mainly due to the correction for the ω–meson. Finally the symmetry energy coefficient a_s decreased by about 2.2 MeV compared to the DBHF results. These changes should not effect the astrophysical properties of the model in the high density region, what is important to be able to reproduce the heavy neutrons stars.
Altogether the DDRMF model obtained from the DBHF results is regarded to be capable of astrophysical application, what has still to be confirmed by some applications. One of these applications is the nuclear matter in the crust of neutron stars, for which the DDRH model will be compared to the Skyrme interaction and an earlier relativistic approach.

6.2 The Structure of Nuclear "Pasta"

In the first part of this section we are going to discuss the results of Skyrme Hartree–Fock calculations using the Skyrme interaction with the parameter set SLy4 as defined in [CB$^+$98]. The pairing phenomenon is included by the BCS approach of chapter 4 which will be discussed later in section 6.4.
The calculations are performed in a Wigner Seitz (WS) cell within a cubic box. The origin of the coordinate system is put in the center of the box, so that the "size" of the box R is half the length of the edge. With the help of this definition the box size is the same for all different geometries like the so–called spherical box and the cylindrical one. This box size R has been adjusted to minimize the total energy per nucleon for the density under consideration. To apply the conditions for the crust of neutron stars to the cubic box, the calculations have been performed for charge neutral matter containing protons, electrons and neutrons in β–equilibrium

$$\mu_n = \mu_p + \mu_e. \tag{6.6}$$

In Fig. 6.2 a few typical density distributions resulting from these variational calculations are displayed. The average density in the box is increasing from top on the left hand side to the bottom on the right part of the figure.

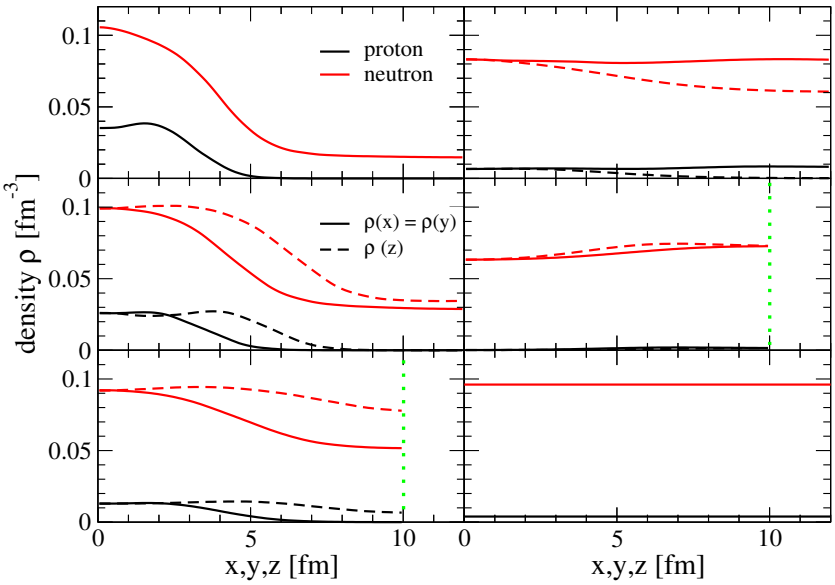

Figure 6.2: Density distributions resulting from Skyrme HF calculations for protons (black color) and neutrons (red color) as a function of Cartesian coordinates x, y, z. The panels in the left column refer to densities 0.0166 fm^{-3} (top), 0.0317 fm^{-3}, and 0.0565 fm^{-3} (bottom), while those in the right column are obtained for baryon densities 0.0681 fm^{-3} (top), 0.079 fm^{-3}, and 0.1 fm^{-3}.

We start our discussion with the top panel in the left column representing a nuclear structure at a baryonic density of 0.0166 fm^{-3}. In this case the density profiles are identical in all three directions. This means that we obtain a quasinuclear structure with spherical symmetry in the center of the WS cell. The proton density drops to zero at a radial distance of about 4 fm. The neutron density profile drops around the same radius from a central density of about 0.1 fm^{-3} to the peripheral value of around 0.01 fm^{-3}. The density distributions for protons and neutrons in the $z = 0$ plane displayed in figure 6.3 confirm these observations and a slight enhancement of the density along the axis is found. Summarizing we have obtained a structure of quasinuclear droplets forming a cubic lattice at this density, which is embedded in a sea of neutrons.

The second panel in the left part of Fig. 6.2 shows the density distributions, which have been obtained at a density of 0.0317 fm^{-3}. In this case we obtain deformed quasinuclear droplets with radii, which are slightly larger in one direction, which is chosen to be the z–direction (dashed curves). This means that we find prolate deformation at this density.

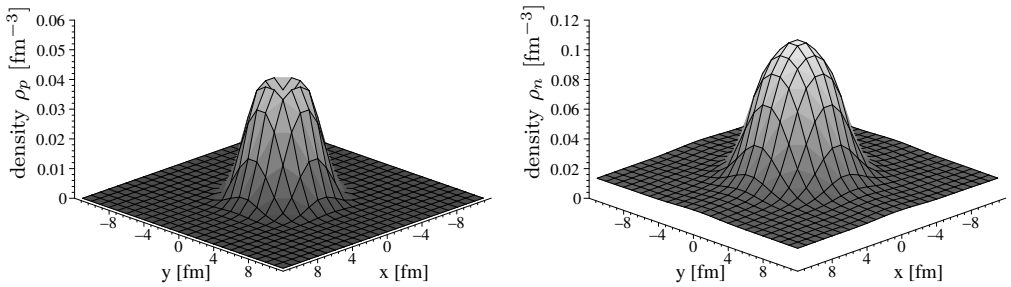

Figure 6.3: Proton and neutron density distribution in the $z = 0$ plane for Skyrme HF + BCS calculation at an average density of $\rho = 0.0166$ fm$^{-}3$.

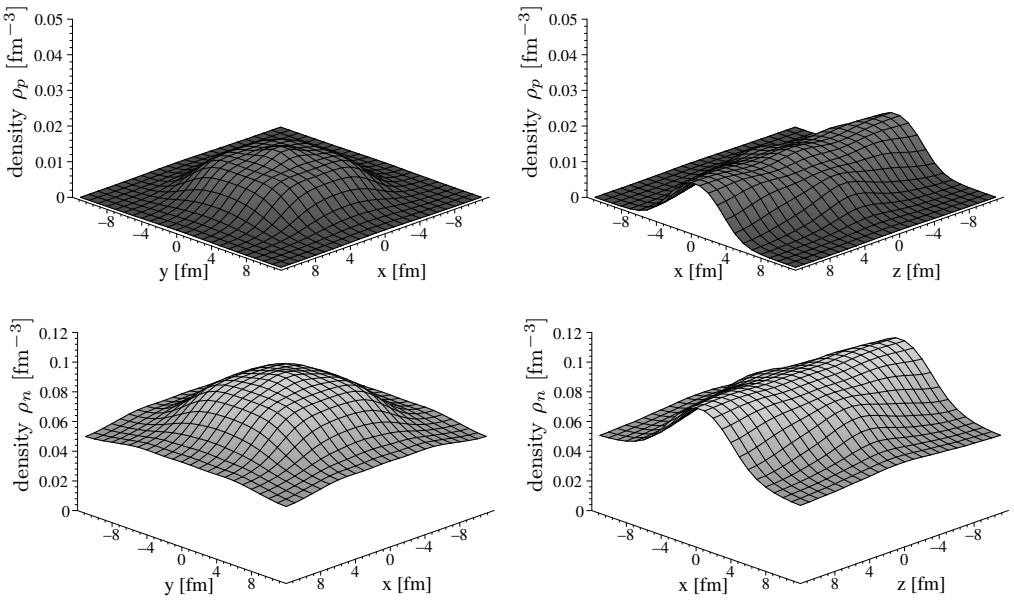

Figure 6.4: Profiles for the proton and neutron density distribution forming a rod structure at a density of 0.0625 fm^{-3}.

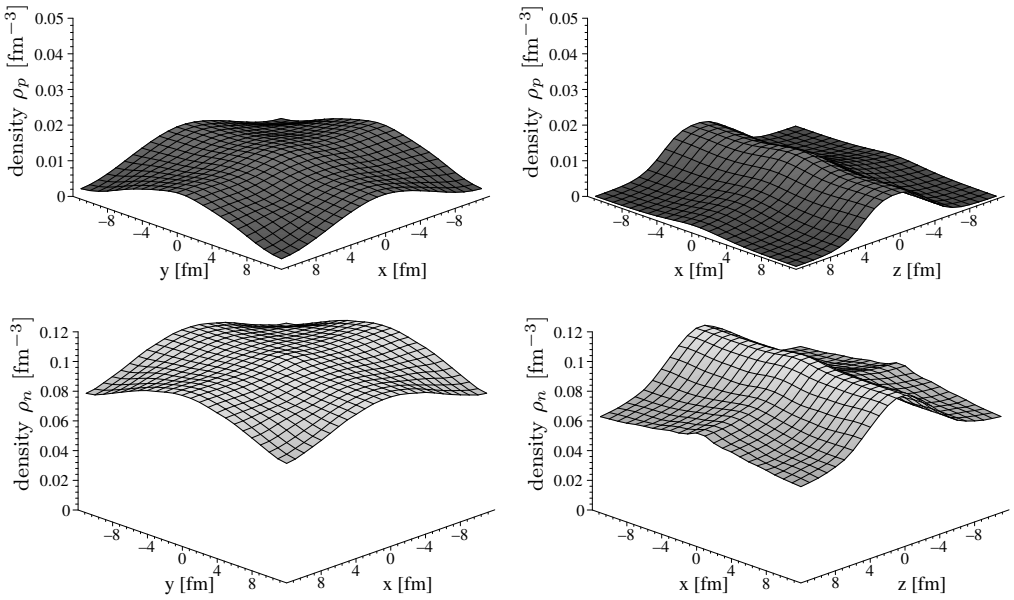

Figure 6.5: The proton and neutron density distributions form a slab structure at a density of 0.0775 fm^{-3}.

At slightly larger densities the deformation of the quasinuclear structures increases until a density is reached at which the proton density does not vanish along one of the three axis. Such an example (baryon density 0.0565 fm^{-3}) is displayed in the bottom panel of the left column. In this case we have quasinuclear structures in the shape of rods parallel to the z–axis. The density of these rods is not homogeneous along the symmetry axes. Note that the size of the WS cell lies within the range displayed in this figure and therefore the boundary has been indicated by the dotted line in this panel. The most designed rod structure is found at a density of 0.0625 fm^{-3}, as shown in Fig. 6.4, where the profile of the proton and neutron densities are displayed in the xy and xz plane, respectively.

Performing HF calculations at a density of 0.0681 fm^{-3} led to a density density distribution as displayed in the top panel of the right column in Fig. 6.2. In this example the proton as well as the neutron density is essentially constant in the $(x, y, z = 0)$ plane. As a function of the third coordinate (z, dashed lines) the proton density is reduced from the central value at $z = 0$ to zero at the border of the WS cell and also the neutron density is reduced by about 25 percent going from the central to the peripheral values of z. Therefore in this case we observe a structure in form of parallel slabs. This slab structure is also shown in Fig. 6.5. From this presentation in particular it gets obvious that the density within such a

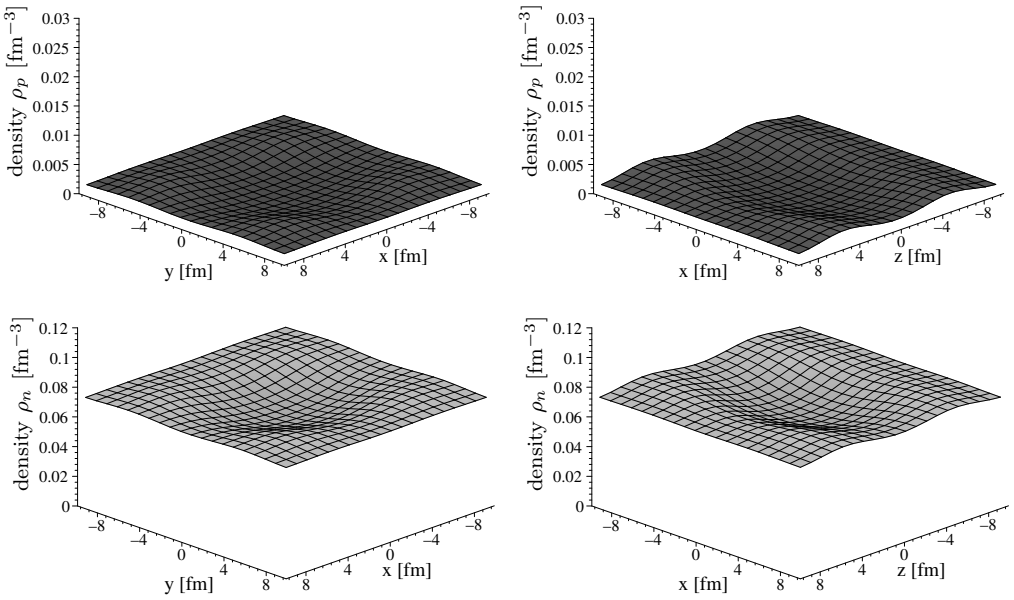

Figure 6.6: Proton and neutron density distributions in the $z = 0$ and $y = 0$ plane at an average density of $\rho = 0.0790$ fm^{-3}.

slab at $z = 0$ is not really a constant but drops in particular along the diagonals of the WS cell with $x = y, z = 0$.

At even larger densities the Skyrme Hartree–Fock calculations in a cubic WS cell yield structures with smaller neutron densities in the center of the WS cell as compared to the boundaries. An example of such an inverse structure, which corresponds to bubbles in the sea of nuclear matter, is displayed in the second panel of the right column of Fig. 6.2 at a density of 0.079 fm^{-3}. The proton density, which is hardly visible in this example, drops from a peripheral value of around 0.004 fm^{-3} to a central value of zero. The density profiles of this structure in the $z = 0$ and $y = 0$ plane are displayed in Fig. 6.6 for protons and neutrons, respectively.

As a final example we present in the bottom panel of the right column of Fig. 6.2 the results of the HF calculation at a baryonic density of 0.1 fm^{-3}. At this and larger densities, the variational calculation yields homogeneous nuclear matter in β–equilibrium. This example also demonstrates that the Cartesian box allows for a clean representation of the limit of homogeneous matter. This is in contrast to calculations employing a spherical WS cell. Depending on the boundary conditions used, calculations within such a spherical box can lead to density profiles, which either show a maximum or a minimum at the boundary. Even if one tries to use a set of boundary conditions, which minimize this effect, the resulting density profile

	Skyrme		RMF		DDRMF
	HF	TF	H	TF	H
droplet–rod	0.042	0.066	0.070	0.062	0.057
rod–slab	0.070	0.078	-	-	-
slab–homogeneous	0.080	0.085	0.075	0.072	0.064

Table 6.3: Comparison of densities at which shape transitions occur using the Skyrme, the Relativistic Mean–Field (RMF) and the density dependent Relativistic Mean–Field (DDRMF) approach at zero temperature. Results are compared, employing the microscopic Hartree–Fock (HF), Hartree (H) or the Thomas–Fermi (TF) approach. All entries are presented in fm^{-3}.

does not correspond to the homogeneous solution [MMM04].

From this discussion we see that the HF calculations in a Cartesian WS cell for densities in the range of 0.01 fm^{-3} to 0.1 fm^{-3} leads to quite a variety of shapes and quasinuclear structures with smooth transitions in between. Following the discussions above these structures may be characterized as quasinuclei, rod structures, slab structures, which are all embedded in a sea of neutrons and, finally, the homogeneous matter. In Table 6.3 the densities at which the transitions from one shape to the other occur are listed for Skyrme HF calculations as well as for the relativistic Hartree and the density dependent relativistic Hartree approach. The transitions in case of Thomas-Fermi approximations are given for comparison for both the non–relativistic Skyrme HF and the linear relativistic Hartree approach. Such Thomas–Fermi approximations are often used in equation of state calculations and discussed in more detail in the next section. The transition densities obtained in Skyrme HF calculations are very similar to those cited in [MHe02].

Besides the Skyrme HF calculation there were performed relativistic mean–field calculations in the same WS cell within β–equilibrium. The Hartree calculations are performed with the parameter set of the linear model L–HS introduced in section 5.3 and the density dependent Hartree calculations with the parameter set introduced in section 6.1. Although the linear model results in underbound nuclei, the application of this model shows the main properties of relativistic effects. As a matter of fact the same shapes are obtained from the relativistic mean–field calculations in both cases: the linear model and the density dependent approach, respectively.

The shapes obtained by RMF calculations are mainly the same as in the case of

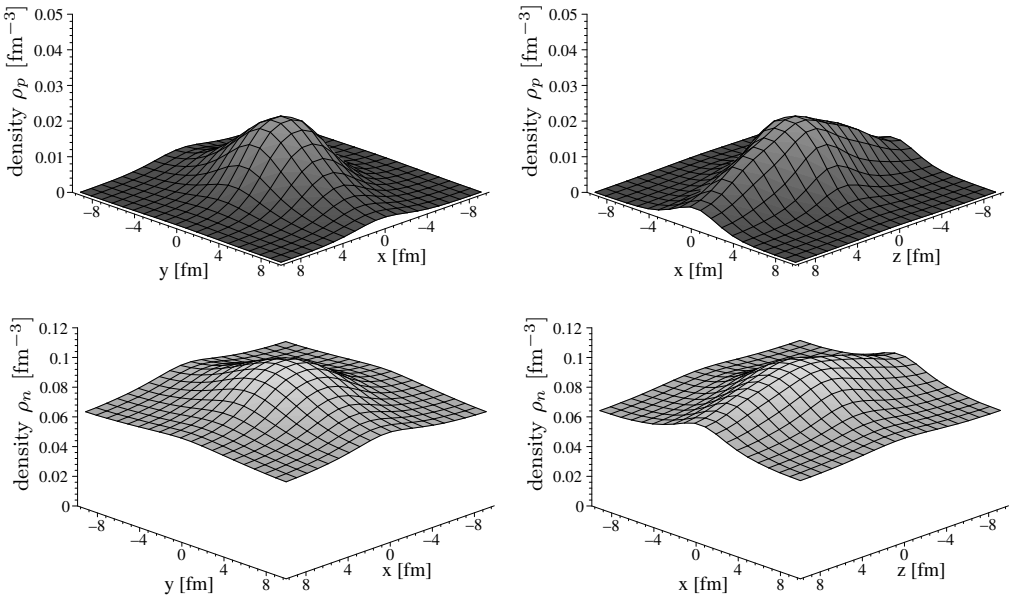

Figure 6.7: Density profiles for protons and neutrons in the $z = 0$ and $y = 0$ plane at an average density of $\rho = 0.071$ fm^{-3} obtained by a RMF calculation with parameter set L–HS.

Skyrme HF calculations in the WS cell. However, the transition to the rod phase occurs at a higher density and the range of the rod phase is quite narrow. In Fig. 6.7 density profiles in the $z = 0$ and in the $y = 0$ plane are displayed from which we see that the rod shape is not fully developed, since the proton density is droping to about half the value if we follow the profile from the center to the edge in z–direction. At the average density of $\rho = 0.075$ fm^{-3} a grid structure is obtained as it is displayed in Fig. 6.8 in the $z = 0$ plane. The density profiles for protons and neutrons are the same in all coordinate planes at this density. In case of the rod structure the protons form a connection between the quasinuclei in one direction. This structure

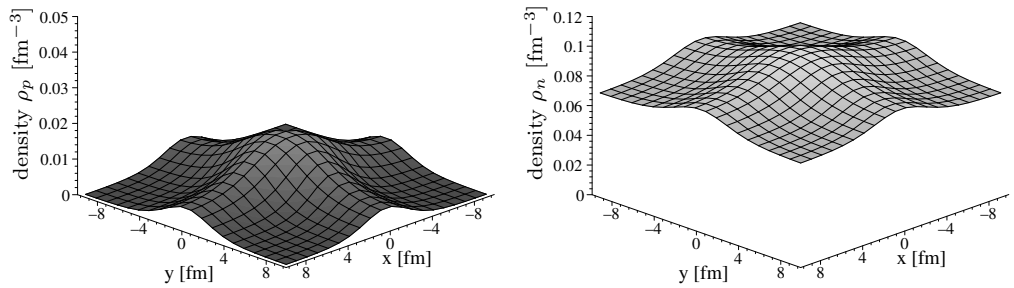

Figure 6.8: Proton and neutron density profiles in the $z = 0$ plane at an average density of $\rho = 0.075$ fm^{-3} obtained with parameter set L–HS.

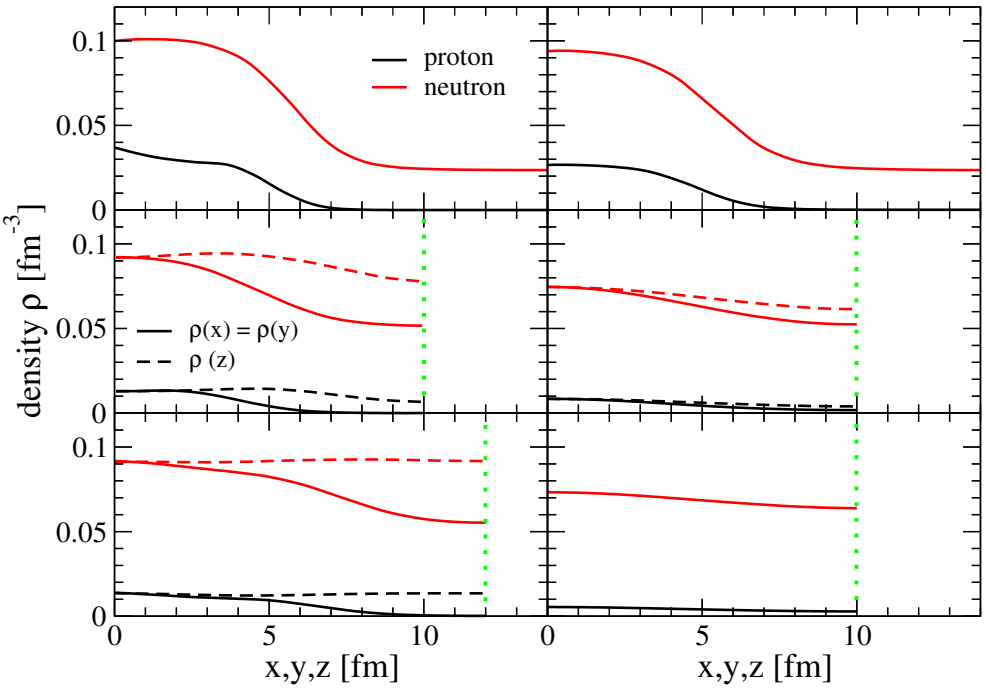

Figure 6.9: Comparison of density distributions at finite temperature with those at zero temperature resulting from Skyrme HF calculations for protons (black color) and neutrons (red color) as a function of Cartesian coordinates x, y, z. The panels in the left column refer to $T = 0$ MeV calculations at the average densities 0.0271 fm^{-3} (top), 0.0565 fm^{-3}, and 0.0625 fm^{-3} (bottom), while those in the right column are obtained for $T = 5$ MeV at the baryon densities 0.0273 fm^{-3} (top), 0.0545 fm^{-3}, and 0.0648 fm^{-3}.

is extended by proton connections in the remaining directions and one ends up with a grid structure. At larger densities the proton density sinks in the center and rises in the periphery, so that the density of $\rho = 0.075$ fm^{-3} can be claimed to be the transition density to homogeneous matter for the RMF approach with the parameter set L–HS.

The Skyrme Hartree–Fock calculations in the Wigner–Seitz cell has been performed also also at the finite temperature of $T = 5$ MeV. Some particular examples out of the various shapes of nuclear structure obtained in these calculations are presented in Fig. 6.9. In the left column shapes of the proton and neutron density profiles for $T = 0$ at different densities are presented, while the shapes resulting from $T = 5$ MeV calculations at comparable average densities as in case of zero temperature are displayed in the right column.

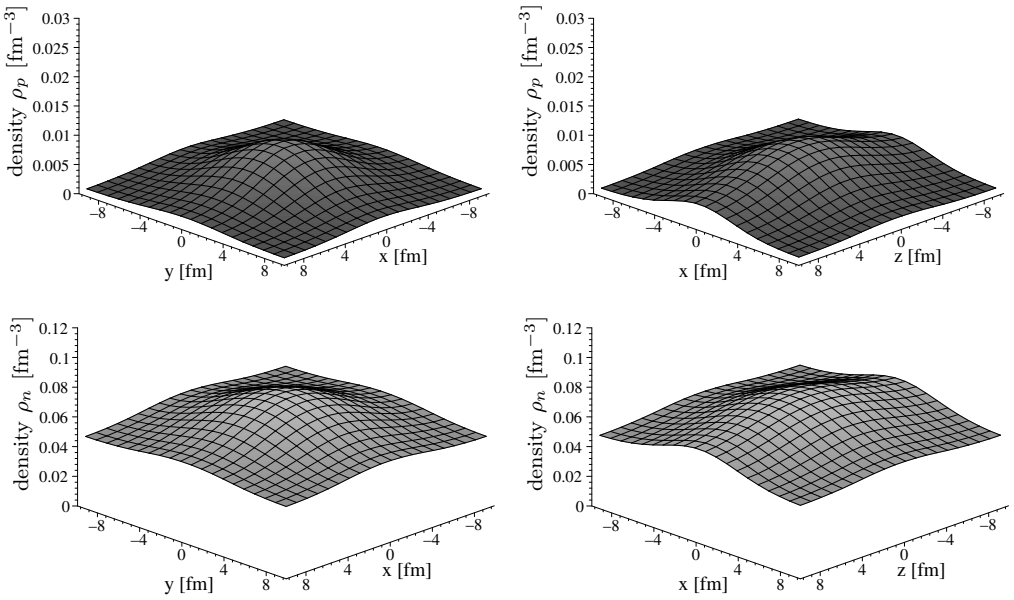

Figure 6.10: Density profiles for protons and neutrons in the $z = 0$ and $y = 0$ plane at an average density of $\rho = 0.0545$ fm^{-3} obtained by a Skyrme HF calculation at $T = 5$ MeV.

At an average density of $\rho = 0.027$ fm^{-3} a droplet structure is obtained for the proton density profile in both cases of $T = 0$ MeV and $T = 5$ MeV, respectively. The only difference is that the density profile is a little smoothed out at $T = 5$ MeV, what is quite expected from the thermal occupation scheme which includes lots of excited states.

As the average density rises in the WS cell, the transition to the rod phase occurs at a slightly lower density in case of the finite temperature approach. The panels in the middle display both a rod structure at average densities of $\rho = 0.0565$ fm^{-3} and $\rho = 0.0545$ fm^{-3}. It strikes that for $T = 5$ MeV the peripheral proton density does not drop to zero, what indicates that the proton density distribution has a homogeneous component on which the structure seems to be built. This gets even more obvious if one considers the density distributions in the $z = 0$ and in the $y = 0$ planes displayed in Fig. 6.10. This homogeneous component is observed for densities $\rho \geq 0.035$ fm^{-3} and the effect increases at larger densities. Summarizing, the rod structure is washed out slightly at $T = 5$ MeV but still present.

The panels in the bottom of Fig. 6.9 display structures obtained at an average density in the WS cell of $\rho = 0.065$ fm^{-3}. At a temperature of 5 MeV the structure already changes the shape towards homogeneous matter as we see from the graph on the

	Skyrme		DDRMF
	HF	TF	H
droplet–rod	0.040	0.048	0.044
rod–slab	-	-	-
slab–homogeneous	0.065	0.048	0.044

Table 6.4: Shape transitions obtained at the finite temperature of $T = 5$ MeV using the Hartree–Fock (HF), the Thomas–Fermi (TF) or the density dependent Hartree (H) approach. All entries are presented in fm^{-3}.

right hand side, while the protons form a clear rod structure at zero temperature. The transition densities for all calculations in the WS cell at a temperature of $T = 5$ MeV are summarized in Table 6.4. If we compare the Skyrme HF transition densities at $T = 5$ MeV with the zero temperature results, the transition densities are lower at finite temperature and the slab structure disappears. Employing the Thomas–Fermi approach the situation at $T = 5$ MeV is even more striking: It does not show the rod structure, what is indicated in the table by the same transition density for the transitions droplet–rod and slab–homogeneous. Here not only the transition densities are shifted but the rod structure can't be reproduced. The results obtained from the density dependent Hartree approach do not show any more a rod structure, but the transition from the droplet structure to homogeneous matter occurs via some grid–like structure which can be regarded as transition to the homogeneous phase. Summarizing the finite temperature lowers the riches of the various "pasta" phases in the neutron star crust significantly for any approach.

6.3 The Equation of State

In the following the equation of state is discussed for a neutron star in the region of the crust where the "Pasta" structures occur. The nuclear force model plugged in the calculation plays an important role. Therefore the non-relativistic Skyrme interaction is compared with the relativistic mean–field calculation. Further the HF and RMF calculations are compared to the corresponding Thomas-Fermi approximations as they are employed in the calculation of equation of state tables like in [ST$^+$98a, ST$^+$98b].

The energies per nucleon and the proton abundances resulting from Skyrme Hartree–

Fock calculations are are displayed in the lower and upper panel of Fig. 6.11, respectively. The solid lines indicate the results for the evaluation of homogeneous matter in β–equilibrium. The results of calculations performed in cubic WS cells are presented in terms of individual symbols. Those symbols, which scatter around the homogeneous matter results are obtained from WS calculations, constraining the HF single–particle wave functions to plane waves. Therefore the scattering of these homogeneous matter calculations within WS cells of finite size around the homogeneous result for infinite matter is a measure of the shell effects in the WS calculations on the calculated energy and proton abundances. Further, these results show that the cubic box provides a good discretisation of the problem since we get fair agreement up to large nuclear densities.

The Hartree–Fock calculations, which allow for the formation of inhomogeneous quasinuclear structures, lead to a reduction of the calculated energy of 1 to 2 MeV per nucleon. This gain in energy is reduced with increasing density up to the density of 0.085 fm^{-3} at which the energies of the inhomogeneous structures merge into the results for the homogeneous matter. At densities below this value of 0.085 fm^{-3} the balance between the gain in binding energy due to a local increase of the baryon density and the loss of binding energy due to the localization of nucleons and surface effects favors the occurrence of inhomogeneities in the baryon densities.

This balance between bulk energy arising from the energy density of nuclear matter treated in a local density approximation and surface effects is also contained in the Thomas–Fermi (TF) approach. In this section we want to investigate to which extent the results of our Hartree-Fock calculations can be reproduced by corresponding TF calculations. For that purpose we consider simple parametrizations for the density distribution for protons and neutrons, which contain a constant peripheral density ρ_q^{out} ($q = p$ or n for protons and neutrons, respectively) and an inner part describing the density distribution in the center of the WS cell. For spherical quasinuclear structures we employ the parametrization of [OI07]

$$\rho_q(r) = \begin{cases} (\rho_q^{in} - \rho_q^{out}) \left[1 - \left(\frac{r}{R_q}\right)^{t_q}\right]^3 + \rho_q^{out}, & r < R_q \\ \rho_q^{out}, & R_q \leq r\,. \end{cases} \tag{6.7}$$

As an alternative we also consider a Wood–Saxon density parametrization of the form

$$\rho_q(r) = (\rho_q^{in} - \rho_q^{out}) \left[1 + \exp\left(\frac{r - r_q}{a_q}\right)\right]^{-1} + \rho_q^{out}\,. \tag{6.8}$$

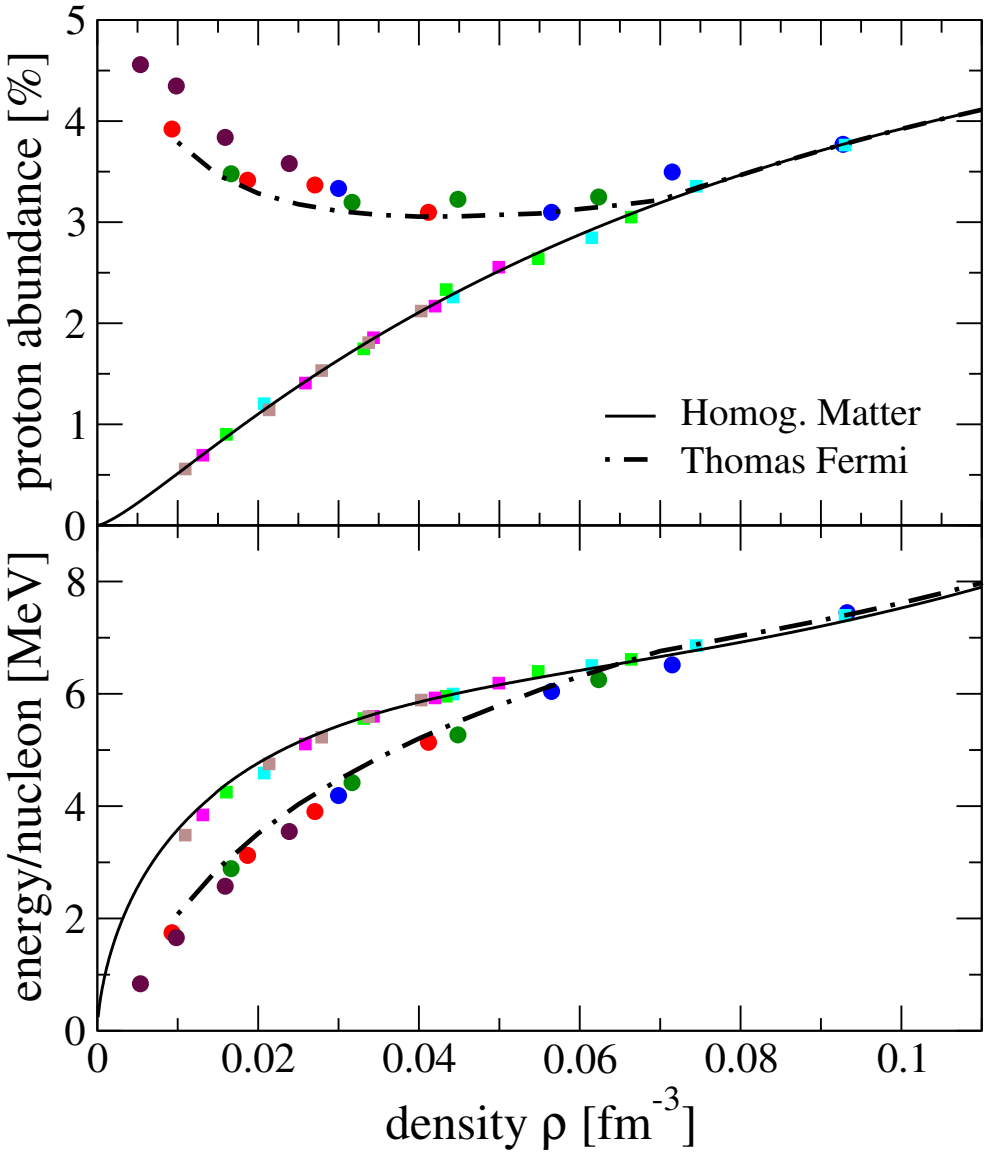

Figure 6.11: Proton abundances and energy per nucleon as obtained from Skyrme Hartree–Fock calculations at different densities. The results evaluated in cubic Wigner Seitz cells (various symbols) are compared to those of homogeneous infinite matter (solid lines) and of Thomas–Fermi calculations (dashed dotted line).

For the description of rod shaped quasinuclear structures cylindrical coordinates are used to parametrize the dependence of the densities on the radial coordinate in a way corresponding to eqs.(6.7) or (6.8). In case of quasinuclear structures in the shape of slabs these parametrizations are considered for the dependence of the densities on the Cartesian z–coordinate.

Assuming those density distributions, the TF energy is calculated as a sum of the bulk energy, i.e. the integrated nuclear matter energy densities, plus the contribution of a surface term of the form [Oya03, OI07]

$$E_{\rm surf} = F_0 \int_{\rm WS\text{-}cell} d^3r \ |\boldsymbol{\nabla}\rho|^2 \ . \tag{6.9}$$

The parameters of the density distributions in(6.7) and (6.8) are varied to minimize the energy of the system under consideration. The Parameter F_0 for the surface energy term in (6.9) has been adjusted in two different ways. In a first approach we have considered the properties of the nucleus ^{208}Pb and adjusted F_0 in such a way that the TF calculation reproduced the energy and radius of this nucleus derived from Skyrme HF. This leads to a value of F_0 of 68.3 MeV fm^5 and 59.7 MeV fm^5 using the parametrization of eq.(6.7) and the Wood–Saxon parametrization of eq.(6.8), respectively.

Adjusting the surface parameter F_0 in this way, one can evaluate the energies of quasinuclear structures in a WS cell using the TF approximation. The results for these TF energies are presented by the dashed dotted line in the lower panel of Fig. 6.11. One finds that this procedure leads to energies, which are consistently larger than those obtained in the HF calculations. It seems that the TF approach, as it is used here, is underestimating the gain in energy due to the formation of inhomogeneous structures. This could be a general problem of the TF approximation or a result of the limitation in the variational ansatz for the density functions.

To investigate these possibilities we have considered the different parametrizations displayed in eqs.(6.7) and (6.8). It turns out that these two parametrizations lead indeed to different density distributions, as displayed in the example of Fig. 6.12, but the resulting energy predictions do not exhibit significant differences, so that we present only one example for the TF approach in Fig. 6.11.

Then the surface term in (6.9) was readjusted to obtain an optimal fit of the HF energies for the quasinuclear structures in β–equilibrium. This readjustment of the surface term leads to values of the surface parameter F_0, which are about a factor of one half smaller than obtained from the fit to the properties of ^{208}Pb. Using these

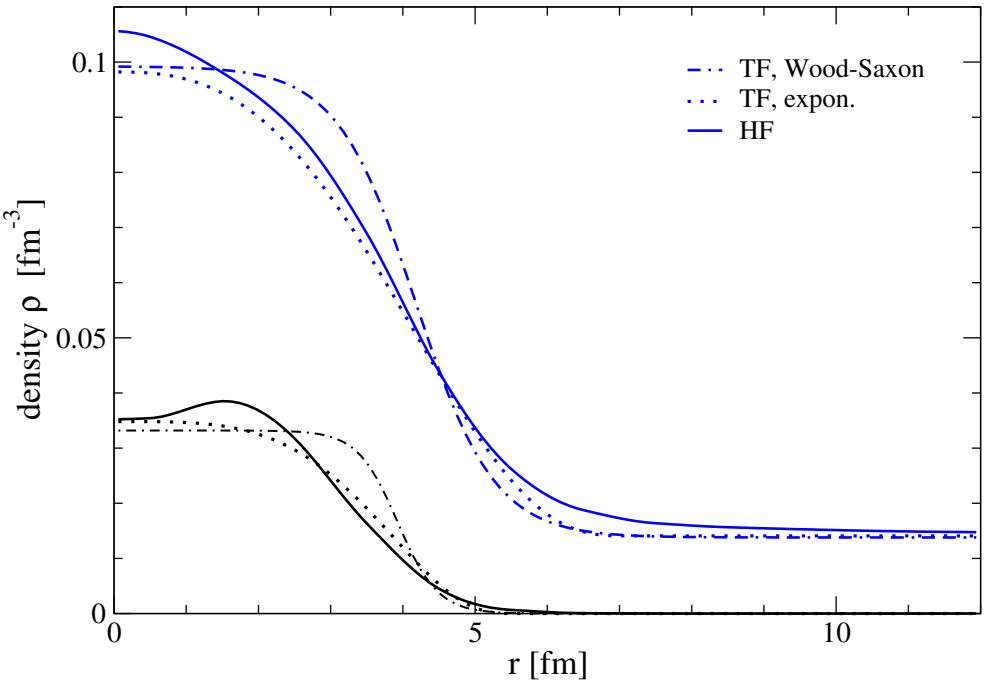

Figure 6.12: Density distributions resulting from Skyrme HF calculations for protons (lower graphs) and neutrons (upper graphs) as a function of the distance from the center of the Wigner Seitz cell. The densities resulting from HF are compared to those determined in Thomas–Fermi (TF) calculations, assuming the parametrizations of (6.7), dotted line, and (6.8), dashed line. The example refers to a global baryon density of 0.0166 fm^{-3}.

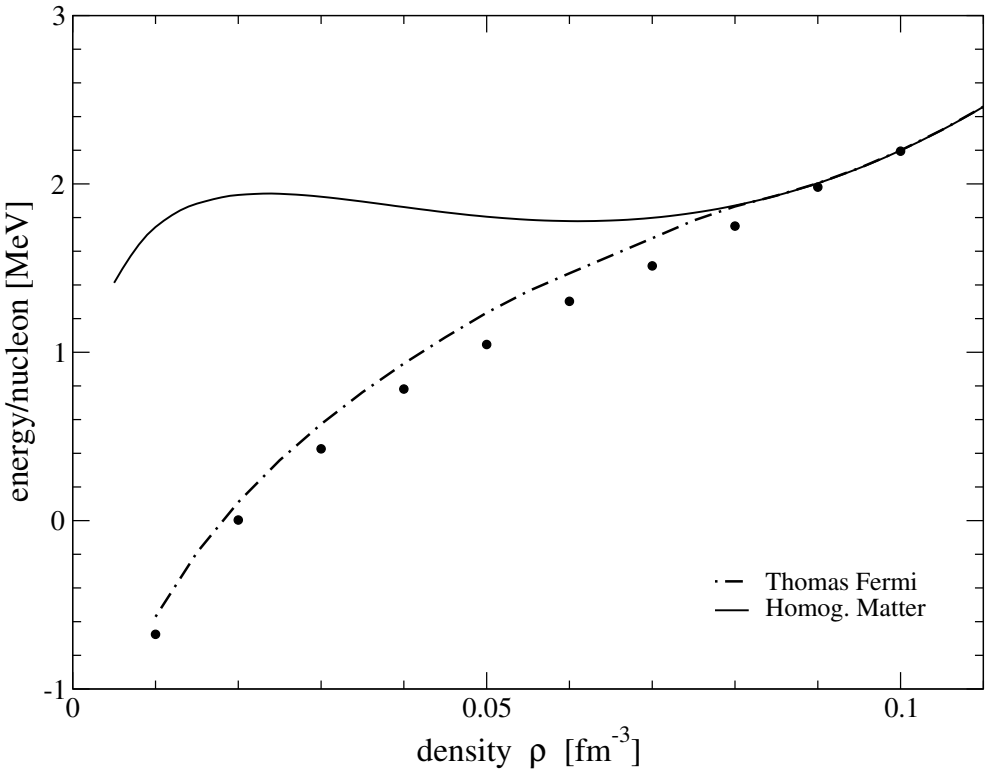

Figure 6.13: Energy per nucleon at a proton abundance $Y_p = 10\%$ from calculations employing the Skyrme interaction SLy4. The HF results obtained in cubic Wigner Seitz cells (circles) are compared to those of homogeneous infinite matter (solid lines) and of Thomas-Fermi calculations (dashed dotted line).

readjusted surface parameter we observe critical densities for the shape transitions of the quasinuclear structures from droplets to rods to slabs and to homogeneous nuclear matter at values which are similar to the results obtained in the HF calculations.

If, however, one uses this reduced values derived from the fit to inhomogeneous matter in β–equilibrium the TF calculation do not give an accurate description of Hartree–Fock energies, in which the proton abundance has been fixed e.g. to a value of 10 percent what is displayed in Fig. 6.13. This result can be taken as an indication that in addition to the isoscalar surface term of (6.9) an isovector surface term might be required in addition to obtain a reliable TF approximation to the results of corresponding HF calculations over a wide range of proton–neutron asymmetries.

The upper panel of Fig. 6.11 contains results on the proton abundances for bary-

onic matter plus electrons in β–equilibrium. The value of the proton abundance assuming homogeneous matter increases with density reaching a value of about 4% at a baryonic density of 0.1 fm^{-3}. Allowing for inhomogeneous, however, this value is almost constant around 3.2% in the density interval from 0.03 to 0.08 fm^{-3} and yields even larger values for densities below 0.03fm^{-3}. This trend is also reproduced in the TF calculations. The increase of the proton abundances at smaller global densities reflects the fact that at those small densities we observe local structures in the center of the WS cells, with large local densities. The proton abundance in these quasinuclear droplets is significantly larger than the proton abundance in the homogeneous matter with the same global density. The scattering of the results for the proton abundances as a function of density resulting from the HF calculations reflects the shell effects, which prefer the formation of quasinuclei with closed shells for the protons.

A comparison of energies resulting from relativistic mean–field calculations in a Wigner Seitz cell are displayed in the lower panel of Fig. 6.14. Comparing these results with the corresponding values displayed in Fig. 6.11 one finds that the energy gain due to the formation of inhomogeneous structures is much weaker in the relativistic mean–field calculations as compared to the Skyrme model. This is also reflected in the corresponding Thomas–Fermi calculations. Note that also in this case we have adjusted the constant F_0 of the surface term in (6.9) to reproduce the bulk properties of ^{208}Pb as predicted by the relativistic mean–field calculations. This leads to a value for F_0 of 87.4 MeV fm^5 and 80.3 MeV fm^5 using the parametrization of eq. (6.7) and the Wood–Saxon parametrization of eq. (6.8), respectively. Both values are significantly larger than the values required for F_0 in the case of the Skyrme model used above.

Employing the density dependent relativistic mean–field parametrization from DBHF introduced in section 6.1 we obtain the proton abundance and energy per nucleon as displayed in Fig. 6.15. First of all the energy per nucleon are significantly lower than those obtained from Skyrme Hartree–Fock calculations and the linear RMF model, what is due to the corresponding DBHF approach. At densities around 0.02 fm^{-3} the gain in energy per nucleon again rises to values comparable to the Skyrme calculations but at densities larger than 0.05 fm^{-3} still the same depletion is observed as for the linear RMF approach. The proton abundance shows a larger minimum compared with the linear RMF approach, but is still below the non–relativistic Skyrme Hartree–Fock calculation. From the minimum towards lower densities the proton

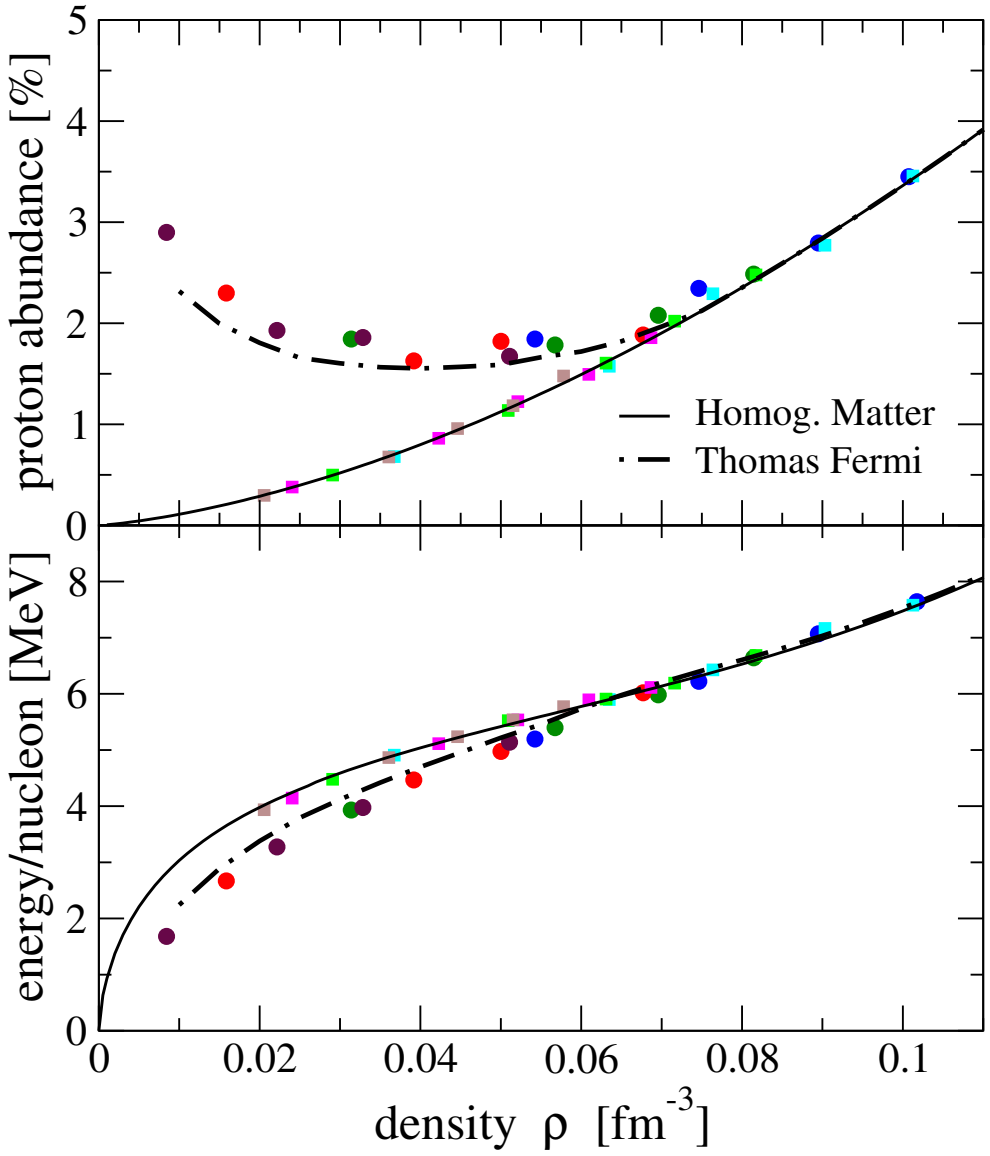

Figure 6.14: Proton abundances and energy per nucleon as obtained from relativistic mean–field calculations at different densities. The results evaluated in cubic Wigner Seitz cells (various symbols) are compared to those of homogeneous infinite matter (solid lines) and of Thomas–Fermi calculations (dashed dotted line).

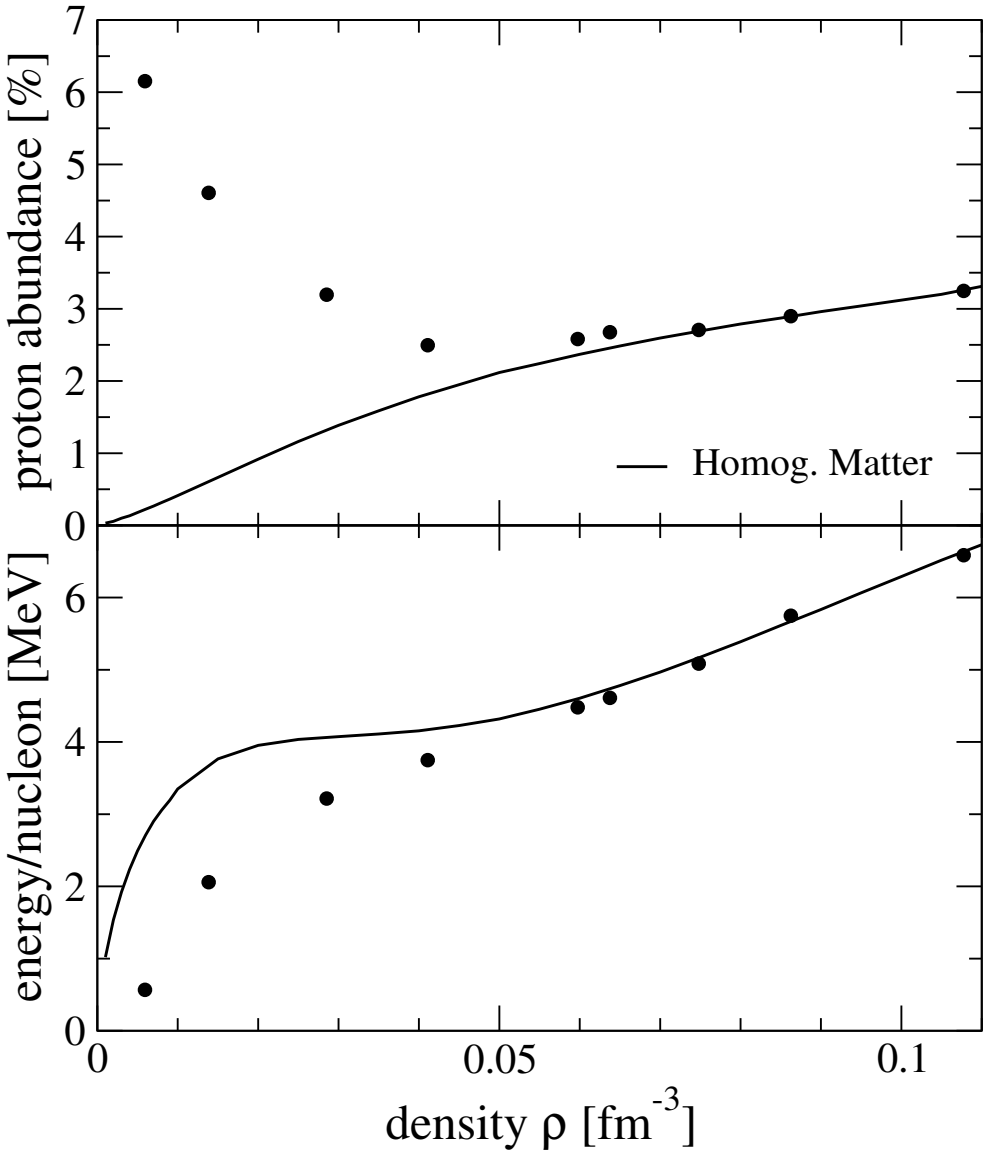

Figure 6.15: Proton abundances and energy per nucleon resulting from density dependent relativistic mean–field calculations at different densities. The results evaluated in cubic Wigner Seitz cells (circles) are compared to those of homogeneous infinite matter (solid lines).

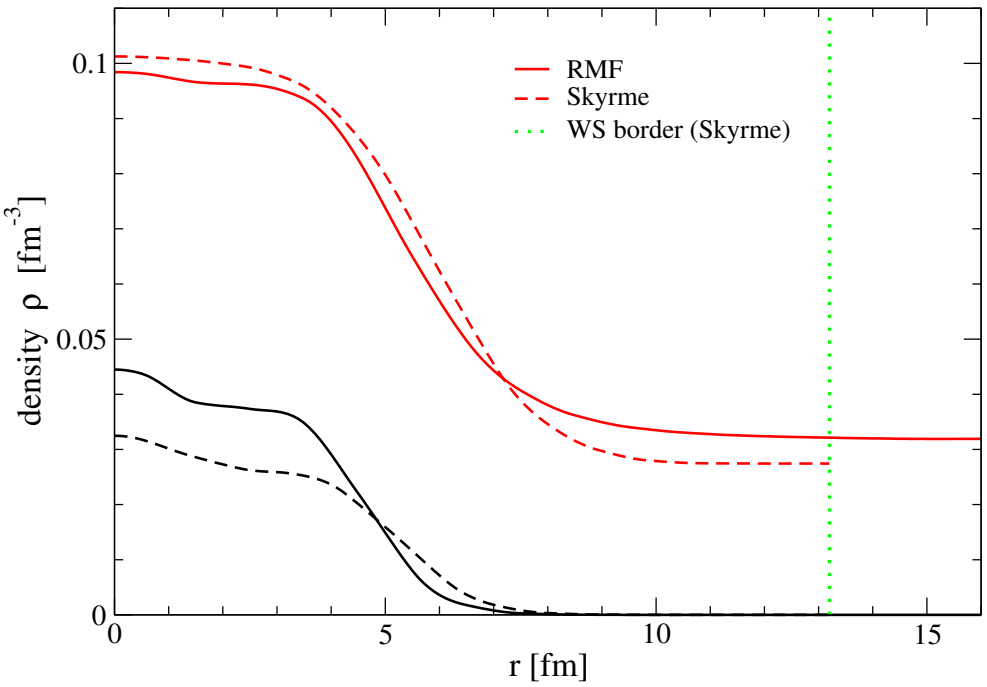

Figure 6.16: Density profiles for protons and neutrons as derived from Skyrme HF and relativistic mean–field calculations at a global density of $\rho = 0.032$ fm^{-3}.

abundance is rising more steeply than the one obtained from the linear RMF and Skyrme Hartree–Fock calculations.

The different interplay between volume, surface, symmetry and Coulomb effects in the relativistic mean–field model as compared to the Skyrme model also leads to smaller values for the proton abundance in the region of nuclear densities, in which inhomogeneous structures emerge. The values around $\rho = 0.02$ fm^{-3}, displayed in the upper panel of Fig. 6.14, are about 40% smaller than the corresponding values obtained in the Skyrme model (see Fig. 6.11). The differences in the balance between volume and surface contributions to the energy also lead to different quasinuclear structures in the nuclear models under consideration. It is worth mentioning that within the relativistic mean–field mode we do not find any formation of slab–like structures. Therefore the Table 6.3 contains for this case only transition densities for droplet to rod structures and the formation of a homogeneous structure.

The density profiles obtained from these two approaches also yield different results. As an example we present in Fig. 6.16 the density profiles at $\rho = 0.032$ fm^{-3}, a density at which both the relativistic as well as the Skyrme model yield a droplet structure. Note, that in the case of the Skyrme calculation we obtain a Wigner–Seitz

cell with a length of 26.4 fm which leads to a borderline as indicated by the dotted line, while the corresponding borderline for the RMF calculation is identical to the frame of the figure.

The Skyrme Hartree–Fock calculations in the Wigner–Seitz cell has been performed also at the finite temperature of $T = 5$ MeV according to section 4.3. At the quite large temperature of $T = 5$ MeV the pairing gap vanishes of course, but the code can be used without changes at different temperatures. The results for the proton abundance, energy per nucleon and free energy per nucleon are displayed in Fig. 6.17 for HF in the cubic cell, the homogeneous infinite matter and the Thomas–Fermi approximation. The latter has been performed employing the surface term F_0 for which the HF results are reproduced at zero temperature.

In the upper panel the proton abundance is displayed which shows a larger maximum as in the zero temperature case for all types of calculations. Especially the proton abundance obtained by homogeneous infinite matter calculation does not tend any more to a minimal value of almost zero as it is the case at zero temperature.

The lower panel shows the energy per nucleon and the free energy per nucleon for the various approaches. In case of the HF and TF calculations the energy per nucleon is reduced compared to the homogeneous nuclear matter result by up to 2 MeV in case of HF and 1 MeV for the TF approach at densities around 0.01 fm^{-3}. In contrast, the reduction of the free energy is not as pronounced as in case of the energy. The free energy is reduced about 0.5 MeV in the HF calculations and about 0.4 MeV in the TF calculations. The lower reduction of the free energy compared to the energy may stem from the entropy which is lower for the more structured nuclear shapes. By this means the reduction of the free energy should be suppressed for sufficiently large temperatures.

The free energy obtained in the Thomas–Fermi calculation deviates only a little from the HF calculation if the surface parameter is adjusted to reproduce the HF results at zero temperature. Unfortunately it is not possible to adjust the surface energy constant F_0 in such a way, that the energy, free energy and proton abundance of the Skyrme HF calculations in the cubic cell are reproduced. However, the free energy and the proton abundance of the HF calculations can simultaneously be reproduced in TF calculation by readjusting the constant F_0. This readjustment leads to the values of 29 MeV fm^5 and 26 MeV fm^5 for the exponential parametrization of eq. (6.7) and the Wood–Saxon parametrization of eq. (6.8), respectively. These parameters are lower by about 15% compared to the values at zero temperature.

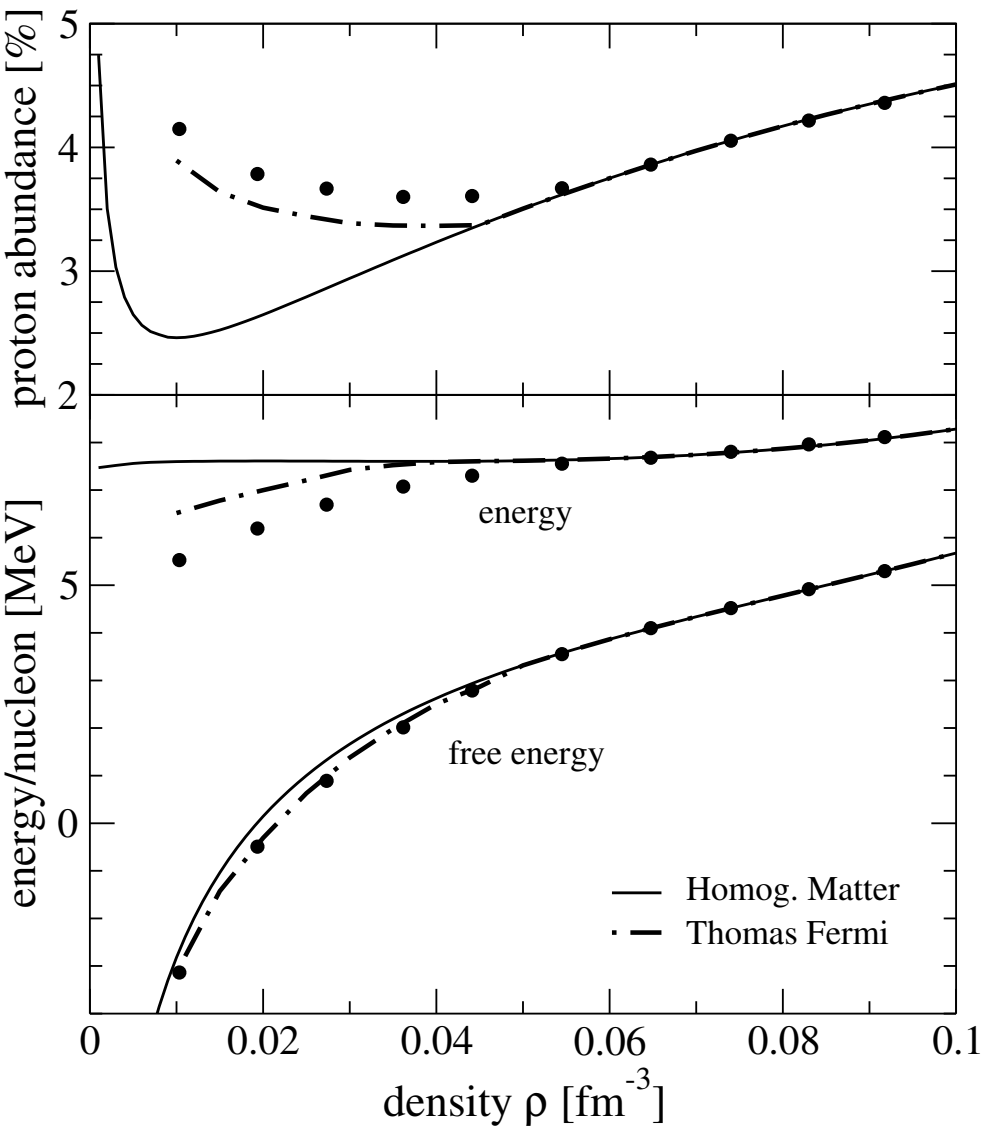

Figure 6.17: Proton abundances, energy per nucleon (upper curves) and free energy per nucleon (lower curves) as obtained from Skyrme calculations at $T = 5$ MeV. The results evaluated by the Hartree–Fock code in cubic Wigner Seitz cells (circles) are compared to those of homogeneous infinite matter (solid lines) and of Thomas–Fermi calculations (dashed dotted line).

Hence a slight modification of the surface energy constant F_0 could improve the Thomas–Fermi approach at finite temperature.

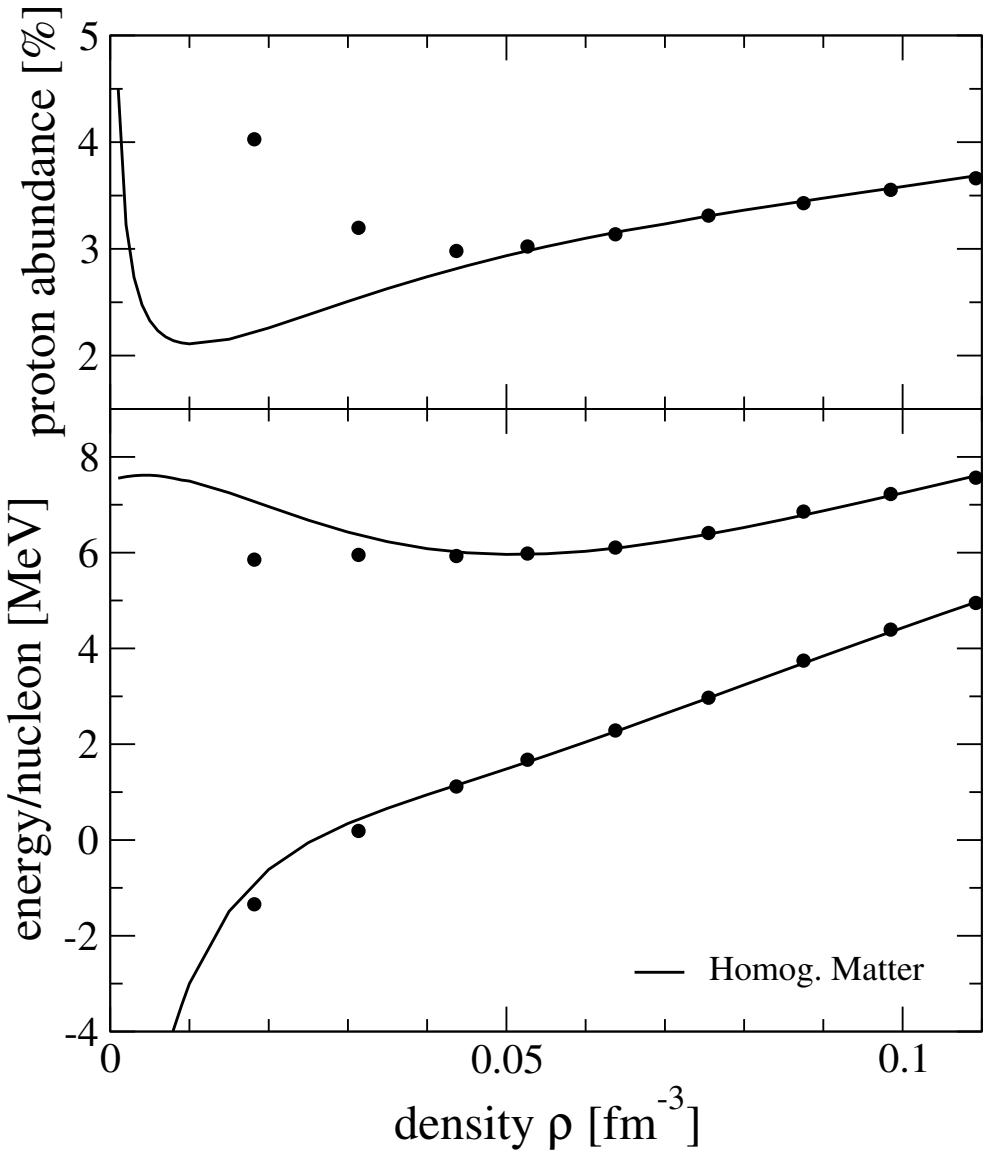

Figure 6.18: Proton abundances and energy per nucleon resulting from density dependent relativistic mean–field calculations at the temperature $T = 5$ MeV. The results evaluated in cubic Wigner Seitz cells (circles) are compared to those of homogeneous infinite matter (solid lines).

For comparison besides the Skyrme HF calculations there has been performed density dependent relativistic mean–field calculations at $T = 5$ MeV for which the results are displayed in Fig. 6.18. The upper panel displays the proton abundance at different densities and it can be observed that the overall behavior is the same as

in case of Skyrme Hartree–Fock. However, a lower value for the proton abundance is observed for the relativistic approach.
The lower panel shows two curves: the energy per nucleon (upper curve) and the free energy per nucleon (lower curve). Comparing with the Skyrme results we recognize, that the the relativistic calculation shows a minimum for the energy per nucleon at a density of about 0.05 fm^{-3} while the Skyrme calculation shows no minimum. Considering the relativistic approach, both curves, the energy curves and the free energy curve, approach the homogeneous matter curves already at the quite low density of 0.045 fm^{-3}. The reduction of the energy at low densities is up to 1.7 MeV, while the reduction of the free energy is again suppressed. Since we obtain the same suppression for different nuclear forces and different approaches we may assume that this effect is due to the entropy as already mentioned.
Despite of the differences between the non–relativistic and the relativistic approach similar overall properties are observed from both approaches for the energy and free energy per nucleon.

6.4 The Pairing Phenomenon

Finally, a feature of the pairing correlations obtained in these calculations shall be discussed. For that purpose the local pairing gap $\Delta(\boldsymbol{r})$ introduced in eq. (4.22) is presented in the upper panel of Fig. 6.19 for the formation of neutron pairs, as obtained in the Skyrme and relativistic mean–field model at $\rho = 0.032$ fm^{-3}. In both of these approaches one observes a suppression of the local gap $\Delta(\boldsymbol{r})$ in the region of the quasinuclear structure, i.e. in the region where the density is large.
This phenomenon has already been observed before [MMM04, MHe02, Ma07, BST07] and has lead to discussions about various phenomena, which are related to to this periodic structure of the gap parameter. It should be noted, however, that this suppression of the gap parameter in the high–density region of the quasinuclear structure is either to the local density approximation, which is used to calculate this local gap or to the assumption of the density dependence of the interaction strength for the pairing interaction, like the one, which we have considered in our calculations (see eq.(4.15)). If, rather than looking at the local gap parameter $\Delta(\boldsymbol{r})$, we inspect the anomalous density $\chi(\boldsymbol{r})$ (see eq.(4.20)), one finds even a small enhancement of the anomalous density in the region of the quasinuclear structure. This suggests that the reduction of the pairing gap in the region of high densities might be an

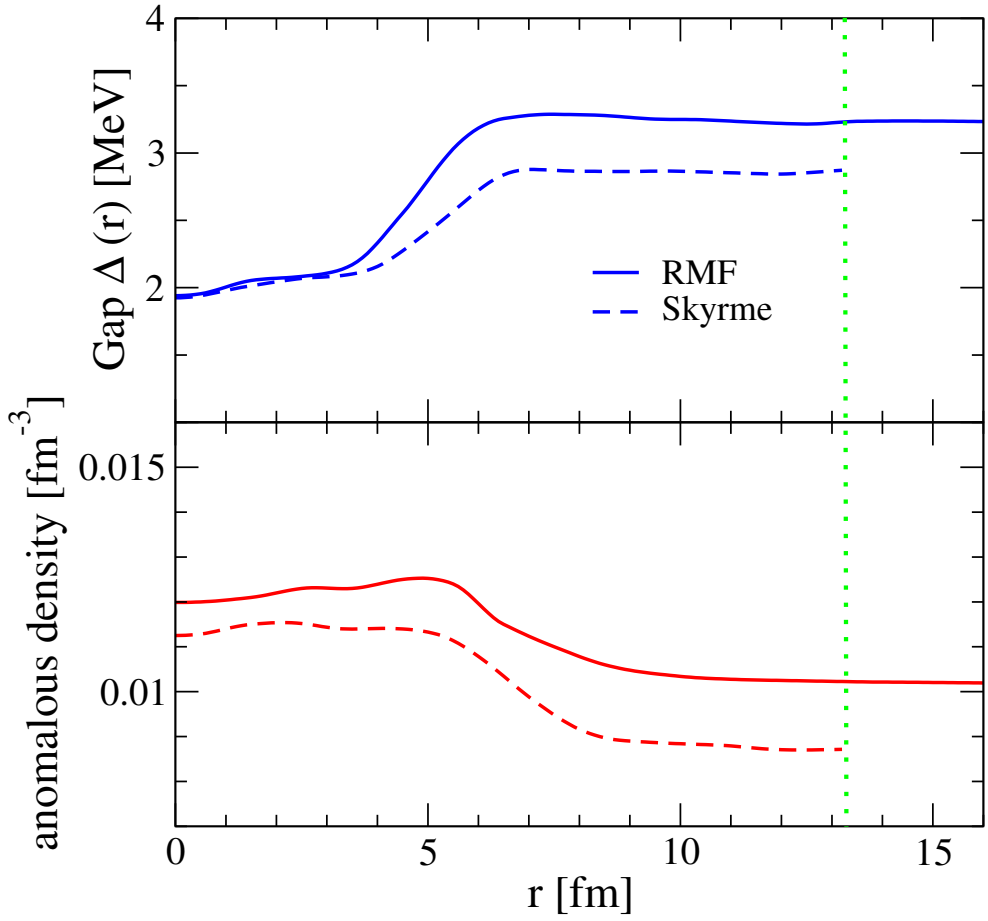

Figure 6.19: Local pairing gap $\Delta(r)$ (upper panel, see eq.(4.22)) and anomalous density $\chi(r)$ (lower panel, see eq.(4.20)) for the configurations which are also considered in Fig. 6.16.

artefact of the special interaction considered.

6.5 Exotic Nuclei

Neutron rich exotic nuclei are of major interest in astrophysics. They occur in a neutron star in the region between the envelope and the crust where the neutrons are about to drip off the nucleus. Their properties are also very important for the understanding of the r–process which forms heavy nuclei [CTT].
Some exotic nuclei have been investigated around the Oxygen and Calcium drip line. A model for finite nuclei should yield reasonable results for the neutron drip line. The approach developed here seems to be very appropriate, since the basis of box eigenfunctions should provide a good discretisation of the continuum states which are partially occupied by pairing correlations.
For the investigation the triaxial relativistic Hartree–Fock model described in section 3.3 has been applied with the parameter set PKO1 summarized in Table 5.6 from [LGM06]. Pairing correlations are treated by a pairing force like in equation (4.15) with the parameters $V_0 = 850.0$ MeV, $\eta = 1.0$, $\kappa = 1.0$ and the energy cut–off $\varepsilon_C = 5.0$ MeV, which are the same parameters as in [LGM06].
Among the bulk properties of nuclei is the root mean square radius which is evaluated by

$$r_{rms} = \sqrt{\langle r^2 \rangle} = \frac{\int d^3r\, r^2 \rho(\boldsymbol{r})}{\int d^3r\, \rho(\boldsymbol{r})}. \tag{6.10}$$

Of special interest is the root mean square charge radius, which can be measured by experiments. In a theoretical calculation the charge density of a nucleus is obtained by folding the proton density distribution with the Gaussian proton form factor for which a value of 0.8 fm is assumed [BM$^+$87]. From the charge density the so–called charge radius r_C is computed by formula (6.10).
The deformation parameters are obtained from the mass quadrupole moment. In our discretisation the quadrupole tensor is diagonal due to the symmetries (5.1) and (5.8) like in [BF$^+$85]. Thus we obtain only the quadrupole momenta Q_k along the axis

$$Q_k = Q_0 \cos(\gamma + \tfrac{2}{3}k\pi), \qquad k = 1, 2, 3, \tag{6.11}$$

where Q_0 is the absolute value of the quadrupole moment and the angle $0 \leq \gamma \leq \frac{1}{3}\pi$ indicates the shape of a triaxial deformation. The quadrupole momenta along the

	^{16}O	^{24}O	^{26}O	^{40}Ca	^{48}Ca	^{54}Ca	^{56}Ca
E/A [MeV]	-7.89	-6.98	-6.56	-8.44	-8.56	-8.12	-7.91
E/A exp. [MeV]	7.98	-7.02	-	-8.55	-8.67	-	-
r_c [fm]	2.72	2.76	2.82	3.47	3.48	3.55	3.60
r_c exp [fm]	2.74	-	-	3.48	3.47	-	-
$r_{rms,p}$ [fm]	2.61	2.65	2.71	3.38	3.40	3.47	3.69
$r_{rms,n}$ [fm]	2.58	3.22	3.38	3.34	3.64	3.90	4.08
β	0.0	0.0024	0.0011	0.0	0.0	0.0011	0.0014
γ [°]	0	60	60	0	0	60	60

Table 6.5: Properties of some Oxygen and Calcium isotopes as obtained from RHF calculations employing parameter set PKO1. Experimental values are taken from [HKL01, Au$^+$03].

axis Q_k are computed by

$$Q_k = \langle 3x_k^2 - \boldsymbol{r}^2 \rangle. \tag{6.12}$$

Solving equation (6.11) for γ and Q_0 yields the deformation parameter β in the following way:

$$\beta = \frac{\sqrt{5\pi}}{3AR_0^2} Q_0, \tag{6.13}$$

where $R_0 = \sqrt{5/3}\, r_{rms}$ is the geometric radius of the nucleus. (compare [MD$^+$00, YCM06]).

The properties of Oxygen and Calcium isotopes within the relativistic Hartree–Fock model are displayed in Table 6.5. Since the model is a phenomenological one, the binding energy and radii of ^{16}O, ^{40}Ca and ^{48}Ca are reproduced well. The ^{24}O nucleus has been experimentally established and we see that the calculated binding energy coincides with the experiment. The atomic mass table of Wapstra and Audi [Au$^+$03] reports values for the binding energy of some other of the investigated nuclei, but they are partially derived from systematic trends. The neutron radii of neutron rich isotopes become quite large, while the proton and charge radii are only slightly enhanced. This means that a neutron–rich surface is obtained for these nuclei. The neutron drip line for Oxygen has been experimentally established. The last stable isotope according to the experiment is ^{24}O while in the RHF model it is ^{26}O. This coincides with the calculated result of the DDRMF model (see section 6.1) and also in a shell model calculation the ^{26}O is still stable [SrM07]. It seems that in many

	^{24}O	^{26}O
$\varepsilon_{F,n}$	-3.2	-1.8
$1d_{5/2}$	-7.6, -7.3, -7.2	-8.0, -7.8, -7.7 (all 0.99)
$2s_{1/2}$	-4.6 (0.99)	-5.1 (0.98)
$1d_{3/2}$	-1.3 (0.01), -1.0 (0.007)	-1.9 (0.54), -1.7 (0.46)
$2p_{3/2}$	-	1.7, 1.8 (all 0.004)
$1f_{7/2}$	-	3.7, 3.8, 3.8 (0.01); 4.1 (0.008)

Table 6.6: Neutron single–particle states of neutron–rich Oxygen nuclei around the Fermi energy $\varepsilon_{F,n}$ obtained from RHF calculations. All energies are given in MeV. Several energies denote splitting according to the magnetic quantum number m_j. Occupation probabilities are given in parentheses if they deviate from one.

theoretical models the neutron drip line is shifted slightly towards larger neutron excess.

In nuclei with partly occupied shells deformations occur. The results obtained for neutron–rich nuclei from the RHF model show all oblate shape. In deformed nuclei the angular momentum is not a good quantum number any more, but as long as the deformation is of axial shape the magnetic quantum number m_j is conserved. In the case of deformations the single–particle energies of one shell split up for different m_j.

The single–particle levels around the Fermi energy of neutron–rich Oxygen nuclei near the neutron drip line are summarized in Table 6.6. It is observed that for the ^{26}O nucleus the states in the $2p_{3/2}$ shell show lower single–particle energies than the one in the $1f_{7/2}$ shell, which are ordered vice versa in a usual nucleus [RS80]. In ^{24}O the same level crossing is observed, but the occupation probability for these levels gets less than 1.0×10^{-4}.

Also for the two neutron–rich Calcium isotopes ^{54}Ca and ^{56}Ca the single particle energies for neutrons are displayed in Table 6.7, where we can observe a level crossing between the $2p_{1/2}$ and the $1f_{5/2}$ shell. In the ^{54}Ca the difference between the levels is already $\Delta\varepsilon = 0.6$ MeV, while in ^{56}Ca it is less pronounced.

The shell structure of the protons may be affected too in such neutron–rich nuclei. Grasso et al. observed in [Gr$^+$07] a crossing of the $2s_{1/2}$ and the $1d_{3/2}$ levels for certain Skyrme interactions and some relativistic mean–field parametrizations. This level crossing is also obtained in the RHF calculation for the ^{54}Ca nucleus by a value

	^{54}Ca	^{56}Ca
$\varepsilon_{F,n}$	-4.1	-4.0
$1f_{7/2}$	-10.0, -9.9, -9.9, -9.8	-10.3, -10.2, -10.1, -10.0 (0.99)
$2p_{3/2}$	-5.7 (0.93), -5.6 (0.92)	-6.4 (0.95), -6.3 (0.94)
$2p_{1/2}$	-4.0 (0.45)	-4.6 (0.69)
$1f_{5/2}$	-3.3 (0.27), -3.2 (0.23), -3.0 (0.20)	-4.3 (0.59), -3.9 (0.44), -3.8 (0.39)
$1g_{9/2}$	1.4–1.9 (0.015–0.012)	0.8–1.7 (0.015-0.010)

Table 6.7: Neutron single–particle states of neutron–rich Calcium nuclei around the Fermi energy $\varepsilon_{F,n}$ obtained from RHF calculations. All energies are given in MeV. Several energies denote splitting according to the magnetic quantum number m_j. Occupation probabilities are given in parentheses if they deviate from one.

of $\Delta\varepsilon = 0.2$ MeV. In case of the ^{56}Ca nucleus the energy difference between these levels is almost zero, what means that in this nucleus the level crossing turns back. In nuclei with even larger neutron excess Grasso et al. observed the usual order of states again.

The results for the relativistic Hartree–Fock model show that deformations occur for neutron rich Oxygen and Calcium isotopes and level crossings take place for neutrons and in Calcium also for protons. It would be interesting if these results hold also for investigations beyond the mean–field.

Chapter 7

Summary and Outlook

In this work the Skyrme Hartree–Fock and Relativistic Hartree–Fock approaches have been considered to describe the structure of nuclear systems ranging from finite nuclei, structures in the crust of neutron stars to homogeneous matter. Effects of pairing correlations and finite temperature are also taken into account. The numerical procedure in the cubic box is described for the Skyrme Hartree–Fock as well as the relativistic Hartree–Fock approach. And finally, results for the crust of neutron stars and exotic nuclei are presented and discussed.

The Skyrme Hartree–Fock theory is a non–relativistic approach to nuclear structure which provides fast calculations due to the zero range Skyrme interaction. This approach has been applied in a cubic Cartesian Wigner–Seitz cell including pairing and finite temperature effects to explore the structure of the so–called nuclear "pasta" phase which occurs in the crust of the neutron star.

Especially in the relativistic Hartree–Fock approach progress has been made in recent years. The operator structure has been confirmed to be similar to that of the Dirac–Brueckner–Hartree–Fock approach. Hence a local density approximation of the DBHF self–energies leads to density dependent coupling for the relativistic Hartree–Fock approach. Using density dependent coupling the rearrangement contribution to the self–energy improves the single–particle energies and wave functions significantly. The triaxial treatment of the relativistic Hartree Fock method has been developed and applied in two cases: Exotic nuclei have been investigated by the relativistic Hartree–Fock approach and the crust of neutron stars has been explored within the relativistic Hartree approach including pairing correlations and finite temperature.

Furthermore a set of density dependent coupling functions to be used in relativistic

Hartree calculations has been fitted to the self–energies of DBHF results of van Dalen et al. [vD$^+$07]. These DBHF calculations are performed employing realistic potentials of the Bonn type and the results provide a good equation of state for neutron stars. A renormalization procedure improves significantly the agreement of the density dependent relativistic mean–field model (DDRMF) with the DBHF results. This procedure modifies in a first step the effective masses of protons and neutrons by absorbing the spatial vector self–energy into the scalar self–energy. In a second step the time–like component of the vector self–energy is modified such that the single–particle energies and the overall binding energies are reproduced. The renormalized DDRMF model still results in underbound nuclei and hence the coupling of the ω–meson has been weakened around the saturation point to be able to reproduce the binding energy of heavy nuclei. The radii of the nuclei are still slightly underestimated. The properties of the resulting DDRMF model are comparable to the original DBHF results. Therefore the DDRMF model should provide a good description of the nuclear equation of state for astrophysical use.

The structure of neutral baryonic matter is investigated in a region of baryon densities between 0.01 and 0.1 fm^{-3} performing various Hartree–Fock and mean–field calculations with inclusion of pairing correlations and finite temperature in a periodic lattice of Wigner–Seitz (WS) cells of cubic shapes. In this region of densities, which should occur in the crust of neutron stars, one observes structures ranging from neutron–rich nuclei embedded in a sea of neutrons up to homogeneous matter. The symmetries of the WS cell allow the formation of triaxial structures which also include rod– and slab–like structures and provide a natural transition to the description of homogeneous matter.

For the baryonic components a Skyrme Hartree–Fock approximation has been compared to the relativistic mean–field model with and without density dependence. All approaches yield an intriguing variety of quasinuclear structures with smooth transitions in between. The occurrence of special structures as well as the critical densities at which transitions between those structures occur depend on the nuclear model considered. Forming such structures the energy is reduced compared to the one in homogeneous nuclear matter and the proton abundance rises.

The resulting energies as well as the proton abundances can fairly well be reproduced by a Thomas–Fermi approach, if the constant, determining the strength of the surface term is adjusted to reproduce the results of the microscopic calculations. A surface term depending on the isospin asymmetry might be required to obtain

Thomas–Fermi results, which are reliable over a large interval of proton-neutron asymmetries.

At finite temperature the richness of the various nuclear shapes obtained from the Skyrme HF and the relativistic mean–field approaches decreases, although some structures are still present. In such an environment the proton abundance is even more enhanced than at zero temperature and the reduction of the free baryonic energy is less pronounced as the one of the baryonic energy due to the lower entropy in the more structured matter. It is possible to reproduce the free energy and the proton abundances by a Thomas–Fermi approach, however, this approach shows deficiencies in reproducing the energy as well as some structures at finite temperature.

Pairing correlations have been evaluated within the BCS approach, assuming a density dependent contact interaction. This leads to local pairing gaps for neutron pairing, which are significantly smaller in the regions of the quasinuclear structures as compared to the bulk of the neutron sea. Since the density dependent pairing interaction leads to an effect which is opposite to the anomalous density, the pairing interaction should be reviewed on the basis of realistic NN potentials. The influence of the superfluid nuclear matter on the rotation properties of the star is another interesting facet of pairing.

The microscopic calculation of single–particle energies and wave functions provide an interesting starting point for further studies on the properties of matter in the crust of neutron stars. Transition matrix elements can be evaluated for various operators what leads to response functions, e.g. the neutrino opacity. Such studies could provide new information about the influence of such nuclear structures on the cooling rate and other properties of the star.

The various nuclear structures which appear in the crust of neutron stars are even more pronounced in core collapse supernovae since the proton abundance rises due to trapped neutrinos. It should be checked if the nuclear structures survive in such an environment at large finite temperatures and if the neutrino opacity undergoes relevant changes.

Properties of exotic neutron–rich nuclei provide a basis for investigations of the formation of heavy nuclei in stars. The observed changes in the shell structure may influence the properties of such nuclei and modify the formation of the heavy ones.

The relativistic Hartree–Fock approach may be improved by parametrizations including density dependent coupling for the tensor self–energy contribution of the ρ–meson. Such parametrizations may be compared from phenomenological fits and

from Dirac–Brueckner–Hartree–Fock calculations.

Calculations with realistic NN potentials should confirm the results obtained employing mean–field approaches in the Wigner–Seitz cell and also for exotic nuclei. A first attempt is already in progress which is based on a low–momentum interaction V_{lowk} in a spherical box with a plane wave basis.

A more improved attempt which combines realistic potentials and relativistic effects would be to perform Dirac–Brueckner–Hartree–Fock calculations in finite nuclei. So far such calculations are regarded as too complex, but may be that things are changing in years to come.

Bibliography

[An+83] M.R. Anastasio, L.S. Celenza, W.S. Pong, and C.M. Shakin: *Relativistic nuclear structure physics*, Phys. Rep. **100** (1983) 327–392.

[Au+03] G. Audi, A.H. Wapstra, and C. Thibault: *The AME2003 atomic mass evaluation. (II.) Tables, graphs and references*, Nucl. Phys. **A729** (2003) 337–676.

[BST07] M. Baldo, E.E. Saperstein, S.V. Tolokonnikov: *A realistic model of superfluidity in the neutron star inner crust*, Eur. Phys. J. **A32** (2007) 97–108 .

[BCS57] J. Bardeen, L.N. Cooper, and J.R. Schrieffer: *Theory of Superconductivity*, Phys. Rev. **108** (1957) 1175–1204.

[BE91] G.F. Bertsch and H. Esbensen: *Pair correlations near the neutron drip line*, Ann. Phys. **209** (1991) 327–363.

[BD64] J.D. Bjorken and S.D. Drell: *Relativistic Quantum Mechanics*, McGraw–Hill, New York, 1964.

[BD65] J.D. Bjorken and S.D. Drell: *Relativistic Quantum Fields*, McGraw–Hill, New York, 1965.

[BK+03] S.K. Bogner, T.T.S. Kuo, and A. Schwenk: *Model–independent low momentum nucleon interaction from phase shift equivalence*, Phys. Rept. **386** (2003) 1–27.

[BDM06] P. Bożek, D.J. Dean, H. Müther: *Correlations and effective interactions in nuclear matter*, Phys. Rev. **C74** (2006) 014303.

[BV81] P. Bonche and D. Vautherin: *A mean–field calculation of the equation of state of supernova matter*, Nucl. Phys. **A372** (1981) 496–526.

[BF+85] P. Bonche, H. Flocard, P.–H. Heenen, S.J. Krieger, and M.S. Weiss: *Self–consistent study of triaxial deformations: Application to the isotopes of Kr, Sr, Zr and Mo*, Nucl. Phys. **A443** (1985) 39–63.

[BM+87] A. Bouyssy, J.–F. Mathiot, N. Van Giai, and S. Marcos: *Relativistic description of nuclear systems in the Hartree–Fock approximation* Phys. Rev. **C36** (1987) 380–401.

[Br78] R. Brockmann: *Relativistic Hartree–Fock description of nuclei*, Phys. Rev. **C18** (1978) 1510–1524.

[BM90] R. Brockmann and R. Machleidt: *Relativistic nuclear structure. I. Nuclear matter*, Phys. Rev. **C42** (1990) 1965–1980.

[CB+97] E. Chabanat, P. Bonche, P. Haensel, J. Meyer, and R. Schaeffer: *A Skyrme parametrization from subnuclear to neutron star densities*, Nucl. Phys. **A627** (1991) 710–746.

[CB+98] E. Chabanat, P. Bonche, P. Haensel, J. Meyer, and R. Schaeffer: *A Skyrme parametrization from subnuclear to neutron star densities Part II. Nuclei far from stabilities*, Nucl. Phys. **A635** (1998) 231–256.

[CMF78] H.–T. Chen, H. Müther and A. Faessler: *Pairing vibrational and isospin rotational states in a particle number and isospin projected generator coordinate method*, Nucl. Phys. **A297** (1978) 445–470.

[Cep95] D.M. Ceperley: *Path integrals in the theory of condensed helium*, Rev. Mod. Phys. **67** (1995) 279–355.

[Co+70] F. Coester, S. Cohen, B. Day, and C. M. Vincent: *Variation in Nuclear–Matter Binding Energies with Phase–Shift–Equivalent Two–Body Potentials*, Phys. Rev. **C1** (1970) 769–776.

[CTT] J.J. Cowan, F.–K. Thielemann and J.W. Truran: *Nuclear Evolution of the Universe*, University of Chicago Press, to be published.

[DA03] N.D. Dang, A. Arima: *Modified Hartree–Fock–Bogoliubov at finite temperature*, Phys. Rev. **C68** (2003) 014318.

[DF+80] K.T.R. Davies, H. Flocard, S. Krieger, and M.S. Weiss: *Application of the Imaginary Time Step Method to the Solution of the Static Hartree–Fock Problem*, Nucl. Phys. **A342** (1980) 111–123.

[DM+92] W.H. Dickhoff and H. Müther: *Nucleon properties in the nuclear medium*, Rep. Prog. Phys. **55** (1992) 1947–2023.

[FT+00] S.A. Fayans, S.V. Tolokonnikov, E.L. Trykov, and D. Zawischa: *Nucler Isotope Shifts within the Local Energy–Density Functional Approach*, Nucl. Phys. **A676** (2000) 49–119.

[Fe28] E. Fermi: *Eine statistische Methode zur Bestimmung einiger Eigenschaften des Atoms und ihre Anwendung auf die Theorie des periodischen Systems der Elemente*, Z. Phys. **48** (1928) 73–79.

[Fr94] R. Fritz: *Korrelationen und Relativistische Effekte in Atomkernen*, Eberhard–Karls–Universität Tübingen, 1994.

[FM94] R. Fritz und H. Müther: *NN correlations and relativistic Hartree-Fock in finite nuclei*, Phys. Rev. **C49** (1994) 633–644.

[FLW95] C. Fuchs, H. Lenske, and H.H. Wolter: *Density Dependent Hadron Field Theory*, Phys. Rev. **C52** (1995) 3043–3060.

[GS+99] E. Garrido, P. Sarriguren, E. Moya de Guerra, and P. Schuck: *Effective density dependent pairing forces in the T=1 and T=0 channels*, Phys. Rev. **C60** (1999) 064312.

[GR65] I.S. Gradshteyn and I.M. Ryzhik: *Table of Integrals, Series and Products*, Academic Press, New York, 1965.

[Gr+07] M. Grasso, Z.Y. Ma, E. Khan, J. Margueron, and N. Van Giai: *Evolution of the proton sd states in neutron-rich Ca isotopes*, preprint arXiv: nucl–th/0706.3287.

[Grn87] W. Greiner *Theoretische Physik: Relativistische Quantenmechanik - Wellengleichungen*, Vol. 6, 2nd ed., Harry Deutsch, Thun and Frankfurt am Main, 1987.

[GM07a] P. Gögelein and H. Müther: *Nuclear matter in the crust of neutron stars*, Phys. Rev. **C76**, 024312 (2007).

[GvD+07] P. Gögelein, E.N.E. van Dalen, C. Fuchs, and H. Müther: *Nuclear matter in the crust of neutron stars derived from realistic NN interactions*, preprint arXiv: nucl–th/0708.2867.

[GM07b] P. Gögelein and H. Müther: in progress.

[Gdm81] A.L. Goodman: *Finite–temperature HFB theory*, Nucl. Phys. **A352** (1981) 30–44.

[HS+84] M. Hashimoto, H. Seki, and M. Yamada: *Shape of Nuclei in the Crust of Neutron Star*, Prog. Theor. Phys, **71** (1984) 320–326.

[HSt52] M.R. Hestenes and E. Stiefel: *Methods of conjugate gradients for solving linear systems*, J. of Res. Nat. Bur. Standards **49** (1952) 409–436.

[HKO95] M. Hjorth–Jensen, T.T.S. Kuo, E. Osnes: *Realistic effective interactions for nuclear systems*, Phys. Rep. **261** (1995) 125–270.

[HKL01] F. Hofmann, C.M. Keil, and H. Lenske: *Density dependent hadron field theory for asymmetric nuclear matter and exotic nuclei*, Phys. Rev. **C64** (2001) 034314.

[HK64] P. Hohenberg and W. Kohn: *Inhomogenous Electron Gas*, Phys. Rev. **136** (1964) B864–B871.

[HSe81] C.J. Horowitz and B.D. Serot: *Self–consistent Hartree description of finite nuclei in a relativistic quantum field theory*, Nucl. Phys. **A368** (1981) 503–528.

[HSe83] C.J. Horowitz and B.D. Serot: *Properties of nuclear and neutron matter in a relativistic Hartree–Fock theory*, Nucl. Phys. **A399** (1983) 529–562.

[Jac75] J.D. Jackson: *Classical Electrodynamics*, 2nd ed., Wiley, New York, 1975.

[KB+06] T. Klähn, D. Blaschke, S. Typel, E.N.E. van Dalen, A. Faessler, C. Fuchs, T. Gaitanos, H. Grigorian, A. Ho, E.E. Kolomeitsev, M. C. Miller, G. Röpke, J. Trümper, D. N. Voskresensky, F. Weber, and H. H. Wolter: *Constraints on*

the high–density nuclear equation of state from the phenomenology of compact stars and heavy-ion collisions, Phys. Rev. **C74** (2006) 035802.

[KF+94] M. Kleinmann, R. Fritz, H. Müther, and A. Ramos: *On the Momentum Dependence of the Nucleon–Nucleus Optical Potential*, Nucl. Phys. **A579** (1994) 85–102.

[KS65] W. Kohn and L.J. Sham: *Self–Consistent Equations Including Exchange and Correlation Effects*, Phys. Rev. **140** (1965) A1133–A1138.

[KM+03] J. Kuckei, F. Montani, H. Müther, and A. Sedrakian: *The structure of nuclear systems derived from low momentum nucleon–nucleon potentials*, Nucl. Phys. **A723** (2003) 32–44.

[LP81] I.E. Lagaris and V.R. Pandharipande: *Phenomenological two–nucleon interaction operator*, Nucl. Phys. **A359** (1981) 331–348.

[LMK91] K. Langanke, J.A. Maruhn, S.E. Koonin: *Computational Physics I, Nuclear Structure*, Springer, Berlin, Heidelberg (1991).

[LGM06] W.H. Long, N. Van Giai, and J. Meng: *Relativistic Hartree–Fock theory. Part I: density–dependent effective Lagrangians*, preprint arXiv: nucl–th/0608009 (2006).

[Ml89] R. Machleidt: *The Meson Theory of Nuclear Forces and Nuclear Structure*, Adv. Nucl. Phys. **19** (1989) 189–376.

[MHe02] P. Magierski and P.–H. Heenen: *Structure of the inner crust of neutron stars: crystal lattice or disordered phase?*, Phys. Rev. **C65** (2002) 045804.

[Ma07] P. Magierski: *Neutron localization induced by the pairing field in inhomogeneous neutron matter*, Phys. Rev. **C75** (2007) 012803.

[MT+05] T. Maruyama, T. Tatsumi, D.N. Voskresensky, T. Tanigawa, and S. Chiba: *Nuclear pasta structures and the charge screening effect*, Phys. Rev. **C72** (2005) 015802.

[MT+06] T. Maruyama, T. Tatsumi, T. Endo, and S. Chiba: *Pasta structures in compact stars*, preprint arXiv: nucl-th/0605075 (2006).

[MD+00] S. Mizutori, J. Dobaczewski, G.A. Lalazissis, W. Nazarewicz, and P.–G. Reinhard: *Nuclear skins and halos in the mean–field theory*, Phys. Rev. **C61** (2000) 044326 .

[MMM04] F. Montani, C. May, and H. Müther: *Mean field and pairing properties in the crust of neutron stars*, Phys. Rev. **C69** (2004) 065801.

[MP00] H. Müther and A. Polls: *Two–Body Correlations in Nuclear Systems*, Prog. Part. Nucl. Phys. **45** (2000) 243–334.

[Ne70] J.W. Negele: *Structure of finite Nuclei in the Local–Density Approximation*, Phys. Rev. **C1** (1970) 1260–1321.

[NV72] J.W. Negele and D. Vautherin: *Density-Matrix Expansion for an Effective Nuclear Hamiltonian*, Phys. Rev. **C5** (1972) 1472–1493.

[NV75] J.W. Negele and D. Vautherin: *Density-Matrix Expansion for an Effective Nuclear Hamiltonian. II*, Phys. Rev. **C11** (1975) 1031–1041.

[Oya03] K. Oyamatsu: *Nuclear shapes in the inner crust of a neutron star*, Nucl. Phys. **A561** (1993) 431–452.

[OI07] K. Oyamatsu and K. Iida: *The symmetry energy at subnuclear densities and nuclei in neutron star crusts*, Phys. Rev. **C75** (2007) 015801.

[PR95] C.J. Pethick and D.G. Ravenhall: *Neutron–rich matter and the crusts of neutron stars*, Ann. Rev. Nucl. Part. Sci. **45** (1995) 429–484.

[Rei71] J.K. Reid (ed.): *Large sparse sets of linear equations*, Academic Press, London and New York, 1971.

[Rcg71] J.K. Reid, *On the method of conjugate gradients for the solution of large sparse systems of linear equations*, in [Rei71] 231–252.

[Rhd89] P.–G. Reinhard: *The relativistic mean–field description of nuclei and nuclear dynamics*, Rep. Prog. Phys. **52** (1989) 439–514.

[RS80] P. Ring and P. Schuck: *The Nuclear Many–Body Problem*, Springer, Berlin Heidelberg New York, 1980.

[RPRM06] A. Rios, A. Polls, A. Ramos, H. Müther: *The entropy of a correlated system of nucleons*, Phys. Rev. **C74** (2006) 054317.

[RR+88] M. Rufa, P.–G. Reinhardt, J. Maruhn, W. Greiner, and M.R. Strayer: *Optimal parametrization for the relativistic mean–field model of the nucleus*, Phys. Rev. **C38** (1988) 390–409.

[Sv+86] R. Schiavilla, V. R. Pandharipande and R. B. Wiringa: *Momentum distributions in $A = 3$ and 4 nuclei*,
Nucl. Phys. **A449** (1986) 219–242.

[SM01] E. Schiller and H. Müther: *Correlations and the Dirac Structure of the Nucleon Self–Energy*, Eur. Phys. J. **A11** (2001) 15–24.

[Sch00] E. Schiller: *Die relativistische Struktur der Nukleon–Nukleon Wechselwirkung im Medium*, Eberhard–Karls–Universität Tübingen, 2000.

[Sm04] K.W. Schmid: *On the use of general symmetry–projected Hartree–Fock–Bogoliubov configurations in variational approaches to the nuclear many–body problem*, Prog. Part. Nucl. Phys. **52** (2004) 565–633.

[SR91] K.W. Schmid and P.–G. Reinhard: *Center–of–mass projection of skyrme–hartree–fock densities*, Nucl. Phys. **A530** (1991) 283–302.

[SW86] B.D. Serot and J.D. Walecka: *The Relativistic Nuclear Many–Body Problem*, Adv. Nucl. Phys. **16** (1986).

[ST+98b] H.Shen, H.Toki, K.Oyamatsu, K.Sumiyoshi: *Relativistic Equation of State of Nuclear Matter for Supernova Explosion*,
Prog. Theor. Phys. **100** (1998) 1013.

[ST+98a] H.Shen, H.Toki, K.Oyamatsu, K.Sumiyoshi: *Relativistic Equation of State of Nuclear Matter for Supernova and Neutron Star*,
Nucl. Phys. **A637** (1998) 435–450.

[Sk59] T.H.R. Skyrme: *Effective nucleon potential*,
Nucl. Phys. **9** (1959) 615–634.

[SrM07] P.C. Srivastava, and I. Mehrotra: *Shell model study of neutron rich oxygen isotopes*, preprint arXiv: nucl–th/0706.1812.

[SR07] J.R. Stone and P.–G. Reinhard: *The Skyrme Interaction in finite nuclei and nuclear matter*, Prog. Part. Nucl. Phys. **58** (2007) 587–657.

[Th27] L.H. Thomas: *The calculation of atomic fields*, Proc. Camb. Phil. Soc. **23** (1927) 542–548.

[UM97] S. Ulrych and H. Müther: *Relativistic structure of the nucleon self–energy in asymmetric nuclei*, Phys. Rev. **C56** (1997) 1788–1794.

[vD+07] E.N.E. van Dalen, C. Fuchs, and A. Faessler *Dirac–Brueckner–Hartree–Fock calculations for isospin asymmetric nuclear matter based on improved approximation schemes*, Eur. Phys. J. **A31** (2007) 29–42.

[Va+95] A. Valcarce, A. Buchmann, F. Fernández, and A. Faessler: *Spin–orbit force in a quark model based nucleon–nucleon potential*, Phys. Rev. **C51** (1995) 1480–1487.

[VB72] D. Vautherin and D.M. Brink: *Hartree–Fock Calculations with Skyrme's Interaction. I. Spherical Nulei*, Phys. Rev. **C5** (1972) 626–647.

[Vau73] D. Vautherin:, *Hartree–Fock Calculations with Skyrme's Interaction. II. Axially Deformed Nuclei*, Phys. Rev. **C7** (1973) 296–316

[WFF88] R.B. Wiringa, V. Fiks, and A. Fabrocini: *Equation of state for dense nuclear matter*, Phys. Rev. **C38** (1988) 1010–1037.

[YCM06] J.M. Yao, H. Chen, and J. Meng: *Time–odd triaxial relativistic mean field approach for nuclear magnetic moments*, Phys. Rev. **C74** (2006) 024307.

[Yse86] H. Yserentant: *Hierarchical bases give conjugate gradient type methods a multigrid speed of convergence*, Appl. Math. Comput. **19**, no. 1–4 (1986) 347–358.

Zusammenfassung in deutscher Sprache

In dieser Arbeit wurde die Struktur nuklearer Systeme mit Hilfe des Skyrme Hartree–Fock und des relativistischen Hartree–Fock Modells beschrieben. Die nuklearen Systeme reichen von Kernen über Strukturen in der Kruste eines Neutronensterns bis zur homogenen Materie, wobei auch die Paarkorrelationen der Nukleonen und die Temperatur berücksichtigt wird. Das numerische Verfahren wird für den Skyrme–Hartree–Fock und den relativistischen Hartree–Fock Ansatz in einer kubischen Zelle beschrieben und durchgeführt. Den Abschluss der Arbeit bilden die Ergebnisse für die Strukturen in der Kruste eines Neutronensterns und für einige neutronenreiche exotische Kerne.

Die Skyrme Hartree–Fock Theorie ist eine nicht–relativistische Dichtefunktionaltheorie zur Berechnung nuklearer Strukturen, die aufgrund der punktweisen Skyrme–Wechselwirkung für schnelle Berechnungen geeignet ist. Dieser Ansatz wird in einer kubischen Wigner–Seitz Zelle zusammen mit Paarbildung– und Temperatureffekten angewendet, um die Struktur der sogenannten "Pasta"–Phase zu untersuchen, die in der Kruste eines Neutronensterns vorkommt.

In den letzten Jahren wurde der relativistische Hartree–Fock Ansatz weiterentwickelt. Es wurde bestätigt, dass die Operatorenstruktur des relativistischen Brueckner–Hartree–Fock Ansatzes für Kernmaterie auf die des relativistischen Hartree–Fock Ansatzes projeziert werden kann. Durch dieses Verfahren gewinnt man eine lokale Dichtenäherung der Brueckner G–Matrix, die Zweiteilchenstreuung im Medium beschreibt. Die Selbstenergien der Nukleonen im relativistichen oder Dirac–Brueckner–Hartree–Fock Verfahren (DBHF) führen zu dichteabängigen Kopplungskonstanten für die Nukleon–Meson Vertices im relativistischen Hartree–Fock Ansatz. Durch die Variationsrechnung erhält man im Zusammenhang mit solchen dichteabhängigen Kopplungskonstanten den sogenannten Rearrangement–Beitrag zur Nu-

kleonselbstenergie, der die Einteilchenenergien und die Wellenfunktionen wesentlich verbessert. Die triaxiale numerische Behandlung des relativistischen Hartree–Fock Ansatzes wurde entwickelt und auf zwei nukleare Systeme angewandt: Exotische neutronenreiche Kerne werden mit dem relativistischen Hartree–Fock Ansatz untersucht und die nukleare Materie in der Kruste der Neutronensterne wird mit dem relativistischen Hartree Verfahren unter Berücksichtigung der Paarkorrelations– und Temperatureffekte modelliert.

Darüberhinaus wurden dichteabhängige Kopplungsfunktionen für relativistische Hartree Berechnungen an die Selbstenergieen einer Dirac–Brueckner–Hartree–Fock Berechnung von van Dalen et al. [vD$^+$07] angefittet. Diese DBHF Berechnungen, die mit realistischen Nukleon–Nukleon Potentialen [Ml89] durchgefürt wurden, ergeben eine gute Zustandsgleichung für Neutronensterne. Eine Renormalisierung verbessert die Übereinstimmung dieses sogenannten dichteabhängigen relativistischen mittleren Feld Modells (DDRMF) mit den Ergebnissen der DBHF Berechnung. Dieses Verfahren modifiziert in einem ersten Schritt die effektiven Massen der Nukleonen, indem der Effekt der raumartigen vektoriellen Selbstenergie auf die skalare Selbstenergie berücksichtigt wird. In einem zweiten Schritt wird die zeitartige Komponente der vektoriellen Selbstenergie modifiziert um das Einteilchenspektrum und die Bindungsenergie der DBHF Berechnung reproduzieren zu können. Da im renormalisierten Modell die endlichen Atomkerne immer noch zu schwach gebunden sind, wurde die Repulsion des ω–Mesons um die Sättigungsdichte herum etwas geschwächt um die Bindungsenergie schwerer Kerne reproduzieren zu können. Die Radien der Atomkerne werden etwas unterschätzt. Die Eigenschaften deses DDRMF Modells sind mit denen des ursprünglichen DBHF Modells vergleichbar und daher sollte dieses Modell eine gute Beschreibung der nuklearen Zustandsgleichung für die Astrophysik ermöglichen.

Als ein Modell für die Kruste eines Neutronensterns wird die Struktur neutraler baryonischer Materie im Dichtebereich zwischen 0.01 und 0.1 fm^{-3} mit Hilfe von verschiedenen Hartree–Fock und mittlere Feld Berechnungen inklusive Paarkorrelations– und Temperatureffekten in einem periodischen Gitter aus kubischen Wigner–Seitz (WS) Zellen untersucht. In diesem Dichtebereich werden Strukturen beobachtet, die von neutronenreichen, in einen Neutronensee eingebetteten Kernen bis zu homogener nuklearer Materie reichen. Die Symmetrieen dieser Wigner–Seitz Zelle ermöglichen die Ausbildung triaxialer Strukturen, die auch stabförmige und plattenartige Strukturen beinhalten, und damit einen natürlichen Übergang zur homogenen Materie

beschreiben können.

Für die baryonische Materie wird eine Skyrme Hartree–Fock Näherung mit der relativistischen mittleren Feld Näherung (RMF) und der dichteabhängigen relativistischen mittleren Feld Näherung (DDRMF) verglichen. Alle Ansätze führten zu einer verblüffenden Vielfalt quasinuklearer Strukturen mit allmählichen, gleichmäßigen Übergängen. Die Erscheinung spezieller Strukturen und auch die Übergangsdichten zwischen diesen Strukturen hängen vom gewählten nuklearen Modell ab. Durch die Bildung solcher Strukturen wird die Energie gegenüber der in homogener Materie abgesenkt und der Protonenanteil steigt an.

Die Energien als auch der Protonenanteil können von einer Thomas–Fermi Berechnung (Lokale Dichtenäherung der Energie) gut reproduziert werden, wenn die Konstante des Oberflächenterms an die Ergebnisse der mikroskopischen Berechnungen angepasst wird. Eine zuverlässige Thomas–Fermi Berechnung für einen großen Bereich von Proton–Neutron–Asymmetrieen erhält man nur, wenn dieser Oberflächenterm von der Isospin–Asymmetrie abhängt.

Bei nichtverschwindender Temperatur zeigen die Skyrme Hartree–Fock und relativistichen mittleren Feld Näherungen weniger ausgeprägte nukleare Strukturen, sie sind aber immer noch vorhanden. Der Protonenanteil ist gegenüber demjenigen bei verschwindender Temperatur leicht erhöht, und die Absenkung der freien baryonischen Eenergie ist weniger ausgeprägt als diejenige der baryonischen Energie aufgrund der geringeren Entropie in der strukturierteren Materie. Die freie Energie und der Protonenanteil kann ebenfalls mit Thomas–Fermi Berechnungen reproduziert werden, obwohl dieser Ansatz bei der Reproduktion der Energie und einiger Strukturen Mängel zeigt.

Die Paarkorrelationen werden mit dem BCS–Ansatz ausgewertet, wobei eine dichteabhängige Kontaktwechselwirkung angenommen wird. Die Paarverteilungsfunktion der Neutronen zeigt im Bereich der Quasikerne niedrigere Werte als im Neutronensee, obwohl die anomale Dichte, die diese Paarkraft bewirkt, steigt. Dieser Effekt sollte anhand einer realistischen Wechselwirkung überprüft werden, da er ein Artefakt der dichteabhängigen Paarkraft sein könnte.

Die mikroskopischen Berechnungen der Einteilchenenergieen und Wellenfunktionen liefern eine Basis für weitere Untersuchungen der Eigenschaften der Materie in der Kruste der Neutronensterne und auch in Supernovae vom Typ II. Es können Übergangsmatrixelemente für verschiedene Operatoren ausgewertet werden, wodurch Responsefunktionen und z. B. die mittlere freie Weglänge der Neutrinos, berechnet

werden können. Diese Untersuchungen können neue Informationen über den Einfluss solcher nuklearer Strukturen auf die Kühlrate und andere Eigenschaften des Sterns zu Tage bringen.
Exotische neutronenreiche Kerne bilden eine Basis für die Bildung schwerer Kerne in Sternen. Eine veränderte Schalenstruktur solcher Kerne kann ihre Eigenschaften, wie z. B. die Halbwertszeit, beeinflussen, die sich auf die Bildung schwerer Kerne auswirken.
Berechnungen aufgrund von realistischen Nukleon–Nukleon Potentialen sollten die Ergebnisse dieser Arbeit bestätigen, die in der mittleren Feld Näherung berechnet wurden. Ein erster Anlauf ist bereits in Bearbeitung, der eine impulsrenormierte Wechselwirkung V_{lowk} verwendet.

Danksagung

Mein besonderer Dank gilt meinem Doktorvater, Herrn Prof. Dr. Herbert Müther, der mich bei der Bearbeitung des Themas unterstützt und beraten hat. Er war stets bereit zu fachlichen Diskussionen und hat mich kompetent beraten. Darüber hinaus ermöglichte er mir zahlreiche internationale Aufenthalte, z. B. bei Herrn Prof. Dr. Arturo Polls in Barcelona, die zum Gelingen dieser Arbeit beigetragen haben.
Dem internationalen Graduiertenkolleg "Hadrons in Vacuum in Nuclei and Stars" (Basel, Graz, Tübingen), das von der DFG finanziell unterstützt wird, danke ich für die finanzielle Unterstützung dieser Arbeit und die Bereitstellung einer hoch motivierenden Umgebung mit Vorträgen, Seminaren und dem Aufenthalt in einer Partneruniversität. An dieser Stelle möchte ich dem ehemaligen Sprecher Prof. Dr. Amand Faessler und dem neuen Sprecher Prof. Dr. Josef Jochum danken, die das Graduiertenkolleg in Tübingen organisieren.
Herrn Prof. Dr. Friedrich-Karl Thielemann danke ich für die Betreuung in Basel und den Einblick in die Astrophysik. Auch Herrn Dr. Matthias Liebendörfer und Tobias Fischer möchte ich für die angeregten Diskussionen über die Simulation der Supernova danken.
Den Herren Dominique Epple, Oliver Plohl, Dr. Markus Quandt, Prof. Dr. Kurt Langfeld, und Markus Leder danke ich für die Administration des PTWAP Computer Clusters, auf dem die Software für diese Arbeit betrieben wurde.
Meinen Freunden danke ich für die moralische Unterstützung und dem Interesse am Fortgang der Arbeit, besonders meinem Studienfreund Marc Preunkert.
Meiner Frau Evgeniya und ihrer Familie danke ich herzlich, die mich mit viel Geduld, Liebe, und Ermutigung bei dieser Arbeit begleitet haben.
Vor allem aber danke ich GOTT, der mir immer wieder neue Ideen und Durchhaltevermögen gegeben hat. IHM allein sei Ehre.